Modern theory of nuclear forces

E. Epelbaum*

Institut für Kernphysik (IKP-3) and Jülich Center for Hadron Physics, Forschungszentrum Jülich, D-52425 Jülich, Germany
and Helmholtz-Institut für Strahlen- und Kernphysik (Theorie) and Bethe Center for Theoretical Physics, Universität Bonn, D-53115 Bonn, Germany

H.-W. Hammer†

Helmholtz-Institut für Strahlen- und Kernphysik (Theorie) and Bethe Center for Theoretical Physics, Universität Bonn, D-53115 Bonn, Germany

Ulf-G. Meißner‡

Helmholtz-Institut für Strahlen- und Kernphysik (Theorie) and Bethe Center for Theoretical Physics, Universität Bonn, D-53115 Bonn, Germany
and Institut für Kernphysik (IKP-3), Institute for Advanced Simulation, and Jülich Center for Hadron Physics, Forschungszentrum Jülich, D-52425 Jülich, Germany

(Published 21 December 2009)

Effective field theory allows for a systematic and model-independent derivation of the forces between nucleons in harmony with the symmetries of quantum chromodynamics. The foundations of this approach are reviewed and its application for light nuclei at various resolution scales is discussed. The extension of this approach to many-body systems is sketched.

DOI: 10.1103/RevModPhys.81.1773 PACS number(s): 21.30.−x, 21.45.−v, 12.38.Lg, 12.39.Fe

CONTENTS

*e.epelbaum@fz-juelich.de
†hammer@hiskp.uni-bonn.de
‡meissner@hiskp.uni-bonn.de

I. QUANTUM CHROMODYNAMICS AND NUCLEAR FORCES

Within the standard model of particle physics, the strong interactions are described by quantum chromodynamics (QCD). QCD is a fascinating theory with many intriguing manifestations. Its structure and interactions are governed by a local non-Abelian gauge symmetry, namely, $SU(3)_{\text{color}}$. Its fundamental degrees of freedom, the quarks (the matter fields) and gluons (the force carriers), have never been observed in isolation (confinement). The strong coupling constant α_S exhibits a very pronounced running and is of order 1 in the typical energy scales of nuclear physics. The bound states made from the basic constituents are the hadrons, the strongly interacting particles. The particle spectrum shows certain regularities that can be traced back to the flavor symmetries related to the fermions building up these states. More precisely, there are six quark flavors. These can be grouped into two very different sectors. While the light quarks (u,d,s) are almost massless and thus have to be treated relativistically, bound states made from heavy quarks allow for a precise nonrelativistic treatment. In what follows, we consider only the light quarks at low energies, where perturbation theory in α_S is inapplicable (this regime is frequently called "strong QCD"). A further manifestation of strong QCD is the appearance of nuclei, shallow bound states composed of

 ©2009 The American Physical Society

protons, neutrons, pions, or strange particles such as hyperons. The resulting nuclear forces that are responsible for the nuclear binding are residual color forces, much like the van der Waals forces between neutral molecules. It is the aim of this article to provide the link between QCD and its symmetries, in particular, the spontaneously and explicitly broken chiral symmetry, and the nuclear forces which allow one to put nuclear physics on firm theoretical grounds and also give rise to an accurate calculational scheme for nuclear forces and the properties of nuclei.

This review is organized as follows: in this section, we discuss some of the concepts underlying the chiral effective field theory (EFT) of the nuclear forces and make contact to *ab initio* lattice simulations of two-baryon systems as well as to more phenomenological approaches. Section II deals with the foundations and applications of nuclear EFT and should be considered the central piece of this review. In particular, tests of these forces in few-nucleon systems are discussed. Attempts to tackle nuclear matter and finite nuclei are considered in Sec. III. We end with a short summary and outlook.

A. Chiral symmetry

First, we must discuss chiral symmetry in the context of QCD. Chromodynamics is a non-Abelian $SU(3)_{color}$ gauge theory with $N_f=6$ flavors of quarks, three of them being light (u,d,s) and the other three heavy (c,b,t). Here light and heavy refer to a typical hadronic scale of about 1 GeV. In what follows, we consider light quarks only (the heavy quarks are to be considered as decoupled). The QCD Lagrangian reads

$$\mathcal{L}_{\rm QCD} = -\frac{1}{2g^2}\mathrm{Tr}(G_{\mu\nu}G^{\mu\nu}) + \bar{q}i\gamma^\mu D_\mu q - \bar{q}\mathcal{M}q$$
$$= \mathcal{L}^0_{\rm QCD} - \bar{q}\mathcal{M}q, \tag{1.1}$$

where we have absorbed the gauge coupling in the definition of the gluon field and color indices are suppressed. The three-component vector q collects the quark fields, $q^T(x)=(u(s),d(x),s(x))$. As far as the strong interactions are concerned, the different quarks u,d,s have identical properties, except for their masses. The quark masses are free parameters in QCD—the theory can be formulated for any value of the quark masses. In fact, light quark QCD can be well approximated by a fictitious world of massless quarks, denoted $\mathcal{L}^0_{\rm QCD}$ in Eq. (1.1). Remarkably, this theory contains no adjustable parameter—the gauge coupling g merely sets the scale for the renormalization group invariant scale $\Lambda_{\rm QCD}$. Furthermore, in the massless world left- and right-handed quarks are completely decoupled. The Lagrangian of massless QCD is invariant under separate unitary global transformations of the left- and right-hand quark fields, the so-called *chiral rotations*, $q_I \to V_I q_I, V_I \in \mathrm{U}(3), I=L,R$, leading to $3^2=9$ conserved left- and 9-conserved right-handed currents by virtue of Noether's theorem. These can be expressed in terms of vector $(V=L+R)$ and axial-vector $(A=L-R)$ currents,

$$V_0^\mu = \bar{q}\gamma^\mu q, \quad V_a^\mu = \bar{q}\gamma^\mu \frac{\lambda_a}{2} q,$$
$$A_0^\mu = \bar{q}\gamma^\mu\gamma_5 q, \quad A_a^\mu = \bar{q}\gamma^\mu\gamma_5 \frac{\lambda_a}{2} q. \tag{1.2}$$

Here $a=1,\ldots,8$, and the λ_a are Gell-Mann's SU(3) flavor matrices. The singlet axial current is anomalous and thus not conserved. The actual symmetry group of massless QCD is generated by the charges of the conserved currents; it is $G_0=\mathrm{SU}(3)_R\times\mathrm{SU}(3)_L\times\mathrm{U}(1)_V$. The $\mathrm{U}(1)_V$ subgroup of G_0 generates conserved baryon number since the isosinglet vector current counts the number of quarks minus antiquarks in a hadron. The remaining group $\mathrm{SU}(3)_R\times\mathrm{SU}(3)_L$ is often referred to as chiral SU(3). Note that one also considers the light u and d quarks only (with the strange quark mass fixed at its physical value); in that case, one speaks of chiral SU(2) and must replace the generators in Eq. (1.2) by the Pauli matrices. We note that QCD is also invariant under the discrete symmetries of parity (P), charge conjugation (C), and time reversal (T). Although interesting in itself, we do not consider strong CP violation and the related θ term in what follows [see, e.g., Peccei (2008)].

The chiral symmetry is a symmetry of the Lagrangian of QCD but not of the ground state or the particle spectrum—to describe the strong interactions in nature, it is crucial that chiral symmetry is spontaneously broken. This can be most easily seen from the fact that hadrons do not appear in parity doublets. If chiral symmetry was exact, from any hadron one could generate by virtue of an axial transformation another state of exactly the same quantum numbers except of opposite parity. The spontaneous symmetry breaking leads to the formation of a quark condensate in the vacuum $\langle 0|\bar{q}q|0\rangle = \langle 0|\bar{q}_L q_R + \bar{q}_R q_L|0\rangle$, thus connecting the left- with the right-handed quarks. In the absence of quark masses this expectation value is flavor independent: $\langle 0|\bar{u}u|0\rangle = \langle 0|\bar{d}d|0\rangle = \langle 0|\bar{q}q|0\rangle$. More precisely, the vacuum is only invariant under the subgroup of vector rotations times the baryon number current, $H_0=\mathrm{SU}(3)_V\times\mathrm{U}(1)_V$. This is the generally accepted picture that is supported by general arguments (Vafa and Witten, 1984) as well as lattice simulations of QCD [for a recent study, see Giusti and Necco (2007)]. In fact, the vacuum expectation value of the quark condensate is only one of the many possible order parameters characterizing the spontaneous symmetry violation—all operators that share the invariance properties of the vacuum qualify as order parameters. The quark condensate nevertheless enjoys a special role; it can be shown to be related to the density of small eigenvalues of the QCD Dirac operator [see Banks and Casher (1980) and discussions in Leutwyler and Smilga (1992) and Stern (1998)], $\lim_{\mathcal{M}\to 0}\langle 0|\bar{q}q|0\rangle = -\pi\rho(0)$. For free fields, $\rho(\lambda)\sim\lambda^3$ near $\lambda=0$. If the eigenvalues accumulate near zero only then one obtains a nonvanishing

condensate. This scenario is indeed supported by lattice simulations and many model studies involving topological objects such as instantons or monopoles.

Before discussing the implications of spontaneous symmetry breaking for QCD, we remind the reader of Goldstone's theorem (Goldstone, 1961; Goldstone *et al.*, 1962): to every generator of a spontaneously broken symmetry corresponds a massless excitation of the vacuum. These states are the *Goldstone bosons*, collectively denoted as pions $\pi(x)$ in what follows. Through the corresponding symmetry current the Goldstone bosons couple directly to the vacuum,

$$\langle 0|A^0(0)|\pi\rangle \neq 0. \tag{1.3}$$

In fact, the nonvanishing of this matrix element is a necessary and sufficient condition for spontaneous symmetry breaking. In QCD, we have eight [three] Goldstone bosons for SU(3) [SU(2)] with spin 0 and negative parity—the latter property is a consequence that these Goldstone bosons are generated by applying the axial charges on the vacuum. The dimensionful scale associated with the matrix element [Eq. (1.3)] is the pion decay constant (in the chiral limit),

$$\langle 0|A_\mu^a(0)|\pi^b(p)\rangle = i\delta^{ab}Fp_\mu, \tag{1.4}$$

which is a fundamental mass scale of low-energy QCD. For massless quarks, the value of F differs from the physical value by terms proportional to the quark masses, to be introduced later, $F_\pi = F[1+\mathcal{O}(\mathcal{M})]$. The physical value of F_π is 92.4 MeV, determined from pion decay, $\pi \to \nu\mu$.

Of course, in QCD the quark masses are not exactly zero. The quark mass term leads to the so-called explicit chiral symmetry breaking. Consequently, the vector and axial-vector currents are no longer conserved (with the exception of the baryon number current),

$$\partial_\mu V_a^\mu = \tfrac{1}{2}i\bar{q}[\mathcal{M},\lambda_a]q, \quad \partial_\mu A_a^\mu = \tfrac{1}{2}i\bar{q}\{\mathcal{M},\lambda_a\}\gamma_5 q. \tag{1.5}$$

However, the consequences of the spontaneous symmetry violation can still be analyzed systematically because the quark masses are *small*. QCD possesses what is called an approximate chiral symmetry. In that case, the mass spectrum of the unperturbed Hamiltonian and the one including the quark masses cannot be significantly different. Stated differently, the effects of the explicit symmetry breaking can be analyzed in perturbation theory. As a consequence, QCD has a remarkable mass gap—the pions (and, to a lesser extent, the kaons and the eta) are much lighter than all other hadrons. To be more specific, consider chiral SU(2). The second formula of Eq. (1.5) is a Ward identity that relates the axial current $A^\mu = \bar{d}\gamma^\mu\gamma_5 u$ with the pseudoscalar density $P = \bar{d}i\gamma_5 u$,

$$\partial_\mu A^\mu = (m_u + m_d)P. \tag{1.6}$$

Taking on-shell pion matrix elements of this Ward identity, one arrives at

$$M_\pi^2 = (m_u + m_d)G_\pi/F_\pi, \tag{1.7}$$

where the coupling G_π is given by $\langle 0|P(0)|\pi(p)\rangle = G_\pi$. This equation leads to some intriguing consequences: In the chiral limit, the pion mass is exactly zero, in accordance with Goldstone's theorem. More precisely, the ratio G_π/F_π is a constant in the chiral limit and the pion mass grows as $\sqrt{m_u+m_d}$ if the quark masses are turned on.

There is even further symmetry related to the quark mass term. It is observed that hadrons appear in isospin multiplets, characterized by very small splittings of the order of a few MeV. These are generated by the small quark mass difference $m_u - m_d$ and also by electromagnetic effects of the same size (with the notable exception of the charged to neutral pion mass difference that is almost entirely of electromagnetic origin). This can be made more precise: For $m_u = m_d$, QCD is invariant under SU(2) isospin transformations; $q \to q' = Uq$, with U as a unitary matrix. In this limit, up and down quarks cannot be disentangled as far as the strong interactions are concerned. Rewriting of the QCD quark mass term allows one to make the strong isospin violation explicit,

$$\begin{aligned}\mathcal{H}_{\mathrm{QCD}}^{\mathrm{SB}} &= m_u\bar{u}u + m_d\bar{d}d \\ &= \frac{m_u+m_d}{2}(\bar{u}u+\bar{d}d) + \frac{m_u-m_d}{2}(\bar{u}u-\bar{d}d),\end{aligned} \tag{1.8}$$

where the first (second) term is an isoscalar (isovector). Extending these considerations to SU(3), one arrives at the eightfold way of Gell-Mann and Ne'eman that played a decisive role in our understanding of the quark structure of the hadrons. The SU(3) flavor symmetry is also an approximate one, but the breaking is much stronger than for the isospin case. From this, one can directly infer that the quark mass difference $m_s - m_d$ must be much larger than $m_d - m_u$.

The consequences of these broken symmetries can be analyzed systematically in a suitably tailored EFT, as discussed below. At this point, it is important to stress that the chiral symmetry of QCD plays a crucial role in determining the longest ranged parts of the nuclear force, which is given by Goldstone boson exchange between two and more nucleons. This was already stressed long ago [see, e.g., Brown (1970), and references therein] but only with the powerful machinery of chiral effective field theory this connection could be worked out model independently, as we show in what follows.

B. Scales in nuclear physics

To appreciate the complexity related to a theoretical description of the nuclear forces, it is most instructive to discuss the pertinent scales arising in this problem. This can most easily be visualized by looking at the phenomenological central potential between two nucleons, as it appears, e.g., in meson-theoretical approaches to the nuclear force (see Fig. 1). The longest range part of the

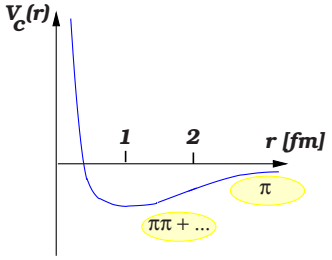

FIG. 1. (Color online) Schematic plot of the central nucleon-nucleon potential. The longest range contribution is the one-pion exchange; the intermediate range attraction is described by two-pion exchanges and other shorter ranged contributions. At even shorter distances, the *NN* interaction is strongly repulsive.

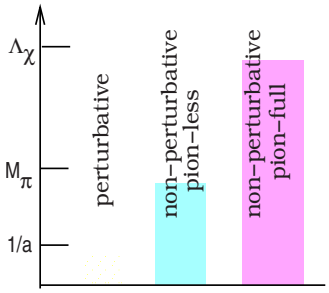

FIG. 2. (Color online) Scales in the two-nucleon problem and the range of validity of the corresponding EFTs as explained in the text. Here Λ_χ is the hard scale related to spontaneous chiral symmetry breaking, with $\Lambda_\chi \simeq M_\rho$, with $M_\rho = 770$ MeV the mass of the rho meson.

interaction is the one-pion exchange (OPE) that is firmly rooted in QCD's chiral symmetry. Thus, the corresponding natural scale of the nuclear force problem is the Compton wavelength of the pion,

$$\lambda_\pi = 1/M_\pi \simeq 1.5 \text{ fm}, \tag{1.9}$$

where $M_\pi = 139.57$ MeV is the charged pion mass. The central intermediate range attraction is given by 2π exchange (and shorter ranged physics). Finally, the wave functions of two nucleons do not like to overlap, which is reflected in a short-range repulsion that can, e.g., be modeled by vector meson exchange. From such considerations, one would naively expect to be able to describe nuclear binding in terms of energy scales of the order of the pion mass. However, the true binding energies of the nuclei are given by much smaller energy scales between 1 and 9 MeV per nucleon. Another measure for the shallow nuclear binding is the so-called binding momentum γ. In the deuteron, $\gamma = \sqrt{mB_D} \simeq 45$ MeV $\ll M_\pi$, with $m = 938.2$ MeV as the nucleon mass and $B_D = 2.224$ MeV as the deuteron binding energy. The small value of γ signals the appearance of energy-momentum scales much below the pion mass. The most dramatic reflection of the complexity of the nuclear force problem is the values of the *S*-wave neutron-proton scattering lengths,

$$|a(^1S_0)| = 23.8 \text{ fm} \gg 1/M_\pi, \quad a(^3S_1) = 5.4 \text{ fm} \gg 1/M_\pi. \tag{1.10}$$

Thus, to properly set up an effective field theory for the forces between two (or more) nucleons, it is mandatory to deal with these very different energy scales. If one was to treat the large *S*-wave scattering lengths perturbatively, the range of the corresponding EFT would be restricted to momenta below $p_{\max} \sim 1/|a(^1S_0)| \simeq 8$ MeV. To overcome this barrier, one must generate the small binding energy scales by a nonperturbative resummation. This can, e.g., be done in a theory without explicit pion degrees of freedom, the so-called pionless EFT. In such an approach, the limiting hard scale is the pion mass. To go further, one must include the pions explicitly, as it is done in the pion-full or chiral nuclear EFT. The relation between these different approaches is schematically shown in Fig. 2. A different and more formal argument that shows the breakdown of a perturbative treatment of the EFT with two or more nucleons is related to the pinch singularities in the two-pion exchange diagram in the static limit as discussed later in the context of the explicit construction of the chiral nuclear EFT.

In addition, if one extends the considerations to heavier nuclei or even nuclear matter, the many-body system exhibits yet another scale, the Fermi momentum k_F, with $k_F \simeq 2M_\pi$ at nuclear matter saturation density. This new scale must be included in a properly modified EFT for the nuclear many-body problem which is not a straightforward exercise as shown below. It is therefore not astonishing that the theory for heavier nuclei is still in a much less developed stage than the one for the few-nucleon problem. These issues will be discussed in Sec. III.

For more extended discussions of scales in the nuclear force problem and in nuclei, see Friar *et al.* (1996), Friar (1997), Delfino *et al.* (2006), and Kaiser *et al.* (2007).

C. Conventional approaches to the nuclear force problem

Before discussing the application of the effective field theory approach to the nuclear force problem, we make a few comments on the highly successful conventional approaches. First, we consider the two-nucleon case. Historically, meson field theory and dispersion relations have laid the foundations for the construction of a two-nucleon potential. All these approaches incorporate the long-range one-pion exchange as proposed by Yukawa in 1935 (Yukawa, 1935) which nowadays is firmly rooted in QCD. Dispersion relations can be used to construct the two-pion exchange contribution to the nuclear force as pioneered at Paris (Cottingham *et al.*, 1973) and Stony Brook (Jackson *et al.*, 1975). For a review, see, e.g., Machleidt and Slaus (2001). In the 1990s, the so-called high-precision potentials have been developed that fit the large basis of *pp* and *np* elastic scattering data with a χ^2/datum $\simeq 1$. One of these is the so-called CD-Bonn potential (Machleidt, 2001). Besides one-pion, ρ and ω

vector-meson exchanges, it contains two scalar-isoscalar mesons in each partial wave up to angular momentum $J=5$ with the mass and coupling constant of the second σ fine tuned in any partial wave. The hadronic vertices are regulated with form factors with cutoffs ranging from 1.3 to 1.7 GeV. Similarly, in the Nijmegen I and II potentials one-pion exchange is supplemented by heavy-boson exchanges with adjustable parameters which are fitted for all (low) partial waves separately (Stoks *et al.*, 1994). The Argonne V18 (AV18) potential starts from a very general operator structure in coordinate space and has fit functions for all these various operators (Wiringa *et al.*, 1995). While these various potentials give an accurate representation of the nucleon-nucleon phase shifts and of most deuteron properties, the situation becomes much less satisfactory when it comes to the much smaller but necessary three-nucleon forces. Such three-body forces are needed to describe the nuclear binding energies and levels, as most systematically shown by the Urbana-Argonne group (Pieper and Wiringa, 2001). Systematic studies of the dynamics and reactions of systems with three or four nucleons further sharpen the case for the necessity of including three-nucleon forces (3NFs) [see, e.g., Glöckle *et al.* (1996)]. The archetype of a 3NF is due to Fujita and Miyazawa (1957), who extended Yukawa's meson exchange idea by sandwiching the pion-nucleon scattering amplitude between nucleon lines, thus generating the 3NF of longest range. In fact, the work of Fujita and Miyazawa has been the seed for many meson-theoretical approaches to the three-nucleon force like the families of Tucson-Melbourne (McKellar and Rajaraman, 1968; Coon *et al.*, 1975), Brazilian (Coelho *et al.*, 1983), or Urbana-Illinois (Pudliner *et al.*, 1997; Pieper *et al.*, 2001) 3NFs.

While the conventional approach outlined here has enjoyed many successes and is frequently used in, e.g., nuclear structure and reaction calculations, it remains incomplete as there are certain deficiencies that can only be overcome based on EFT approaches. These are the following: (i) it is difficult—if not impossible—to assign a trustworthy theoretical error, (ii) gauge and chiral symmetries are difficult to implement, (iii) none of the three-nucleon forces is consistent with the underlying nucleon-nucleon interaction models or approaches, and (iv) the connection to QCD is not at all obvious. There is still a very natural connection between these models and the forces derived from EFT by mapping the complicated physics of the short-distance part of any interaction at length scales $\sim 1/M_\rho$ to the tower of multifermion contact interactions that naturally arise in the EFT description (see Sec. II.B).

D. Brief introduction to effective field theory

EFT is a general approach to calculate the low-energy behavior of physical systems by exploiting a separation of scales in the system [for reviews see, e.g., Georgi (1993), Manohar (1996), and Burgess (2007)]. Its roots can be traced to the renormalization group (Wilson, 1983) and the intuitive understanding of ultraviolet divergences in quantum field theory (Lepage, 1989). A succinct formulation of the underlying principle was given in Weinberg (1979): If one starts from the most general Lagrangian consistent with all symmetries of the underlying interaction, one will get the most general S matrix consistent with these symmetries. Together with a power counting scheme that specifies which terms are required at a desired accuracy leads to a predictive paradigm for a low-energy theory. The expansion is typically in powers of a low-momentum scale $M_{\rm low}$ which can be the typical external momentum over a high-momentum scale $M_{\rm high}$. However, what physical scales $M_{\rm high}$ and $M_{\rm low}$ are identified with depends on the considered system. In its most simple setting, consider a theory that is made of two particle species, the light and the heavy ones with $M_{\rm low} \ll M_{\rm high}$. Consider now soft processes in which the energies and momenta are of the order of the light particle mass (the so-called soft scale). Under such conditions, the short-distance physics related to the heavy particles can never be resolved. However, it can be represented by light-particle contact interactions with increasing dimension (number of derivatives). Consider, e.g., heavy-particle exchange between light ones in the limit that $M_{\rm high} \to \infty$ while keeping the ratio $g/M_{\rm high}$ fixed, with g the light-heavy coupling constant. As shown in Fig. 3, one can represent such exchange diagrams by a sum of local operators of the light fields with increasing number of derivatives. In a highly symbolic notation

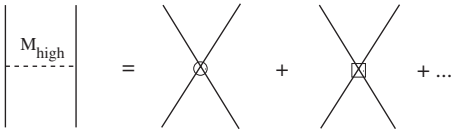

FIG. 3. Expansion of a heavy-particle exchange diagram in terms of local light-particle operators. The solid and dashed lines denote light and heavy particles, respectively. The filled circle and square denote insertions with zero and two derivatives in order. The ellipsis stands for operators with more derivatives.

$$\frac{g^2}{M_{\rm high}^2 - t} = \frac{g^2}{M_{\rm high}^2} + \frac{g^2 t}{M_{\rm high}^4} + \cdots , \tag{1.11}$$

with t the squared invariant momentum transfer. In many cases, the corresponding high-energy theory is not known. The framework of EFT still offers a predictive and systematic framework for performing calculations in the light particle sector. Denote by Q a typical energy or momentum of the order of $M_{\rm low}$ and by Λ the hard scale where the EFT will break down. In many cases, this scale is set by the masses of the heavy particles not considered explicitly. In such a setting, any matrix element or Green's function admits an expansion in the small parameter Q/Λ (Weinberg, 1979),

$$\mathcal{M} = \sum_{\nu} \left(\frac{Q}{\Lambda}\right)^{\nu} \mathcal{F}\left(\frac{Q}{\mu}, g_i\right), \tag{1.12}$$

where $\mathcal{F}$ is a function of order 1 (naturalness), μ a regularization scale (related to the UV divergences appearing in the loop graphs), and g_i denotes a collection of coupling constants, often called low-energy constants (LECs). These parametrize (encode) the unknown high-energy (short-distance) physics and must be determined by a fit to data (or can be directly calculated if the corresponding high-energy theory is known or can be solved). The counting index ν in general depends on the fields in the effective theory, the number of derivatives, and the number of loops. This defines the so-called power counting which allows one to categorize all contributions to any matrix element at a given order. It is important to stress that ν must be bounded from below to define a sensible EFT. In QCD this is a consequence of the spontaneous breaking of its chiral symmetry. The contributions with the lowest possible value of ν define the so-called leading-order (LO) contribution, the first corrections with the second smallest allowed value of ν define the next-to-leading-order (NLO) terms, and so on. In contrast to more conventional perturbation theory, the small parameter is not a coupling constant (such as quantum electrodynamics) but rather one expands in small energies or momentum, where small refers to the hard scale Λ. The archetype of such a perturbative EFT is chiral perturbation theory (CHPT) that exploits the structures of the spontaneous and explicit chiral symmetry breaking in QCD (Gasser and Leutwyler, 1984, 1985). Here the light degrees of freedom are the pions, which are generated through the symmetry violation. Heavier particles, such as, vector mesons, only appear indirectly as they generate local four-pion interactions with four, six, etc., derivatives. For a recent review, see Bernard and Meißner (2007). Of course, the pions also couple to heavy matter fields—such as nucleons—which can also be included in CHPT, as reviewed in Bernard (2008).

So far, we have made the implicit assumption of naturalness, which implies, that the scattering length a is of natural size as, e.g., in CHPT, where the scale is set by $1/\Lambda_\chi \simeq 1$ GeV$^{-1} \simeq 0.2$ fm. This also implies that there are no bound states close to the scattering thresholds. In many physical systems and of particular interest here, especially in the two-nucleon system, this is not the case, but one rather has to deal with unnaturally large scattering lengths (and also shallow bound states). Specifically we consider nucleon-nucleon scattering at very low energies in the $^1S_0$ channel [cf. Eq. (1.10)]. For such low energies, even the pions can be considered heavy and are thus integrated out. To construct an EFT that is applicable for momenta $p > 1/a$, one must retain all terms $ap \sim 1$ in the scattering matrix. This requires a nonperturbative resummation and is most elegantly done in the power divergence scheme of Kaplan, Savage, and Wise (1998a, 1998b). This amounts to summing the leading four-nucleon contact term $\sim C_0(\psi^\dagger\psi)^2$ to all orders in C_0 and matching the scale-dependent LEC C_0 to the scattering length. This leads to the T matrix,

$$T = \frac{4\pi}{m}\frac{1}{1/a + ip}[1 + \mathcal{O}(p^2)], \tag{1.13}$$

where the expansion around the large scattering length is made explicit. Note that a small negative value of a corresponds to attraction. All other effects, such as effective range corrections, are treated perturbatively. This compact and elegant scheme is, however, not sufficient for discussing nuclear processes with momenta $p \geqslant M_\pi$. We return to this topic when we give the explicit construction of the chiral nuclear EFT in Sec. II.B. It is important to stress that such EFTs with unnaturally large scattering length can exhibit universal phenomena that can be observed in physical systems which differ in their typical energy scale by many orders of magnitude [for a review see Braaten and Hammer (2006)]. We note that there are many subtleties in constructing a proper EFT, but space forbids to discuss these here. Whenever appropriate and/or necessary, we mention these in the following sections and provide explicit references.

E. First results from lattice QCD

Lattice QCD (LQCD) is a promising tool to calculate hadron properties *ab initio* from the QCD Lagrangian on a discretized Euclidean space-time. This requires state-of-the-art high performance computers and refined algorithms to analyze the QCD partition function by Monte Carlo methods. Only recently software and hardware developments have become available that allow for full QCD simulations at small enough quark masses (corresponding to pion masses below 300 MeV), large enough volumes (corresponding to spatial dimensions larger than 2.5 fm), and sufficiently fine lattice spacing ($a \simeq 0.05$ fm) so that the results are not heavily polluted by computational artifacts and can really be connected to the physical quark masses by sensible chiral extrapolations.

For the nuclear force problem, there are two main developments in LQCD reviewed here. These concern the extraction of hadron-hadron scattering lengths from unquenched simulations and the first attempts to construct a nuclear potential. These are groundbreaking studies, but at present one has not yet achieved an accuracy to obtain high-precision predictions for nuclear properties. We look forward to the development of these approaches in the future.

The first exploratory study of the nucleon-nucleon scattering lengths goes back to Fukugita *et al.* (1994, 1995) in the quenched approximation. They make use of an elegant formula, frequently called the Lüscher formula, which relates the S-wave scattering length a_0 between two hadrons h_1 and h_2 to the energy shift $\delta E = E_{h_1h_2} - (m_1 + m_2)$ of the two-hadron state at zero relative momentum confined in spatial box of size L^3. It is given by (Hamber *et al.*, 1983; Lüscher, 1986, 1991),

$$\delta E = -\frac{2\pi a_0}{\mu L^3}\left[1 + c_1\frac{a_0}{L} + c_2\frac{a_0^2}{L^2}\right] + \mathcal{O}(L^{-6}), \tag{1.14}$$

with $\mu = m_1 m_2/(m_1+m_2)$ the reduced mass and $c_1 = 2.837\,297$ and $c_2 = 6.375\,183$. A generalization of this formalism was given in Beane *et al.* (2004) utilizing methods developed for the so-called pionless nuclear EFT [EFT with contact interactions; for a review see, e.g., Bedaque and van Kolck (2002)]. It reads

$$p \cot \delta_0(p) = \frac{1}{\pi L}\mathcal{S}((Lp/2\pi)^2),$$

$$\mathcal{S}(\eta) = \sum_{\vec{j}}^{\Lambda_j}\frac{1}{|\vec{j}|^2 - \eta} - 4\pi\Lambda_j, \tag{1.15}$$

which gives the location of all energy eigenstates in the box. Here δ_0 is the S-wave phase shift. The sum over all three-vectors of integers $\vec{j}$ is such that $|\vec{j}| < \Lambda_j$ and the limit $\Lambda_j \to \infty$ is implicit. In the limit $L \gg |a_0|$, Eq. (1.15) reduces to the Lüscher formula [Eq. (1.14)]. On the other hand, for large scattering length, $|(p \cot \delta_0)^{-1}| \gg L$, the energy of the lowest state is given by

$$E_0 = \frac{4\pi^2}{\mu L^2}[d_1 + d_2 Lp \cot \delta_0 + \cdots], \tag{1.16}$$

with $d_1 = 0.472\,895$, $d_2 = 0.079\,023\,4$, and $p \cot \delta_0$ is evaluated at the energy $E = 4\pi^2 d_1/\mu L^2$. Within this framework, Beane *et al.* (2006) performed the first fully dynamical simulation of the neutron-proton scattering lengths, with a lowest pion mass of 354 MeV. This mass is still too high to perform a precise chiral extrapolation to the physical pion mass, but this calculation demonstrates the feasibility of this approach (see also Sec. II.H). This scheme can also be extended to hyperon-nucleon interactions [see Beane *et al.* (2005)]. A first signal for $p\Lambda$ and $n\Sigma^-$ scattering was reported in Beane *et al.* (2007). For a recent review on these activities of the NPLQCD Collaboration, see Beane *et al.* (2008).

Another interesting development was initiated and carried out in Aoki, Hatsuda, and Ishii (2007b). They generalized the two-center Bethe-Salpeter wave-function approach of the CP-PACS Collaboration (Aoki *et al.*, 2005), which offers an alternative to Lüscher's formula, to the NN system. Given an interpolating field for the neutron and for the proton, the NN potential can be defined from the properly reduced six-quark Bethe-Salpeter amplitude $\phi(\vec{r})$. The resulting Lippmann-Schwinger equation defines a nonlocal potential for a given fixed separation $r = |\vec{r}|$. Performing a derivative expansion, the central potential $V_c(r)$ at a given energy E is extracted from

$$V_c(r) = E + \frac{1}{m}\frac{\vec{\nabla}^2\phi(r)}{\phi(r)}. \tag{1.17}$$

Monte Carlo simulations are then performed to generate the six-quark Bethe-Salpeter amplitude in a given spin and isospin state of the two-nucleon system on a large lattice, $V = (4.4\text{ fm})^4$ in the quenched approximation for pion masses between 380 and 730 MeV. Despite these approximations, the resulting effective potential extracted using Eq. (1.17) shares the features of the phenomenological NN potentials—a hard core (repulsion) at small separation surrounded by an attractive well at intermediate and larger distances (see Fig. 4). Furthermore, the asymptotic form of this potential has exactly the form of the OPE, provided one rescales

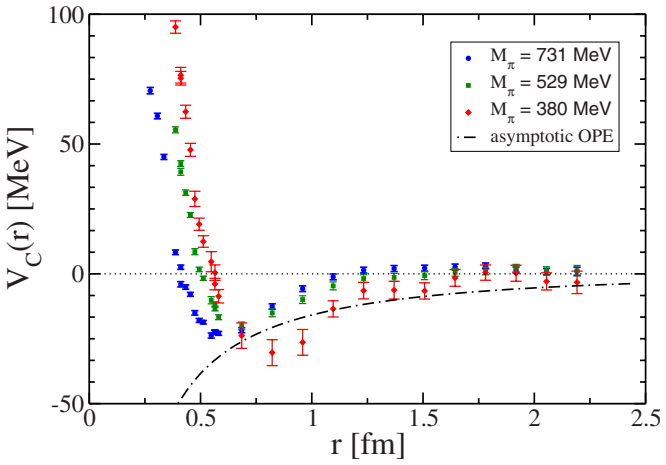

FIG. 4. (Color online) Effective potential in the $^1S_0$ channel for three different quark masses in quenched LQCD. The dashed line is the asymptotic OPE for $M_\pi = 380$ MeV, $m = 1.2$ GeV, and $g_{\pi N}^2/(4\pi) = 14.0$. From Ishii *et al.*, 2007a.

$$V_c^{\rm OPE}(r) = \frac{g_{\pi N}^2}{4\pi}\boldsymbol{\tau}_1\cdot\boldsymbol{\tau}_2\frac{\vec{\sigma}_1\cdot\vec{\sigma}_2}{3}\left(\frac{M_\pi}{2m}\right)^2\frac{e^{-M_\pi r}}{r} \tag{1.18}$$

with the pion and nucleon masses used in the simulations but keeping the pion-nucleon coupling at its physical value $g_{\pi N}^2/(4\pi) \simeq 14.0$. These interesting results have led to some enthusiastic appraisal [see, e.g., Wilczek (2007)]. However, it is important to note that the so-calculated potential is not unique, especially its properties at short distances, since it depends on the definition of the interpolating nucleon fields. Furthermore, the quenched approximation is known to have uncontrolled systematic uncertainties as it does not even define a quantum field theory. In this context, Aoki *et al.* (2005) reported on the numerical absence of the large-distance-dominating η exchange from the flavor-singlet hair-pin diagram. One would still like to see this promising calculation repeated with dynamical quarks of sufficiently small masses. Nemura *et al.* (2008) used this framework to study the ΞN interaction. Interestingly, the central potential of the $p\Xi^0$ interaction looks very similar to the central np potential. It would be interesting to extend these calculations to other hyperon-nucleon channels and also study the effects of SU(3) symmetry breaking. We return to these issues in the context of a three-flavor chiral EFT in Sec. II.F. For recent developments in this scheme concerning the calculation of the tensor force, the energy dependence of the NN potential, and pre-

liminary results for full QCD (2+1 flavors), see Aoki, Ishii, and Nemura (2008).

F. Observables and not-so observable quantities

There is an extensive literature, primarily from the 1960s and 1970s, on the role of off-shell physics in nuclear phenomena [see, e.g., Srivastava and Sprung (1975), and references therein]. This includes not only few-body systems (e.g., the triton) and nuclear matter but also interactions of two-body systems with external probes, such as nucleon-nucleon bremsstrahlung and the electromagnetic form factors of the deuteron. The implicit premise was that there is a true underlying potential governing the nucleon-nucleon force, so that its off-shell properties can be determined. Indeed, the nuclear many-body problem has traditionally been posed as finding approximate solutions to the many-particle Schrödinger equation, given a fundamental two-body interaction that reproduces two-nucleon observables.

In contrast, effective field theories are determined completely by on-energy-shell information up to a well-defined truncation error. In writing down the most general Lagrangian consistent with the symmetries of the underlying theory, many-body forces arise naturally. Even though they are usually suppressed at low energies, they enter at some order in the EFT expansion. These many-body forces have to be determined from many-body data. The key point is, however, that no off-energy-shell information is needed or experimentally accessible. A fundamental theorem of quantum field theory states that physical observables (or more precisely S-matrix elements) are independent of the choice of interpolating fields that appear in a Lagrangian (Haag, 1958; Coleman *et al.*, 1969). Equivalently, observables are invariant under a change in field variables in a field theory Lagrangian (or Hamiltonian),

$$\psi(x) \to \psi(x) + \eta P[\psi], \tag{1.19}$$

where $P[\psi]$ is a local polynomial of the field ψ and its derivatives and η is an arbitrary counting parameter. Newly generated contributions to observables have to cancel separately at each order in η. This "equivalence theorem" holds for renormalized field theories. In an EFT, one exploits the invariance under field redefinitions to eliminate redundant terms in the effective Lagrangian and to choose the most convenient or efficient form for practical calculations (Politzer, 1980; Georgi, 1991; Kilian and Ohl, 1994; Arzt, 1995; Scherer and Fearing, 1995b). Since off-shell Green's functions and the corresponding off-shell amplitudes do change under field redefinitions, one must conclude that off-shell properties are unobservable.

Several recent works have emphasized from a field theory point of view the impossibility of observing off-shell effects. Fearing (1998) and Fearing and Scherer (2000) used model calculations to illustrate how apparent determinations of the two-nucleon off-shell T matrix in nucleon-nucleon bremsstrahlung are illusory since field redefinitions shift contributions between off-shell contributions and contact interactions. Similarly, it was shown in Scherer and Fearing (1995a) that Compton scattering on a pion cannot be used to extract information on the off-shell behavior of the pion form factor. Cohen *et al.* (1996) and Friar *et al.* (1999) emphasized the nonuniqueness of chiral Lagrangians for three-nucleon forces and pion production. Field redefinitions lead to different off-shell forms that yield the same observables within a consistent power counting. Kaplan *et al.* (1999) showed that an interaction proportional to the equation of motion has no observable consequence for the deuteron electromagnetic form factor even though it contributes to the off-shell T matrix.

In systems with more than two nucleons, one can trade off-shell two-body interactions for many-body forces. This explains how two-body interactions related by unitary transformations can predict different binding energies for the triton (Afnan and Serduke, 1973) if many-body forces are not consistently included. These issues were discussed from the viewpoint of unitary transformations in Polyzou and Glöckle (1990) and Amghar and Desplanques (1995). The extension to many-fermion systems in the thermodynamic limit was considered in Furnstahl *et al.* (2001). The effects of field redefinitions were illustrated using the EFT for the dilute Fermi gas (Hammer and Furnstahl, 2000). For a related discussion, see Krippa *et al.* (2003). If many-body interactions generated by the field redefinitions are neglected, a Coester line similar to the one observed for nuclear matter (Coester *et al.*, 1970) is generated. Moreover, the connection to more traditional treatments using unitary transformations was elucidated. The question of whether occupation numbers and momentum distributions of nucleons in nuclei are observables was investigated by Furnstahl and Hammer (2002). Field redefinitions lead to variations in the occupation numbers and momentum distributions that imply the answer is negative. The natural size of the inherent ambiguity (or scheme dependence) in these quantities is determined by the applicability of the impulse approximation. If the impulse approximation is well justified, the ambiguity is small and these quantities are approximately scheme independent. This has important implications for the interpretation of $(e,e'p)$ experiments with nuclei. Whether the stark difference in occupation numbers between nonrelativistic and relativistic Brueckner calculations can be explained by this ambiguity is another interesting question (Jaminon and Mahaux, 1990).

II. EFT FOR FEW-NUCLEON SYSTEMS: FOUNDATIONS AND APPLICATIONS

A. EFT with contact interactions and universal aspects

In nuclear physics, there are a number of EFTs which are all useful for a certain range of systems (cf. Fig. 2). The simplest theories include only short-range interactions and even integrate out the pions. At extremely low energies, $M_{\rm high}$ is given by the inverse of the NN scattering lengths and one can formulate a perturbative EFT in

powers of the typical momentum k divided by $M_{\rm high}$. Since the NN scattering lengths are large this theory has a very limited range of applicability. It is therefore useful to construct another EFT with short-range interactions that resums the interactions generating the large scattering length. This so-called pionless EFT can be understood as an expansion around the limit of infinite scattering length or equivalently around threshold bound states. Its breakdown scale is set by one-pion exchange, $M_{\rm high}\sim M_\pi$, while $M_{\rm low}\sim 1/a\sim k$. For momenta k of the order of the pion mass M_π, pion exchange becomes a long-range interaction and has to be treated explicitly. This leads to the chiral EFT whose breakdown scale $M_{\rm high}$ is set by the chiral symmetry breaking scale Λ_χ and will be discussed in detail below.

The pionless theory relies only on the large scattering length and is independent of the mechanism responsible for it. It is very general and can be applied in systems ranging from ultracold atoms to nuclear and particle physics. It is therefore ideally suited to unravel universal phenomena driven by the large scattering length such as limit cycle physics (Braaten and Hammer, 2003; Mohr *et al.*, 2006) and the Efimov effect (Efimov, 1970). For recent reviews of applications to the physics of ultracold atoms, see Braaten and Hammer (2006, 2007). Here we consider applications of this theory in nuclear physics.

The pionless EFT is designed to reproduce the well known effective range expansion. The leading-order Lagrangian can be written as

$$\mathcal{L}=N^\dagger\left(i\partial_0+\frac{\vec{\nabla}^2}{2m}\right)N-C_0^t(N^T\tau_2\sigma_i\sigma_2N)^\dagger(N^T\tau_2\sigma_i\sigma_2N)$$
$$-C_0^s(N^T\sigma_2\tau_a\tau_2N)^\dagger(N^T\sigma_2\tau_a\tau_2N)+\cdots, \qquad (2.1)$$

where the dots represent higher-order terms suppressed by derivatives and more nucleon fields. The Pauli matrices σ_i (τ_a) operate in spin (isospin) space. The contact terms proportional to C_0^t (C_0^s) correspond to two-nucleon interactions in the ${}^3S_1$ (${}^1S_0$) NN channels. Their renormalized values are related to the corresponding large scattering lengths a_t and a_s in the spin-triplet and spin-singlet channels, respectively. The exact relation, of course, depends on the renormalization scheme. Various schemes can be used, such as a momentum cutoff or dimensional regularization. Convenient schemes that have a manifest power counting at the level of individual diagrams are dimensional regularization with power divergence subtraction (PDS), where poles in two and three spatial dimensions are subtracted (Kaplan *et al.*, 1998b), or momentum subtraction schemes as in Gegelia (1998). However, a simple momentum cutoff can be used as well.

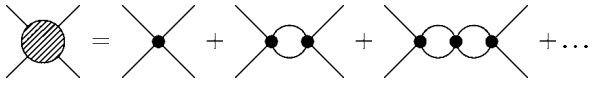

FIG. 5. The bubble diagrams with the contact interaction C_0^t or C_0^s contributing to the two-nucleon scattering amplitude.

Since the scattering lengths are set by the low-momentum scale $a\sim 1/M_{\rm low}$, the leading contact interactions have to be resummed to all orders (Kaplan *et al.*, 1998b; van Kolck, 1999). The nucleon-nucleon scattering amplitude in the ${}^3S_1$ (${}^1S_0$) channels is obtained by summing the so-called bubble diagrams with the C_0^t (C_0^s) interactions shown in Fig. 5. This summation gives the exact solution of the Lippmann-Schwinger equation for the C_0^t or C_0^s interactions. Higher-order derivative terms which are not shown explicitly in Eq. (2.1) reproduce higher-order terms in the effective range expansion. Since these terms are natural and their size is set by $M_{\rm high}$, their contribution at low energies is suppressed by powers of $M_{\rm low}/M_{\rm high}$ and can be treated in perturbation theory. The subleading correction is given by the effective range $r_0\sim 1/M_{\rm high}$ and the corresponding diagrams are illustrated in Fig. 6. The renormalized S-wave scattering amplitude to next-to-leading-order in a given channel then takes the form

$$T_2(k)=\frac{4\pi}{m}\frac{1}{-1/a-ik}\left[1-\frac{r_0k^2/2}{-1/a-ik}+\cdots\right], \qquad (2.2)$$

where k is the relative momentum of the nucleons and the dots indicate corrections of order $(M_{\rm low}/M_{\rm high})^2$ for typical momenta $k\sim M_{\rm low}$. The pionless EFT becomes very useful in the two-nucleon sector when external currents are considered and has been applied to a variety of electroweak processes. These calculations are reviewed in detail in Beane *et al.* (2000) and Bedaque and van Kolck (2002). More recently Christlmeier and Grießhammer calculated low-energy deuteron electrodisintegration in the framework of the pionless EFT (Christlmeier and Grießhammer, 2008). For the double-differential cross sections of the $d(e,e')$ reaction at $\theta=180°$ excellent agreement was found with a recent experiment at S-DALINAC (Ryezayeva *et al.*, 2008).[1] The double-differential cross section for an incident electron energy $E_0=27.8$ MeV and $\theta=180°$ is shown in Fig. 7. The data were used to precisely map the $M1$ response which governs the reaction $np\to d\gamma$ relevant to big-bang nucleosynthesis. Finally, the reaction $pp\to pp\pi^0$ near threshold was studied in Ando (2007).

We now proceed to the three-nucleon system. Here it is convenient to rewrite the theory using so-called "dimeron" auxiliary fields (Kaplan, 1997). We need two dimeron fields, one for each S-wave channel: (i) a field t_i with spin (isospin) 1 (0) representing two nucleons interacting in the ${}^3S_1$ channel (the deuteron) and (ii) a field s_a with spin (isospin) 0 (1) representing two nucleons interacting in the ${}^1S_0$ channel (Bedaque *et al.*, 2000),

[1]However, there is a disagreement between theory and data for the small longitudinal-transverse interference contribution σ_{LT} reported in von Neumann-Cosel *et al.* (2002) that is currently not understood (Christlmeier and Grießhammer, 2008).

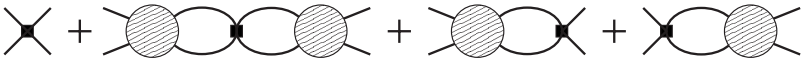

FIG. 6. Diagrams for the inclusion of higher-order contact interactions.

$$\mathcal{L} = N^\dagger\left(i\partial_t + \frac{\vec{\nabla}^2}{2m}\right)N - t_i^\dagger\left(i\partial_t - \frac{\vec{\nabla}^2}{4m} - \Delta_t\right)t_i$$
$$- s_a^\dagger\left(i\partial_t - \frac{\vec{\nabla}^2}{4m} - \Delta_s\right)s_a - \frac{g_t}{2}(t_i^\dagger N^T\tau_2\sigma_i\sigma_2 N + \text{H.c.})$$
$$- \frac{g_s}{2}(s_a^\dagger N^T\sigma_2\tau_a\tau_2 N + \text{H.c.}) - G_3 N^\dagger\Big\{g_t^2(t_i\sigma_i)^\dagger(t_j\sigma_j)$$
$$+ \frac{g_t g_s}{3}[(t_i\sigma_i)^\dagger(s_a\tau_a) + \text{H.c.}] + g_s^2(s_a\tau_a)^\dagger(s_b\tau_b)\Big\}N$$
$$+ \cdots, \tag{2.3}$$

where i,j are spin and a,b are isospin indices while g_t, g_s, Δ_t, Δ_s, and G_3 are the bare coupling constants. This Lagrangian goes beyond leading order and already includes the effective range terms. The coupling constants g_t, Δ_t, g_s, Δ_s are matched to the scattering lengths a_α and effective ranges $r_{0\alpha}$ in the two channels ($\alpha=s,t$). Alternatively, one can match to the position of the bound state or virtual state pole γ_α in the T matrix instead of the scattering length which often improves convergence (Phillips, Rupak, and Savage, 2000). The two quantities are related through

$$\gamma_\alpha = \frac{1}{r_{0\alpha}}(1 - \sqrt{1 - 2r_{0\alpha}/a_\alpha}), \tag{2.4}$$

where $\alpha=s,t$. The term proportional to G_3 constitutes a Wigner-SU(4) symmetric three-body interaction. It only contributes in the spin-doublet S-wave channel. When the auxiliary dimeron fields t_i and s_a are integrated out, an equivalent form containing only nucleon fields is obtained. At leading order when the effective range corrections are neglected, the spatial and time derivatives acting on the dimeron fields are omitted and the field is static. The coupling constants g_α and Δ_α, $\alpha=s,t$ are not independent then and only the combination g_α^2/Δ_α enters in observables. This combination can then be matched to the scattering length or pole position.

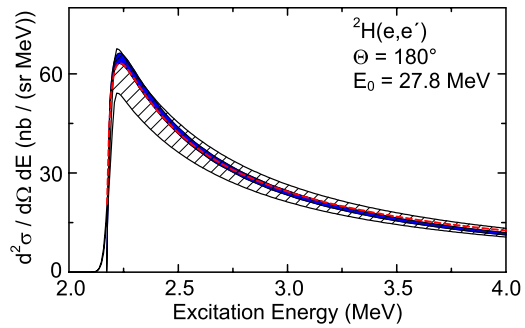

FIG. 7. (Color online) Double-differential cross sections of the ^{2}H(e,e') reaction with errors (hatched bands) extracted from the experiment. The gray bands and dashed lines are calculations in pionless EFT and a potential model (Ryezayeva *et al.*, 2008). Figure is courtesy of H. W. Grießhammer.

The simplest three-body process to consider is neutron-deuteron scattering below the breakup threshold. In order to focus on the main aspects of renormalization, we suppress all spin-isospin indices and complications from coupled channels in the three-nucleon problem. This corresponds to a system of three spinless bosons with large scattering length. If the scattering length is positive, the bosons form a two-body bound state analog to the deuteron which we call dimeron. The leading-order integral equation for boson-dimeron scattering is shown schematically in Fig. 8. For total orbital angular momentum $L=0$, it takes the following form:

$$T_3(k,p;E) = \frac{16}{3a}M(k,p;E) + \frac{4}{\pi}\int_0^\Lambda dq q^2 T_3(k,q;E)$$
$$\times \frac{M(q,p;E)}{-1/a + \sqrt{3q^2/4 - mE - i\epsilon}}, \tag{2.5}$$

where the inhomogeneous term reads

$$M(k,p;E) = \frac{1}{2kp}\ln\left(\frac{k^2+kp+p^2-mE}{k^2-kp+p^2-mE}\right) + \frac{H(\Lambda)}{\Lambda^2}. \tag{2.6}$$

Here H determines the strength of the three-body force $G_3(\Lambda)=2mH(\Lambda)/\Lambda^2$ which enters already at leading order and Λ is a UV cutoff introduced to regularize the integral equation. The magnitude of the incoming (outgoing) relative momenta is k (p) and $E=3k^2/(4m) - 1/(ma^2)$. The on-shell point corresponds to $k=p$ and the phase shift can be obtained via $k\cot\delta = 1/T_3(k,k;E)+ik$. For $H=0$ and $\Lambda\to\infty$, Eq. (2.5) reduces to the integral equation first derived by Skorniakov and Ter-Martirosian (1957). It is well known that this equation has no unique solution (Danilov, 1961). The regularized equation has a unique solution for any given (finite) value of the ultraviolet cutoff Λ, but the amplitude in the absence of the three-body force shows an oscillatory behavior on $\ln\Lambda$. Cutoff independence of the amplitude is restored by an appropriate "running" of $H(\Lambda)$ which turns out to be a limit cycle (Bedaque *et al.*, 1999a, 1999b)

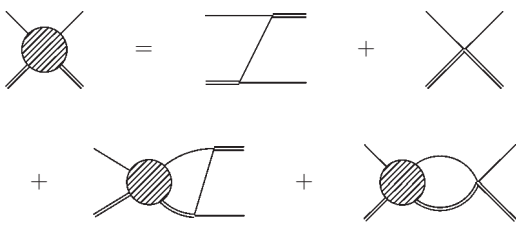

FIG. 8. The integral equation for the boson-dimeron scattering amplitude. The single (double) line indicates the boson (dimeron) propagator.

$$H(\Lambda) = \frac{\cos[s_0 \ln(\Lambda/\Lambda_*) + \arctan s_0]}{\cos[s_0 \ln(\Lambda/\Lambda_*) - \arctan s_0]}, \tag{2.7}$$

where Λ_* is a dimensionful three-body parameter generated by dimensional transmutation. Adjusting Λ_* to a single three-body observable allows us to determine all other low-energy properties of the three-body system. Note that the choice of the three-body parameter Λ_* is not unique and there are other definitions more directly related to experiment (Braaten and Hammer, 2006). Because $H(\Lambda)$ in Eq. (2.7) vanishes for certain values of the cutoff Λ it is possible to eliminate the explicit three-body force from the equations by working with a fixed cutoff that encodes the dependence on Λ_*. This justifies tuning the cutoff Λ in the STM equation to reproduce a three-body datum and using the same cutoff to calculate other observables as suggested by Kharchenko (1973). Equivalently, a subtraction can be performed in the integral equation (Hammer and Mehen, 2001; Afnan and Phillips, 2004). In any case, one three-body input parameter is needed for the calculation of observables. A comprehensive study of the range corrections to the three-boson spectrum was carried out in Platter *et al.* (2008). They showed that all range corrections vanish in the unitary limit due to the discrete scale invariance. While the corrections proportional to r_0/a vanish trivially, this includes also the corrections proportional to $\kappa_* r_0$, where $\kappa_* = \sqrt{mB_3^*}$ is the binding momentum of the Efimov state fixed by the chosen renormalization condition. Moreover, they have calculated the corrections to the Efimov spectrum for finite scattering length. The range corrections are negligible for the shallow states but become important for the deeper bound states.

The integral equations for the three-nucleon problem derived from the Lagrangian (2.3) are a generalization of Eq. (2.5). [For their explicit form and derivation, see, e.g., Bedaque, Rupak, *et al.* (2003).] For S-wave nucleon-deuteron scattering in the spin-quartet channel only the spin-1 dimeron field contributes. This integral equation has a unique solution for $\Lambda \to \infty$ and there is no three-body force in the first few orders. The spin-quartet scattering phases can therefore be predicted to high precision from two-body data (Bedaque and van Kolck 1998; Bedaque *et al.*, 1998). In the spin-doublet channel both dimeron fields as well as the three-body force in the Lagrangian (2.3) contribute (Bedaque *et al.*, 2000). This leads to a pair of coupled integral equations for the T matrix. Thus, one needs a new parameter which is not determined in the NN system in order to fix the (leading) low-energy behavior of the $3N$ system in this channel. The three-body parameter gives a natural explanation of universal correlations between different three-body observables such as the Phillips line, a correlation between the triton binding energy and the spin-doublet neutron-deuteron scattering length (Phillips, 1968). These correlations are purely driven by the large scattering length independent of the mechanism responsible for it. As a consequence, they occur in atomic systems such as ^{4}He atoms as well (Braaten and Hammer, 2006).

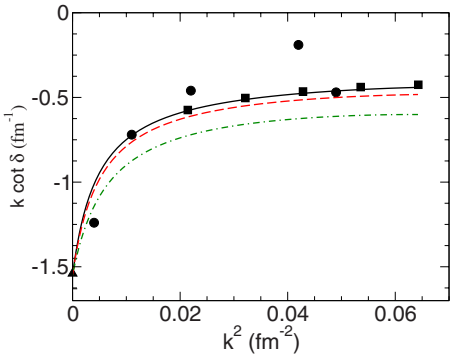

FIG. 9. (Color online) Phase shifts for neutron-deuteron scattering below the deuteron breakup at LO (dash-dotted line), NLO (dashed line), and next-to-next-to-leading order N^{2}LO (solid line). The filled squares and circles give the results of a phase shift analysis and a calculation using AV18 and the Urbana IX three-body force, respectively. Figure is courtesy of L. Platter.

Higher-order corrections to the amplitude including the ones due to NN effective range terms can be included perturbatively. This was first done at NLO for the scattering length and triton binding energy by Efimov (1991) and for the energy dependence of the phase shifts by Hammer and Mehen (2001). Bedaque, Rupak, *et al.* (2003) and Grießhammer (2004) demonstrated that it is convenient to iterate certain higher-order range terms in order to extend the calculation to N^{2}LO. Here a subleading three-body force was also included as required by dimensional analysis. More recently, Platter and Phillips showed using the subtractive renormalization that the leading three-body force is sufficient to achieve cutoff independence up to N^{2}LO in the expansion in $M_{\rm low}/M_{\rm high}$ (Platter and Phillips, 2006). Whether the subleading three-body force is required for consistent renormalization at N^{2}LO or not is still an open question. The results for the spin-doublet neutron-deuteron scattering phase shift at LO (Bedaque *et al.*, 2000), NLO (Hammer and Mehen, 2001), and N^{2}LO (Platter, 2006) are shown in Fig. 9. There is excellent agreement with the available phase shift analysis and a calculation using a phenomenological NN interaction. Whether there is a suppression of the subleading three-body force or simply a correlation between the leading and subleading contributions is not fully understood. The extension to $3N$ channels with higher orbital angular momentum is straightforward (Gabbiani *et al.*, 2000) and three-body forces do not appear until very high orders. A general counting scheme for three-body forces based on the asymptotic behavior of the solutions of the leading order STM equation was proposed in Grießhammer (2005). A complementary approach to the few-nucleon problem is given by the renormalization group where the power counting is determined from the scaling of operators under the renormalization group transformation (Wilson, 1983). This method leads to consistent results for the power counting (Barford and Birse, 2005; Ando and Birse, 2008; Birse, 2008). Universal low-energy proper-

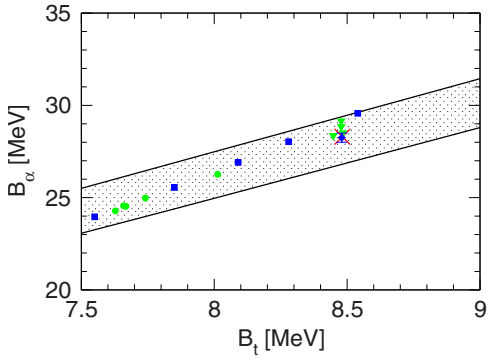

FIG. 10. (Color online) The Tjon line correlation as predicted by the pionless theory. The gray circles and triangles show various calculations using phenomenological potentials (Nogga *et al.*, 2000). The squares show the results of chiral EFT at NLO for different cutoffs, while the diamond gives the N^2LO result (Epelbaum *et al.*, 2001; Epelbaum, Nogga, Glöckle, Kamada, Meißner, and Witała, 2002). The cross shows the experimental point.

ties of few-body systems with short-range interactions and large two-body scattering length were reviewed in Braaten and Hammer (2006). [See also Efimov (1981) for an early work on this subject.] Three-body calculations with external currents are still in their infancy. However, a few exploratory calculations have been carried out. Universal properties of the triton charge form factor were investigated in Platter and Hammer (2006) and neutron-deuteron radiative capture was calculated in Sadeghi and Bayegan (2005) and Sadeghi *et al.* (2006). This opens the possibility to carry out accurate calculations of electroweak reactions at very low energies for astrophysical processes.

The pionless approach has also been extended to the four-body sector (Platter *et al.*, 2004, 2005). In order to be able to apply the Yakubovsky equations, an equivalent effective quantum mechanics formulation was used. The study of the cutoff dependence of the four-body binding energies revealed that no four-body parameter is required for renormalization at leading order. As a consequence, there are universal correlations in the four-body sector which are also driven by the large scattering length. The best known example is the Tjon line: a correlation between the triton and alpha particle binding energies B_t and B_α, respectively. Of course, higher-order corrections break the exact correlation and generate a band. Fig. 10, we show this band together with some calculations using phenomenological potentials (Nogga *et al.*, 2000) and a chiral EFT potential with explicit pions (Epelbaum *et al.*, 2001; Epelbaum, Nogga, Glöckle, Kamada, Meißner, and Witała, 2002). All calculations with interactions that give a large scattering length must lie within the band. Different short-distance physics and/or cutoff dependence should only move the results along the band. This can, for example be observed in the NLO results with the chiral potential indicated by the squares in Fig. 10 or in the few-body calculations with the low-momentum *NN* potential $V_{\text{low } k}$ carried out in Nogga *et al.* (2004). The $V_{\text{low } k}$ potential is obtained from phenomenological *NN* interactions by integrating out high-momentum modes above a cutoff Λ but leaving two-body observables (such as the large scattering lengths) unchanged. The results of few-body calculations with $V_{\text{low } k}$ are not independent of Λ but lie all close to the Tjon line (cf. Fig. 2 in Nogga *et al.*, 2004). The studies of the four-body system in the pionless theory were extended further in Hammer and Platter (2007). Here the dependence of the four-body bound state spectrum on the two-body scattering length was investigated in detail and summarized in a generalized Efimov plot for the four-body spectrum.

The question of whether a four-body parameter has to enter at leading order was reanalyzed in Yamashita *et al.* (2006). Within the renormalized zero-range model, they found a strong sensitivity of the deepest four-body energy to a four-body subtraction constant in their equations. They motivated this observation from a general model-space reduction in a realistic two-body interaction close to a Feshbach resonance. The results of Platter *et al.* (2004) for the ^{4}He tetramer that include a four-body parameter were also reproduced. Yamashita *et al.* concluded that a four-body parameter should generally enter at leading order. They argued that four-body systems of ^{4}He atoms and nucleons [where this sensitivity is absent (Nogga *et al.*, 2004; Platter *et al.*, 2004, 2005)] are special because repulsive interactions strongly reduce the probability to have four particles close together. However, the renormalization of the four-body problem was not explicitly verified in their calculation. Another drawback of their analysis is the focus on the deepest four-body state only. Therefore, their findings could be an artifact of their particular regularization scheme. Another recent study by von Stecher *et al.* (2009) confirmed the absence of a four-body parameter for shallow states, while some sensitivity was found for the deepest four-body state.

The pionless theory has also been extended to more than four particles using it within the no-core shell model approach. Here the expansion in a truncated harmonic oscillator basis is used as the ultraviolet regulator of the EFT. The effective interaction is determined directly in the model space, where an exact diagonalization in a complete many-body basis is performed. Stetcu, Barrett, and van Kolck (2007) calculated the 0^+ excited state of ^{4}He and the ^{6}Li ground state using the deuteron, triton, and alpha particle ground states as input. The first $(0^+;0)$ excited state in ^{4}He is calculated within 10% of the experimental value, while the ^{6}Li ground state comes out at about 70% of the experimental value in agreement with the 30% error expected for the leading-order approximation. These results are promising and should be improved if range corrections are included. Finally, the spectrum of trapped three- and four-fermion systems was calculated using the same method (Stetcu, Barrett, van Kolck, and Vary, 2007). In this case the harmonic potential is physical and not simply used as an ultraviolet regulator.

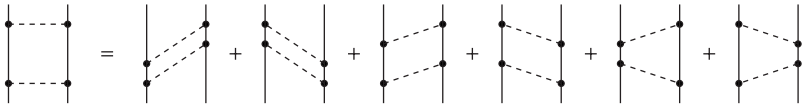

FIG. 11. Representation of the two-pion exchange Feynman diagram in terms of time-ordered graphs. Solid and dashed lines represent nucleons and pions, respectively.

B. Chiral EFT for few nucleons: Foundations

The extension of the previously discussed EFT with contact interactions to higher energies requires the inclusion of pions as explicit degrees of freedom. The interaction between pions and nucleons can be described in a systematic way using chiral perturbation theory. In contrast, the interaction between the nucleons is strong and leads to nonperturbative phenomena at low energy such as, e.g., shallow-lying bound states. This breakdown of perturbation theory can be linked to the fact that the interaction between the nucleons is not suppressed in the chiral limit contrary to the pion and pion-nucleon interactions. Moreover, an additional enhancement occurs for Feynman diagrams involving two and more nucleons due to the appearance of the so-called pinch singularities in the limit of the infinite nucleon mass. Although such infrared singularities disappear if one keeps the nucleon mass at its physical value, they do generate large enhancement factors which destroy the chiral power counting. This can be more easily understood utilizing the language of time-ordered perturbation theory. Consider, for example, the two-pion exchange box diagram shown in Fig. 11. While all intermediate states in the first two time-ordered graphs, often referred to as irreducible, involve at least one virtual pion and thus lead to energy denominators of the expected size, $E-E_i \sim M_\pi$, the remaining reducible diagrams involve an intermediate state with nucleons only which produces unnaturally small energy denominators of the order $E-E_i \sim M_\pi^2/m \ll M_\pi$. Clearly, the enhanced reducible time-ordered diagrams are nothing but the iterations of the Lippmann-Schwinger equation with the kernel which contains all possible irreducible diagrams and defines the nuclear Hamiltonian. It is free from infrared enhancement factors and can be worked out systematically using the machinery of chiral perturbation theory as suggested in Weinberg's seminal work (Weinberg, 1990, 1991).[2] This natural reduction to the quantum mechanical A-body problem is a welcome feature for practical calculations as it allows one to apply various existing few-body techniques such as, e.g., the Faddeev-Yakubovsky scheme, the no-core shell model, Green's function Monte Carlo method, and hyperspherical harmonics method. On the other hand, the framework offers a systematic and perturbative scheme to derive nuclear forces and current operators in harmony with the chiral symmetry of QCD. The expansion parameter is given by the ratio Q/Λ, where Q is the soft scale associated with the pion mass and/or external nucleon momenta and Λ is the pertinent hard scale. For a given connected irreducible diagram with N nucleons, L pion loops, and V_i vertices of type i, the power ν of the soft scale Q which determines its importance can be obtained based on naive dimensional analysis (i.e., assuming classical scaling dimensions for various operators in the effective Lagrangian),

$$\nu = -4 + 2N + 2L + \sum_i V_i \Delta_i, \quad \Delta_i = d_i + \tfrac{1}{2} n_i - 2. \quad (2.8)$$

Here n_i is the number of nucleon field operators and d_i is the number of derivatives and/or insertions of M_π. The spontaneously broken chiral symmetry of QCD guarantees $\Delta_i \geq 0$. As a consequence, the chiral dimension ν is bounded from below and only a finite number of diagrams contribute at a given order. In addition, Eq. (2.8) provides a natural explanation to the dominance of the two-nucleon interactions and the hierarchy of nuclear forces observed in nuclear physics. In particular, it implies that two-, three-, and four-nucleon forces start to contribute at orders $\nu=0$, 2, and 4, respectively. Note that as argued in Weinberg (1991), the nucleon mass m should be counted as $Q/m \sim Q^2/\Lambda^2$ (which implies that $m \gg \Lambda$) in order to maintain consistency with the appearance of shallow-lying bound states.[3] Note further that according to this counting rule the momentum scale associated with the real pion production is treated as the hard scale, $\sqrt{mM_\pi} \sim \Lambda$, and needs not be explicitly kept track of [see also Mondejar and Soto (2007) and Sec. II.E for a related discussion]. Clearly, such a framework is only applicable at energies well below the pion production threshold. We also emphasize that the validity of the naive dimensional scaling rules for few-nucleon contact operators has been questioned in Nogga *et al.* (2005) and Birse (2006). We return to this issue in Sec. II.C.

Before discussing the chiral expansion of the nuclear forces it is important to clarify the relation between the underlying chiral Lagrangian for pions and nucleons and

[2]An alternative framework based on the perturbative treatment of the pion exchange contributions has been introduced in Kaplan *et al.* (1998a, 1998b) [see Beane *et al.* (2000) and Bedaque and van Kolck (2002)]. As shown in Cohen and Hansen (1999a, 1999b) and Fleming *et al.* (2000), the perturbative inclusion of pions does not allow to significantly increase the applicability range of the theory as compared to pionless EFT. For yet different proposals to include pions in EFT for the nucleon-nucleon system see Lutz (2000), Oller (2008), and Soto and Tarrus (2008).

[3]This statement only applies for the power counting based on naive dimensional analysis.

the nuclear Hamiltonian we are finally interested in. The derivation of the nuclear potentials from field theory is an old and extensively studied problem in nuclear physics. Different approaches have been developed in the 1950s of the last century in the context of the so-called meson theory of nuclear forces [see, e.g., Phillips (1959)]. In the modern framework of chiral EFT, the most frequently used methods besides the already mentioned time-ordered perturbation theory are the ones based on S matrix and the unitary transformation. In the former scheme, the nuclear potential is defined through matching the amplitude to the iterated Lippmann-Schwinger equation (Kaiser *et al.*, 1997). In the second approach, the potential is obtained by applying an appropriately chosen unitary transformation to the underlying pion-nucleon Hamiltonian which eliminates the coupling between the purely nucleonic Fock space states and the ones which contain pions [see Epelbaum *et al.* (1998b) for more details]. We stress that both methods lead to *energy-independent* interactions as opposed by the ones obtained in time-ordered perturbation theory. The energy independence of the potential is a welcome feature which enables applications to three- and more-nucleon systems.

We are now in the position to discuss the structure of the nuclear force at lowest orders of the chiral expansion. The leading-order (LO) contribution results, according to Eq. (2.8), from two-nucleon tree diagrams constructed from the Lagrangian of lowest dimension $\Delta_i=0$, $\mathcal{L}^{(0)}$, which has the following form in the heavy-baryon formulation (Jenkins and Manohar, 1991; Bernard *et al.*, 1992):

$$\mathcal{L}_{\pi}^{(0)} = \frac{F^2}{4}\langle \nabla^\mu U \nabla_\mu U^\dagger + \chi_+ \rangle,$$

$$\mathcal{L}_{\pi N}^{(0)} = \bar{N}(iv\cdot D + \mathring{g}_A u\cdot S)N,$$

$$\mathcal{L}_{NN}^{(0)} = -\tfrac{1}{2}C_S(\bar{N}N)(\bar{N}N) + 2C_T(\bar{N}SN)\cdot(\bar{N}SN), \quad (2.9)$$

where N, v_μ, and $S_\mu \equiv (1/2)i\gamma_5\sigma_{\mu\nu}v^\nu$ denote the large component of the nucleon field, the nucleon four-velocity, and the covariant spin vector, respectively. The brackets $\langle\cdots\rangle$ denote traces in the flavor space while F and $\mathring{g}_A$ refer to the chiral-limit values of the pion decay and the nucleon axial vector coupling constants. The low-energy constants (LECs) C_S and C_T determine the strength of the leading NN short-range interaction. Further, the unitary 2×2 matrix $U(\boldsymbol{\pi})=u^2(\boldsymbol{\pi})$ in the flavor space collects the pion fields,

$$U(\boldsymbol{\pi}) = 1 + \frac{i}{F}\boldsymbol{\tau}\cdot\boldsymbol{\pi} - \frac{1}{2F^2}\boldsymbol{\pi}^2 + \mathcal{O}(\pi^3), \quad (2.10)$$

where τ_i denotes the isospin Pauli matrix. The covariant derivatives of the nucleon and pion fields are defined via $D_\mu=\partial_\mu+[u^\dagger,\partial_\mu u]/2$ and $u_\mu=i(u^\dagger\partial_\mu u - u\partial_\mu u^\dagger)$. The quantity $\chi_+=u^\dagger\chi u^\dagger+u\chi^\dagger u$ with $\chi=2B\mathcal{M}$ involves the explicit chiral symmetry breaking due to the finite light quark masses, $\mathcal{M}=\mathrm{diag}(m_u,m_d)$. The constant B is related to the value of the scalar quark condensate in the chiral limit, $\langle 0|\bar{u}u|0\rangle=-F^2B$, and relates the pion mass M_π to the quark mass m_q via $M_\pi^2=2Bm_q+\mathcal{O}(m_q^2)$. For more details on the notation and the complete expressions for the pion-nucleon Lagrangian including up to four derivatives/M_π insertions see Fettes *et al.* (2000). Expanding the effective Lagrangian in Eqs. (2.9) in powers of the pion fields one can easily verify that the only possible connected two-nucleon tree diagrams are the one-pion exchange and the contact one (see the first line in Fig. 12), yielding the following potential in the two-nucleon center-of-mass system (CMS):

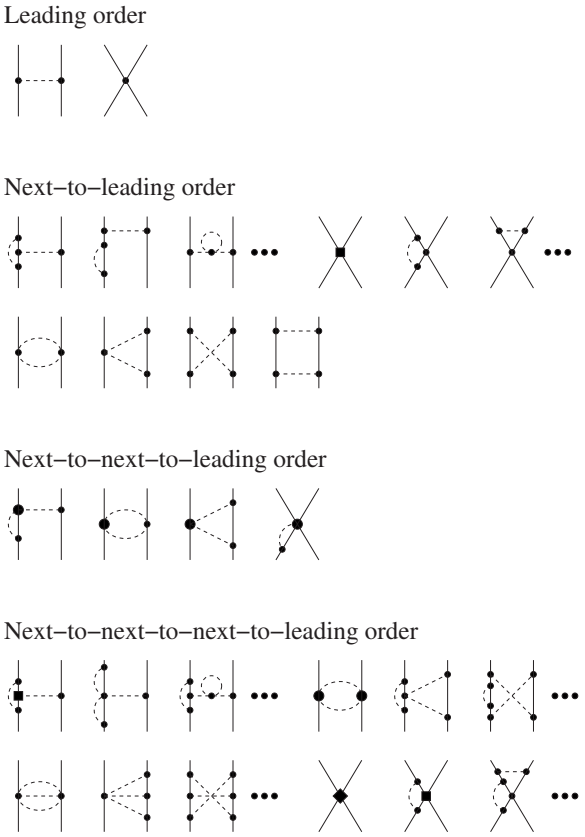

FIG. 12. Chiral expansion of the two-nucleon force up to next-to-next-to-next-to-leading order ($\mathrm{N^3LO}$). Solid dots, filled circles, squares, and diamonds denote vertices with $\Delta_i=0$, 1, 2, and 3, respectively. Only irreducible contributions of the diagrams are taken in to account as explained in the text.

$$V_{NN}^{(0)} = -\frac{g_A^2}{4F_\pi^2}\frac{\vec{\sigma}_1\cdot\vec{q}\,\vec{\sigma}_2\cdot\vec{q}}{\vec{q}^{\,2}+M_\pi^2}\boldsymbol{\tau}_1\cdot\boldsymbol{\tau}_2 + C_S + C_T\vec{\sigma}_1\cdot\vec{\sigma}_2, \quad (2.11)$$

where the superscript of V_{NN} denotes the chiral order ν, σ_i are the Pauli spin matrices, $\vec{q}=\vec{p}\,'-\vec{p}$ is the nucleon momentum transfer, and $\vec{p}$ ($\vec{p}\,'$) refers to initial (final) nucleon momenta in the CMS. Further, $F_\pi=92.4$ MeV and $g_A=1.267$ denote the pion decay and the nucleon axial coupling constants, respectively.

The first corrections to the LO result are suppressed by two powers of the low-momentum scale. The absence of the contributions at order $\nu=1$ can be traced back to

parity conservation which forbids $(\bar{N}N)(\bar{N}N)$ vertices with one spatial derivative and πNN vertices with two derivatives (i.e., $\Delta_i=1$). The next-to-leading-order (NLO) contributions to the 2NF therefore result from tree diagrams with one insertion of the $\Delta_i=2$ interaction and one-loop diagrams constructed from the lowest-order vertices (see Fig. 12). The relevant terms in the effective Lagrangian read (Gasser *et al.*, 1988)

$$\mathcal{L}_{\pi}^{(2)} = \frac{l_3}{16}\langle\chi_+\rangle^2 + \frac{l_4}{16}[2\langle\nabla_\mu U\nabla^\mu U^\dagger\rangle\langle\chi_+\rangle + 2\langle\chi^\dagger U\chi^\dagger U + \chi U^\dagger\chi U^\dagger\rangle - 4\langle\chi^\dagger\chi\rangle - \langle\chi_-\rangle^2] + \cdots,$$

$$\mathcal{L}_{\pi N}^{(2)} = \bar{N}\left(\frac{1}{2\mathring{m}}(v\cdot D)^2 - \frac{1}{2\mathring{m}}D\cdot D + d_{16}S\cdot u\langle\chi_+\rangle + id_{18}S^\mu[D_\mu,\chi_-] + \cdots\right)N,$$

$$\mathcal{L}_{NN}^{(2)} = -\tilde{C}_1\{(\bar{N}DN)\cdot(\bar{N}DN) + [(D\bar{N})N]\cdot[(D\bar{N})N]\} - 2(\tilde{C}_1+\tilde{C}_2)(\bar{N}DN)\cdot[(D\bar{N})N] - \tilde{C}_2(\bar{N}N)\cdot[(D^2\bar{N})N + \bar{N}D^2N] + \cdots, \quad (2.12)$$

where l_i, d_i, and $\tilde{C}_i$ denote further LECs and $\mathring{m}$ is the nucleon mass in the chiral limit. The ellipses in the pion and pion-nucleon Lagrangians refer to terms which do not contribute to the nuclear force at NLO. In the case of the nucleon-nucleon Lagrangian $\mathcal{L}_{NN}^{(2)}$ only a few terms are given explicitly. The complete reparametrization-invariant set of terms can be found in Epelbaum (2000). The NLO contributions to the two-nucleon potential have been first considered in Ordonez *et al.* (1994, 1996) utilizing the framework of time-ordered perturbation theory. The corresponding energy-independent expressions have been worked out in Friar and Coon (1994) using the method described in Friar (1977) and then rederived in Kaiser *et al.* (1997) using an S-matrix-based approach and, independently, in Epelbaum *et al.* (1998b, 2000) based on the method of unitary transformation. The one-pion (1π) exchange diagrams at NLO do not produce any new momentum dependence. Apart from renormalization of various LECs in Eq. (2.11), one obtains the leading contribution to the Goldberger-Treiman discrepancy (Epelbaum *et al.*, 2003),

$$\frac{g_{\pi N}}{m} = \frac{g_A}{F_\pi} - \frac{2M_\pi^2}{F_\pi}d_{18} + \cdots, \quad (2.13)$$

where the ellipsis refers to higher-order terms. Similarly, loop diagrams involving NN short-range interactions only lead to (M_π-dependent) shifts in the LO contact terms. The remaining contributions to the 2NF due to higher-order contact interactions and two-pion exchange have the form

$$V_{NN}^{(2)} = -\frac{\boldsymbol{\tau}_1\cdot\boldsymbol{\tau}_2}{384\pi^2F_\pi^4}L^{\tilde{\Lambda}}(q)\left(4M_\pi^2(5g_A^4-4g_A^2-1) + \vec{q}^{\,2}(23g_A^4-10g_A^2-1) + \frac{48g_A^4M_\pi^4}{4M_\pi^2+\vec{q}^{\,2}}\right) - \frac{3g_A^4}{64\pi^2F_\pi^4}L^{\tilde{\Lambda}}(q)(\vec{\sigma}_1\cdot\vec{q}\,\vec{\sigma}_2\cdot\vec{q} - \vec{\sigma}_1\cdot\vec{\sigma}_2\vec{q}^{\,2}) + C_1\vec{q}^{\,2} + C_2\vec{k}^{\,2} + (C_3\vec{q}^{\,2} + C_4\vec{k}^{\,2})\vec{\sigma}_1\cdot\vec{\sigma}_2 + iC_5\frac{1}{2}(\vec{\sigma}_1+\vec{\sigma}_2)\cdot\vec{q}\times\vec{k} + C_6\vec{q}\cdot\vec{\sigma}_1\vec{q}\cdot\vec{\sigma}_2 + C_7\vec{k}\cdot\vec{\sigma}_1\vec{k}\cdot\vec{\sigma}_2, \quad (2.14)$$

where $q\equiv|\vec{q}|$ and the LECs C_i can be written as linear combinations of $\tilde{C}_i$ in Eq. (2.12). The loop function $L^{\tilde{\Lambda}}(q)$ is defined in the spectral function regularization (Epelbaum *et al.*, 2004a, 2004b) as

$$L^{\tilde{\Lambda}}(q) = \theta(\tilde{\Lambda}-2M_\pi)\frac{\omega}{2q}\ln\frac{\tilde{\Lambda}^2\omega^2 + q^2s^2 + 2\tilde{\Lambda}q\omega s}{4M_\pi^2(\tilde{\Lambda}^2+q^2)}, \quad (2.15)$$

where we have introduced the following abbreviations: $\omega=\sqrt{4M_\pi^2+\vec{q}^{\,2}}$ and $s=\sqrt{\tilde{\Lambda}^2-4M_\pi^2}$. Here $\tilde{\Lambda}$ denotes the ultraviolet cutoff in the mass spectrum of the two-pion-exchange potential. If dimensional regularization (DR) is employed, the expression for the loop function simplifies to

$$L(q) = \lim_{\tilde{\Lambda}\to\infty} L^{\tilde{\Lambda}}(q) = \frac{\omega}{q}\ln\frac{\omega+q}{2M_\pi}. \quad (2.16)$$

In addition to the two-nucleon contributions, at NLO one also needs to consider three-nucleon diagrams shown in the first line of Fig. 13. The first diagram does not involve reducible topologies and, therefore, can be dealt with using the Feynman graph technique. It is then easy to verify that its contribution is shifted to higher orders due to the additional suppression by the factor of $1/m$ caused by the appearance of time derivative at the leading-order $\pi\pi\bar{N}N$ vertex, the so-called Weinberg-Tomozawa vertex. The two remaining diagrams have been considered in Weinberg (1990, 1991) and later in Ordonez and van Kolck (1992) using the energy-dependent formulation based on time-ordered perturbation theory. In this approach, it was shown that the resulting 3NF cancels exactly (at the order one is working) against the recoil correction to the 2NF when the latter is iterated in the dynamical equation. In energy-independent approaches—such as, e.g., the method of unitary transformation—which are employed in most of the existing few-nucleon calculations one observes that the irreducible contributions from the last two diagrams in the first line of Fig. 13 are suppressed by the factor $1/m$ and thus occur at higher orders (Epelbaum, 2000)

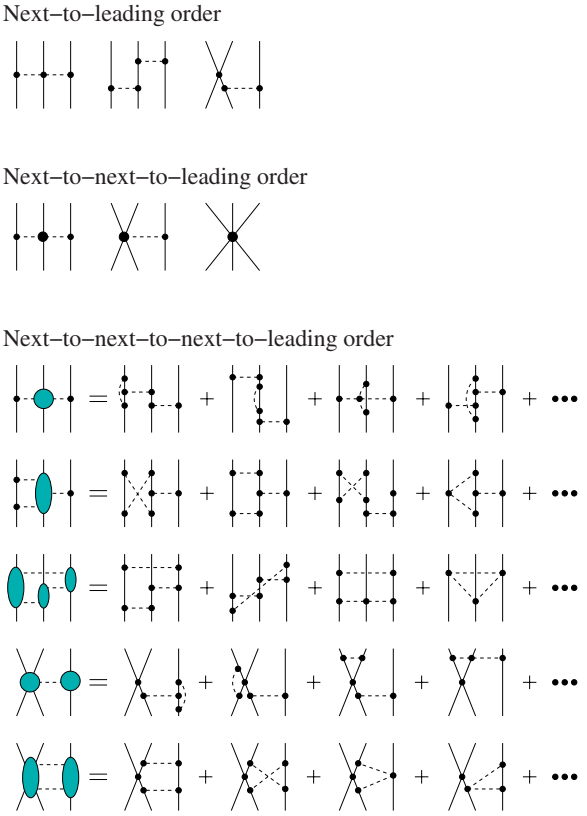

FIG. 13. (Color online) Chiral expansion of the three-nucleon force up to N^{3}LO. Diagrams in the first line (NLO) yield vanishing contributions to the 3NF if one uses energy-independent formulations as explained in the text. The five topologies at N^{3}LO involve the two-pion exchange, one-pion-two-pion-exchange, ring, contact-one-pion exchange, and contact-two-pion-exchange diagrams in order. Shaded blobs represent the corresponding amplitudes. For remaining notation see Fig. 12.

[see also Coon and Friar (1986) and Eden and Gari (1996)]. Consequently, there is no 3NF at NLO in the chiral expansion.

The contributions at N^{2}LO involve one-loop diagrams with one insertion of the subleading vertices of dimension $\Delta_i=1$ (see Fig. 12). The corresponding Lagrangians read

$$\mathcal{L}_{\pi N}^{(1)} = \bar{N}\{c_1\langle\chi_+\rangle + c_2(v\cdot u)^2 + c_3 u\cdot u + c_4[S^\mu,S^\nu]u_\mu u_\nu + c_5\langle\hat{\chi}_+\rangle\}N,$$

$$\mathcal{L}_{\pi NN}^{(1)} = \frac{D}{2}(\bar{N}N)(\bar{N}S\cdot uN), \tag{2.17}$$

where $\hat{\chi}_+ \equiv \chi_+ - \langle\chi_+\rangle/2$ and D, c_i are the LECs. The 1π-exchange loop diagram again only lead to renormalization of the corresponding LECs. Similarly, the contribution from the last diagram which involves the two-nucleon contact interaction can be absorbed into a redefinition of the LECs $C_{S,T}$ and C_i in Eqs. (2.11) and (2.14) (provided one is not interested in the quark mass dependence of the nuclear force). Further, the football diagram yields vanishing contribution due to the anti-symmetric (with respect to pion isospin quantum numbers) nature of the Weinberg-Tomozawa vertex. Thus, the only nonvanishing contribution at this order results from the 2π-exchange triangle diagram,

$$V_{NN}^{(3)} = -\frac{3g_A^2}{16\pi F_\pi^4}[2M_\pi^2(2c_1-c_3)-c_3\vec{q}^2] \times(2M_\pi^2+\vec{q}^2)A^{\tilde{\Lambda}}(q) - \frac{g_A^2 c_4}{32\pi F_\pi^4}\boldsymbol{\tau}_1\cdot\boldsymbol{\tau}_2(4M_\pi^2 + q^2)A^{\tilde{\Lambda}}(q)(\vec{\sigma}_1\cdot\vec{q}\,\vec{\sigma}_2\cdot\vec{q}-\vec{q}^2\vec{\sigma}_1\cdot\vec{\sigma}_2), \tag{2.18}$$

where the loop function $A^{\tilde{\Lambda}}(q)$ is given by

$$A^{\tilde{\Lambda}}(q) = \theta(\tilde{\Lambda}-2M_\pi)\frac{1}{2q}\arctan\frac{q(\tilde{\Lambda}-2M_\pi)}{q^2+2\tilde{\Lambda}M_\pi}. \tag{2.19}$$

In DR, the expression for $A(q)$ takes the following simple form:

$$A(q) \equiv \lim_{\tilde{\Lambda}\to\infty} A^{\tilde{\Lambda}}(q) = \frac{1}{2q}\arctan\frac{q}{2M_\pi}. \tag{2.20}$$

Notice that the triangle diagram also generates short-range contributions which may be absorbed into redefinition of contact interactions. The isoscalar central contribution proportional to the LEC c_3 is attractive and very strong. It is by far the strongest two-pion exchange contribution and reaches a few tens of MeV (depending on the choice of regularization) at internucleon distances of the order $r\sim M_\pi^{-1}$. The origin of the unnaturally strong subleading 2π-exchange contributions can be traced back to the (numerically) large values of the LECs $c_{3,4}$ and is well understood in terms of resonance exchange related to Δ excitation (Bernard *et al.*, 1997). We return to this issue in Sec. II.D where the chiral EFT formulation with explicit Δ degrees of freedom will be discussed. The central 2π-exchange potential was also calculated in Robilotta (2001) using the infrared-regularized version of chiral EFT which enables one to sum up a certain class of relativistic corrections (Becher and Leutwyler, 1999). He found that the results in the heavy-baryon limit overestimate the ones obtained using infrared regularization by about 25% [see also Epelbaum (2006a) for a related discussion]. Last but not least, the chiral 2π-exchange potential up to N^{2}LO has been tested in the Nijmegen partial wave analysis (PWA) of both proton-proton and neutron-proton data (Rentmeester *et al.*, 1999, 2003) where also an attempt has been done to determine the values of the LECs $c_{3,4}$. As demonstrated in these studies, the representation of the (strong) long-range interaction based on the combination of the 1π- and the chiral 2π-exchange potentials rather than on the pure 1π-exchange potential allows one to considerably reduce the number of phenomenological parameters entering the energy-dependent boundary conditions which are needed to parametrize the missing short- and medium-range interactions. Also the extracted values of the LECs $c_{3,4}$ agree reasonably well with various determinations in the pion-nucleon

system. These studies provide confirmation of the important role of the 2π-exchange potential in nucleon-nucleon scattering observables [see, however, Entem and Machleidt (2003b) for a criticism]. For a similar work utilizing the distorted-wave methods see Birse and McGovern (2004) and Birse (2007).

The first nonvanishing contributions to the 3NF also show up at N^{2}LO and arise from tree diagrams shown in Fig. 13 which involve a single insertion of the subleading vertices $\mathcal{L}^{(1)}$ in Eq. (2.17) and

$$\mathcal{L}^{(1)}_{NNN} = -\frac{E}{2}(\bar{N}N)(\bar{N}\boldsymbol{\tau}N)\cdot(\bar{N}\boldsymbol{\tau}N), \tag{2.21}$$

where E is a low-energy constant. The corresponding 3NF expression reads

$$V^{(3)}_{3N} = \frac{g_A^2}{8F_\pi^4}\frac{\vec{\sigma}_1\cdot\vec{q}_1\vec{\sigma}_3\cdot\vec{q}_3}{[q_1^2+M_\pi^2][q_3^2+M_\pi^2]}[\boldsymbol{\tau}_1\cdot\boldsymbol{\tau}_3(-4c_1M_\pi^2 + 2c_3\vec{q}_1\cdot\vec{q}_3) + c_4\boldsymbol{\tau}_1\times\boldsymbol{\tau}_3\cdot\boldsymbol{\tau}_2\vec{q}_1\times\vec{q}_3\cdot\vec{\sigma}_2] - \frac{g_AD}{8F_\pi^2}\frac{\vec{\sigma}_3\cdot\vec{q}_3}{q_3^2+M_\pi^2}\boldsymbol{\tau}_1\cdot\boldsymbol{\tau}_3\vec{\sigma}_1\cdot\vec{q}_3 + \frac{1}{2}E\boldsymbol{\tau}_2\cdot\boldsymbol{\tau}_3, \tag{2.22}$$

where the subscripts refer to the nucleon labels and $\vec{q}_i = \vec{p}_i' - \vec{p}_i$, with $\vec{p}_i'$ and $\vec{p}_i$ the final and initial momenta of the nucleon i. The expressions in Eq. (2.22) correspond to a particular choice of nucleon labels. The full expression for the 3NF results by taking into account all possible permutations of the nucleons (for three nucleons there are altogether six permutations), i.e.,

$$V^{\text{full}}_{3N} = V_{3N} + \text{all permutations}. \tag{2.23}$$

We further emphasize that the expressions for the 3NF given in Ordonez and van Kolck (1992) and van Kolck (1994) contain one redundant 1π-exchange and two redundant contact interactions. As shown in Epelbaum, Nogga, Glöckle, Kamada, Meißner, and Witała (2002), only one independent linear combination contributes in each case if one considers matrix elements between antisymmetrized few-nucleon states [see also Bedaque *et al.* (2000) for a related discussion].

We now turn to N^{3}LO and discuss first the corrections to the 2NF. As follows from Eq. (2.8), one has to account for contributions from tree diagrams with one insertion from $\mathcal{L}^{(4)}$ or two insertions from $\mathcal{L}^{(2)}$, one-loop diagrams with one insertion from $\mathcal{L}^{(2)}$ or two insertions from $\mathcal{L}^{(1)}$ as well as two-loop graphs constructed from the lowest-order vertices (see Fig. 12). Apart from renormalization of various LECs, the 1π-exchange potential receives at this order [in the scheme based on the counting $m \sim \mathcal{O}(\Lambda^2/M_\pi)$] the first relativistic corrections proportional to m^{-2}. These are scheme-dependent and have to be chosen consistently with the $1/m$ corrections to the 2π-exchange potential and the relativistic extension of the dynamical equation [see Friar (1999) for a comprehensive discussion.] The two-pion exchange contributions at N^{3}LO were worked out in Kaiser (2001a) based on the one-loop representation of the πN scattering amplitude. We refrain from giving here the rather involved expressions for the subsubleading 2π-exchange potential and refer to the original work (Kaiser, 2001a) where the results are given in terms of the corresponding spectral functions. For certain classes of contributions, the integrals over the two-pion exchange spectrum could be performed analytically and are given in Entem and Machleidt (2002). Notice further that the subleading (i.e., the ones proportional to m^{-2}) relativistic corrections of the 2π-exchange range have also been worked out in Kaiser (2002a). In the counting scheme with $m \sim \mathcal{O}(\Lambda^2/M_\pi)$, these terms, however, would only appear at next-to-next-to-next-to-next-to-next leading order (N^{5}LO). It should also be emphasized that the N^{3}LO contributions to the 2π-exchange potential were worked out in the covariant version of chiral EFT [more precisely, using the formulation in Becher and Leutwyler (1999)] by Higa *et al.* (Higa and Robilotta 2003; Higa *et al.*, 2004, 2005).

3π-exchange contributions also appear at this order in the chiral expansion and have been worked out in Kaiser (2000a, 2000b) [see also Pupin and Robilotta (1999) for a related work]. The resulting potentials turn out to be rather weak. For example, the strongest contribution is of the isoscalar spin-spin type (i.e., proportional to $\vec{\sigma}_1\cdot\vec{\sigma}_2$) and about ten times weaker than the corresponding 2π-exchange contribution at the same order at relative distances $r \sim M_\pi^{-1}$. It should, however, be emphasized that the subleading 3π-exchange contributions at next-to-next-to-next-to-next leading order (N^{4}LO) are larger in size (Kaiser, 2001b) which, again, can be traced back to the large values of the LECs c_i. Finally, the last type of the 2NF corrections at this order results from diagrams involving contact interactions. The most general polynomial (in momenta) representation of the short-range part of the potential involves, apart from the two leading and seven subleading terms given in Eqs. (2.11) and (2.14), 15 new contact interactions (in the isospin invariant sector) yielding in total 24 LECs to be determined from nucleon-nucleon data.

The 3NF contributions at N^{3}LO feed into five different topologies (see Fig. 13) and are currently being worked out. Presently, the expressions for the first three topologies which do not involve short-range contact interactions are available. The one-loop corrections to the 2π-exchange diagrams can, to a large extent, be accounted for by a finite shift $c_i \to \bar{c}_i = c_i + \delta c_i$ of the LECs c_i (Ishikawa and Robilotta, 2007; Bernard *et al.*, 2008),

$$\delta c_1 = -g_A^2 M_\pi/64\pi F_\pi^2, \quad \delta c_3 = -\delta c_4 = g_A^4 M_\pi/16\pi F_\pi^2. \tag{2.24}$$

Numerically, these corrections are of the order of 20% of the corresponding LECs and are consistent with the difference in values of c_i between the order-Q^2 and Q^3

determinations from the pion-nucleon system [see Bernard *et al.* (1995, 1997), Fettes *et al.* (1998), and Buettiker and Meißner (2000)]. The only 2π-exchange contribution that cannot be cast into redefinition of the LECs c_i arises from the diagram which involves pions interacting in flight [see Ishikawa and Robilotta (2007) and Bernard *et al.* (2008) for the explicit expression]. We also emphasize that there are no 2π-exchange contributions from tree diagrams with one insertion from $\mathcal{L}_{\pi N}^{(2)}$ in Eq. (2.12) (except for the relativistic corrections). This is because diagrams involving subleading πNN interaction do not yield any irreducible contributions while the ones with the $\pi\pi NN$ vertices of dimension $\nu=2$ involve at least one time derivative and are, therefore, suppressed by a factor of $1/m$. This observation is consistent with the absence of logarithmic ultraviolet divergences in the loop diagrams. In this context, it should be emphasized that the requirement of renormalizability at N^{3}LO (and, presumably, also at higher orders) was found to impose strong constraints on the unitary ambiguity in the form of the resulting nuclear potentials. This issue is discussed in Epelbaum (2007) and may remind one of the recent findings in the context of large-N_c QCD (Belitsky and Cohen, 2002; Cohen, 2002; Cohen and Gelman, 2002) where it was shown that the multiple-meson-exchange potential derived in the energy-dependent formulation is inconsistent with large-N_c counting rules. The consistency could be maintained using a different (but equivalent up to the considered order) form of the potential based on the energy-independent formalism [see Cohen (2002) for more details]. The contributions from the two-pion-one-pion exchange and ring diagrams are given explicitly in Bernard *et al.* (2008) where expressions are shown in both momentum and coordinate spaces. Especially in the case of ring diagrams where loop integrals involve two independent external momenta and, therefore, yield rather involved expressions in momentum space, it is advantageous to switch to coordinate space where a much more compact representation emerges. Notice further that ring diagrams were already studied in the pioneering work of Fujita *et al.* (1962). The calculation of the last two topologies involving the leading contact interactions is in progress. Last but not least, one should also take into account the leading relativistic $1/m$ corrections to the NLO three-nucleon diagrams (see the first line in Fig. 13). Again, these contributions are scheme dependent and should be chosen consistently with the relativistic corrections to the 2NF and the form of the dynamical equation. The $1/m$ corrections to the 2π-exchange 3NF have already been worked out long time ago by Coon and Friar and are given in the most general form in Coon and Friar (1986). Notice further that at this order one needs to account for the dependence of the 2NF on the total momentum of the NN system (effects due to drift of the CMS of a two-body subsystem). Such boosted NN operators may, in fact, also be viewed as $3N$ operators. In the context of chiral EFT, this kind of corrections is discussed in Robilotta (2006).

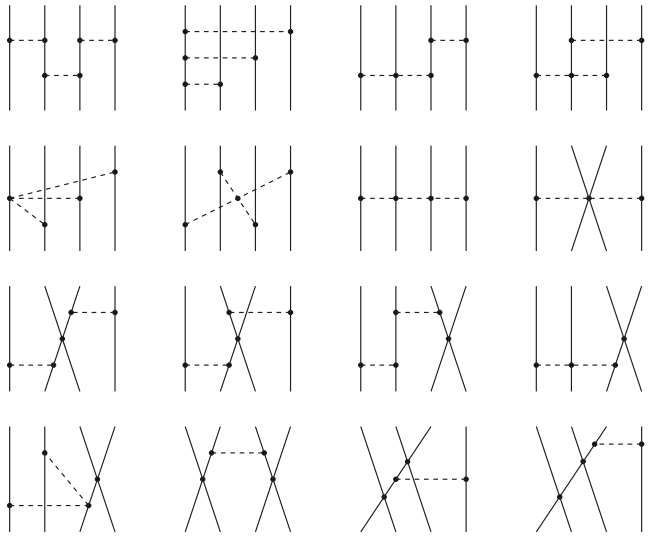

FIG. 14. Diagrams contributing to the four-nucleon force at N^{2}LO. For notation see Fig. 12.

The last type of N^{3}LO contributions arises from four-nucleon tree diagrams constructed from the lowest-order vertices (see Fig. 14), which have been evaluated recently using the method of unitary transformation (Epelbaum, 2006b, 2007).

Notice that the first two diagrams in the second line were already discussed long ago [see, e.g., McManus and Riska (1980) and Robilotta (1985)]. Furthermore, it should be emphasized that disconnected diagrams calculated, e.g., in van Kolck (1994), using time-ordered perturbation theory do not contribute to the nuclear force in the method of unitary transformation. It has been conjectured by Robilotta (1985) that $4N$ diagrams which involve reducible topologies do not generate irreducible pieces in the amplitude and thus lead to vanishing 4NFs. While this is indeed the case for the leading $3N$ diagrams at NLO, it is explicitly shown in Epelbaum (2006b, 2007) that many of the reducible-like diagrams in Fig. 14 do generate nonvanishing 4NFs which are not suppressed by inverse powers of the nucleon mass. As a representative example, we give here the g_A^6 contribution which results entirely from the first diagram in Fig. 14 (the second graph appears to be truly reducible and does not produce any contribution to the 4NF),

$$V_{4N}^{(4)} = -\frac{2g_A^6}{(2F_\pi)^6}\frac{\vec{\sigma}_1\cdot\vec{q}_1\vec{\sigma}_4\cdot\vec{q}_4}{[\vec{q}_1^{\,2}+M_\pi^2][\vec{q}_{12}^{\,2}+M_\pi^2]^2[\vec{q}_4^{\,2}+M_\pi^2]}[(\boldsymbol{\tau}_1\cdot\boldsymbol{\tau}_4\boldsymbol{\tau}_2\cdot\boldsymbol{\tau}_3-\boldsymbol{\tau}_1\cdot\boldsymbol{\tau}_3\boldsymbol{\tau}_2\cdot\boldsymbol{\tau}_4)\vec{q}_1\cdot\vec{q}_{12}\vec{q}_4\cdot\vec{q}_{12}+\boldsymbol{\tau}_1\times\boldsymbol{\tau}_2\cdot\boldsymbol{\tau}_4\vec{q}_1\cdot\vec{q}_{12}\vec{q}_{12}$$
$$\times\vec{q}_4\cdot\vec{\sigma}_3+\boldsymbol{\tau}_1\times\boldsymbol{\tau}_3\cdot\boldsymbol{\tau}_4\vec{q}_4\cdot\vec{q}_{12}\vec{q}_1\times\vec{q}_{12}\cdot\vec{\sigma}_2+\boldsymbol{\tau}_1\cdot\boldsymbol{\tau}_4\vec{q}_{12}\times\vec{q}_1\cdot\vec{\sigma}_2\vec{q}_{12}\times\vec{q}_4\cdot\vec{\sigma}_3]+\text{all permutations}, \tag{2.25}$$

where $\vec{q}_{12}=\vec{q}_1+\vec{q}_2=-\vec{q}_3-\vec{q}_4=-\vec{q}_{34}$ is the momentum transfer between the nucleon pairs 12 and 34. The complete expression for the leading 4NF in both momentum and coordinate space can be found in Epelbaum (2007). A rough estimation of the 4NF contributions to, e.g., the α-particle binding energy is provided by the strength of the corresponding r-space potentials expressed in terms of dimensionless variables $r_{ij}M_\pi$. One then finds, e.g., for the g_A^6 terms $g_A^6 M_\pi^7(16\pi F_\pi^2)^{-3}\sim 50$ keV. This agrees qualitatively with a more accurate numerical estimation carried out in Rozpedzik *et al.* (2006) which, however, still involved severe approximations to simplify the calculations.

So far we only discussed isospin-invariant contributions to the nuclear forces. It is well established that nuclear forces are charge dependent [for reviews see, e.g., Miller *et al.* (1990) and Miller and Van Oers (1994)]. For example, in the nucleon-nucleon $^1S_0$ channel one has for the scattering lengths a and the effective ranges r (after removing electromagnetic effects),

$$a_{\rm CIB}=\tfrac{1}{2}(a_{nn}+a_{pp})-a_{np}=5.64\pm 0.40\ \text{fm},$$

$$r_{\rm CIB}=\tfrac{1}{2}(r_{nn}+r_{pp})-r_{np}=0.03\pm 0.06\ \text{fm}. \tag{2.26}$$

These numbers for charge independence breaking (CIB) are taken from the recent compilation of Machleidt (2001). The charge independence breaking in the scattering lengths is large, of the order of 25%, since $a_{np}=-23.740\pm 0.020$ fm. Of course, it is magnified at threshold due to kinematic factors (as witnessed by the disappearance of the effect in the effective range). In addition, there are charge symmetry breaking (CSB) effects leading to different values for the pp and nn phase shifts and threshold parameters,

$$a_{\rm CSB}=a_{pp}-a_{nn}=1.6\pm 0.6\ \text{fm},$$

$$r_{\rm CSB}=r_{pp}-r_{nn}=0.10\pm 0.12\ \text{fm}. \tag{2.27}$$

Combining these numbers gives as central values $a_{nn}=-18.9$ fm and $a_{pp}=-17.3$ fm. Notice that this value for a_{nn} is in agreement with the recent experimental determinations from the reaction $\pi^- d\to nn\gamma$, $a_{nn}=-18.5\pm 0.5$ fm (Howell *et al.*, 1998), and the kinematically complete deuteron breakup reaction $nd\to nnp$ at $E_{\rm lab}=13$ MeV, $a_{nn}=-18.7\pm 0.6$ fm (Gonzalez Trotter *et al.*, 1999). However, another recent experiment also based on the deuteron breakup reaction at $E_{\rm lab}=25.2$ MeV yielded a considerably smaller value, $a_{nn}=-16.3\pm 0.4$ fm (Huhn *et al.*, 2000). For a review of indirect methods to measure the $^1S_0$ nn scattering length and the current experimental status for this observable see Howell (2008).

Within the standard model, isospin violation has its origin in the different masses of the up and down quarks and the electromagnetic interactions. Chiral EFT is well suited to explore the consequences of these two effects for low-energy dynamics of few- and many-nucleon systems. Consider first the strong isospin-violating effects. The QCD quark mass term can be written in the two-flavor case as

$$\mathcal{L}_{\rm mass}^{\rm QCD}=-\tfrac{1}{2}\bar{q}(m_u+m_d)(1+\epsilon\tau^3)q, \tag{2.28}$$

where the superscript of the Pauli isospin matrix denotes the corresponding Cartesian component and

$$\epsilon\equiv\frac{m_u-m_d}{m_u+m_d}\sim-\frac{1}{3}. \tag{2.29}$$

Here the numerical estimation corresponds to the modified subtraction $\overline{\rm MS}$ scheme at a renormalization scale of 1 GeV (Leutwyler, 1996). In Eq. (2.28), the isoscalar term breaks chiral but preserves isospin symmetry. It is responsible, e.g., for the nonvanishing pion mass $M^2=(m_u+m_d)B$, $M_\pi^2=M^2+\mathcal{O}(m_{u,d}^2)$ and generates a string of chiral-symmetry-breaking terms in the effective hadronic Lagrangian proportional to M^{2n} with $n=1,2,\ldots$. The isovector term gives rise to the strong isospin breaking and leads to hadronic effective interactions $\propto(\epsilon M^2)^n$. Consequently, the typical size of the strong isospin violation in hadronic observables is given by $\epsilon M_\pi^2/\Lambda^2\sim 1\%$ if one takes $\Lambda=M_\rho$ (this, however, does not apply, e.g., to the pion masses). The leading and subleading strong isospin-violating contributions are already incorporated in the Lagrangians $\mathcal{L}_\pi^{(2)}$ and $\mathcal{L}_{\pi N}^{(1,2)}$ in Eqs. (2.9), (2.12), and (2.17) and correspond to terms involving χ, $\chi_\pm$. Notice that the strong isospin violation is additionally suppressed in the meson sector (due to G parity). In particular, the charged-to-neutral pion mass difference is almost entirely of electromagnetic origin. Electromagnetic terms in the effective Lagrangian resulting from exchange of hard virtual photons can be generated using the method of external sources (Gasser and Leutwyler, 1984). All such terms are proportional to positive powers of the nucleon charge matrix $Q=e(1+\tau^3)/2$, where e denotes the electric charge. In addition, soft photons have to be included explicitly. For more details on the inclusion of virtual photons in chiral EFT see Urech (1995), Neufeld and Rupertsberger (1996), Meißner *et al.* (1997), Knecht and Urech (1998), Meißner and Steininger (1998), Müller and Meißner (1999), and Gasser *et al.* (2002).

To explore isospin-breaking (IB) effects in nuclear forces and few-nucleon observables it is useful to relate the corresponding small parameters ϵ and e to the chiral expansion parameter M_π/Λ. Clearly, this can be done in various ways. For example, in Walzl *et al.* (2001), Epelbaum and Meißner (2005), and Epelbaum, Meißner, and Palomar (2005) the following rules have been adopted:

$$\epsilon\sim e\sim\frac{M_\pi}{\Lambda},\quad \frac{e^2}{(4\pi)^2}\sim\frac{M_\pi^4}{\Lambda^4}. \tag{2.30}$$

Note that the factor $1/(4\pi)^2$ arises from the integration of hard virtual photons. Similar counting rules were also used in van Kolck (1993), van Kolck *et al.* (1996), Friar and van Kolck (1999), and Friar *et al.* (2003, 2004, 2005). Notice, however, that in the meson and single-baryon

sectors one usually counts $\epsilon \sim 1$ but $e \sim M_\pi/\Lambda$. Utilizing the counting rules in Eq. (2.30), the leading and subleading IB contributions from the hard virtual photons have the forms (Müller and Meißner, 1999)

$$\mathcal{L}^{(2)}_{\pi,\mathrm{em}} = C\langle QUQU^\dagger\rangle,$$

$$\mathcal{L}^{(3)}_{\pi N,\mathrm{em}} = F^2\bar{N}(f_1\langle\tilde{Q}_+^2 - \tilde{Q}_-^2\rangle + f_2\langle Q_+\rangle\tilde{Q}_+ + f_3\langle\tilde{Q}_+^2 + \tilde{Q}_-^2\rangle)N, \tag{2.31}$$

where $\tilde{Q}_\pm \equiv Q_\pm - 1/2\langle Q_\pm\rangle$ and f_i refer to the corresponding LECs. The leading Lagrangians for the strong and electromagnetic IB contact interactions $\mathcal{L}^{(3)}_{NN,\mathrm{str}}$ and $\mathcal{L}^{(4)}_{NN,\mathrm{em}}$ are given explicitly in Walzl *et al.* (2001).

We first discuss IB contributions to the pion and nucleon masses. As already pointed out, the leading contribution to the charged-to-neutral pion mass difference is entirely of electromagnetic origin,

$$\delta M_\pi^2 \equiv M_{\pi^\pm}^2 - M_{\pi^0}^2 \simeq \frac{2}{F^2}e^2C. \tag{2.32}$$

The experimentally known pion mass difference $M_{\pi^\pm} - M_{\pi^0} = 4.6$ MeV allows us to fix the value of the LEC C, $C = 5.9\times10^{-5}$ GeV^4. Notice that the natural scale for this LEC is $F_\pi^2\Lambda^2/(4\pi)^2 \sim 3\times10^{-5}$ GeV^4 if one adopts $\Lambda \sim M_\rho$. Writing the nucleon mass m as

$$m \equiv \mathrm{diag}(m_p, m_n) = m + \tfrac{1}{2}\delta m\,\tau^3, \tag{2.33}$$

one obtains for the proton-to-neutron mass difference δm,

$$\delta m = -4c_5\epsilon M_\pi^2 - f_2e^2F_\pi^2 + \cdots, \tag{2.34}$$

where the ellipsis refers to higher-order corrections. Notice that the f_3 term in Eq. (2.31) is isospin invariant. On the other hand, the f_1 term does produce IB vertices with two and more pions but does not contribute to the leading electromagnetic nucleon mass shift. The LECs c_5 and f_2 can be determined from the strong and electromagnetic nucleon mass shifts,

$$(m_p - m_n)^{\mathrm{str}} = (\delta m)^{\mathrm{str}} = -2.05 \pm 0.3 \text{ MeV},$$

$$(m_p - m_n)^{\mathrm{em}} = (\delta m)^{\mathrm{em}} = 0.76 \pm 0.3 \text{ MeV}, \tag{2.35}$$

which lead to (Meißner and Steininger, 1998)

$$c_5 = -0.09 \pm 0.01 \text{ GeV}^{-1}, \quad f_2 = -0.45 \pm 0.19 \text{ GeV}^{-1}.$$

The values for the strong and electromagnetic nucleon mass shifts are taken from Gasser and Leutwyler (1982). Notice that the recent lattice QCD result (Beane, Orginos, and Savage, 2007) for the strong nucleon mass shift $(\delta m)^{\mathrm{str}} = -2.26 \pm 0.57 \pm 0.42 \pm 0.10$ MeV is in agreement with the one of Gasser and Leutwyler (1982). We further emphasize that according to the counting rules in Eq. (2.30) the electromagnetic contribution to the nucleon mass shift is formally of higher order than the strong one. Based on naive dimensional analysis, these contributions are expected to be of the size $|(\delta m)^{\mathrm{str}}| \sim \epsilon M_\pi^2/M_\rho \sim 8$ MeV and $|(\delta m)^{\mathrm{em}}| \sim e^2M_\rho/(4\pi)^2 \sim 0.5$ MeV.

We are now in the position to overview the structure of the IB nuclear forces. The general isospin structure of the two-nucleon force feeds, according to the classification of Henley and Miller (1979), into the four classes: $V^{\mathrm{I}}_{NN} = \alpha + \beta\tau_1\cdot\tau_2$ (isospin invariant), $V^{\mathrm{II}}_{NN} = \alpha\tau_1^3\tau_2^3$ (charge-independence breaking), $V^{\mathrm{III}}_{NN} = \alpha(\tau_1^3 + \tau_2^3)$ (charge-symmetry breaking), and $V^{\mathrm{IV}}_{NN} = \alpha(\tau_1^3 - \tau_2^3) + \beta[\tau_1\times\tau_2]^3$ (isospin mixing). Here α and β denote the corresponding space and spin operators. Notice that for the class-IV terms, β has to be odd under a time-reversal transformation. The most general isospin structure of the 3NF is worked out in Epelbaum *et al.* (2005b). While the distinction between the class-I, -II, and -III forces based on the conservation of the total isospin operator $\mathbf{T} = (\Sigma_i\boldsymbol{\tau}_i)/2$ and charge-symmetry operator $P_{cs} = \exp(i\pi T_2)$ can be straightforwardly generalized to any number of nucleons, the conservation of the operator $\mathbf{T}^2$ responsible for the distinction between the class-III and -IV 2NFs depends, in general, on the number of nucleons. In particular, the class-II and -III 2NFs commute with the operator $\mathbf{T}^2_{NN}$ (i.e., do not mix isospin in the NN system) but do not commute with $\mathbf{T}^2_{>NN}$. For this reason, the general isospin structure of the 3NF was classified by Epelbaum, Meißner, and Palomar (2005b) in terms of class-I, -II, and -III contributions.

The dominant IB contribution to the 2NF occurs at NL$\not{0}$ [the slash indicates that we now use the power counting rules extended as in Eq. (2.30)] due to the charge-to-neutral pion mass difference in the 1π-exchange potential. It can be accounted for by taking the proper pion masses in the 1π-exchange potential for various physical channels,

$$V^{pp}_{1\pi} = V^{nn}_{1\pi} = V_{1\pi}(M_{\pi^0}),$$

$$V^{np}_{1\pi} = -V_{1\pi}(M_{\pi^0}) + 2(-1)^{I+1}V_{1\pi}(M_{\pi^\pm}), \tag{2.36}$$

where I denotes the total isospin of the two-nucleon system and

$$V_{1\pi}(M_\pi) = -\frac{g_A^2}{4F_\pi^2}\frac{\vec{\sigma}_1\cdot\vec{q}\,\vec{\sigma}_2\cdot\vec{q}}{\vec{q}^2 + M_\pi^2}. \tag{2.37}$$

Notice that the resulting IB interaction conserves charge symmetry (i.e., class II) and reaches about $\delta M_\pi^2/M_\pi^2 \sim 7\%$ of the strength of the isospin-invariant 1π-exchange potential. It is known to yield a sizable contribution to the CIB in the $^1S_0$ NN scattering length [see, e.g., Walzl *et al.* (2001)]. Another IB effect at the same order comes from the Coulomb interaction between the protons (classes II and III). We emphasize that effects of the purely electromagnetic interactions in two-nucleon scattering observables get enhanced under certain kinematical conditions (low energies and/or forward angles) due to the long-range nature of these interactions. Clearly, such an enhancement goes beyond the simple power counting rules in Eq. (2.30). Consequently, despite the fact that the first corrections to the pointlike

static one-photon exchange (Coulomb interaction) due to recoil and two-photon exchange (Austen and de Swart, 1983), pion loop contributions to the nucleon form factors (Kaiser, 2006c), vacuum polarization (Uehling, 1935; Durand, 1957), and magnetic moment interaction (Stoks, 1990) are suppressed by the factor $1/m^2$ and, according to the power counting, contribute at rather high orders, sizable effects may show up in certain observables. For example, the magnetic moment interaction strongly affects the nucleon analyzing power A_y at low energy and forward angles. Effects of subleading electromagnetic interactions were also investigated in $3N$ continuum using phenomenological nuclear forces (Witała *et al.*, 2003; Kievsky *et al.*, 2004) [see Rupak and Kong (2003) for a formulation based on pionless EFT].

The corrections to the IB 2NF at $\mathrm{N^2LO}$ are CSB and arise from charge dependence of the pion-nucleon coupling constant in the 1π-exchange potential and the derivativeless NN contact interaction $\propto m_u - m_d$ (van Kolck *et al.*, 1996; Epelbaum and Meißner, 2005). Notice, however, that the energy-dependent Nijmegen PWA does not yield any evidence for charge dependence of the pion-nucleon coupling constant (de Swart *et al.*, 1997). The leading CIB contact interactions are of electromagnetic origin and (formally) start to contribute at $\mathrm{N^3LO}$. At this order, one also has to take into account further IB contributions to the 1π-exchange potential at the one-loop level which, to a large extent, can be accounted for by a further (charge-dependent) renormalization of the πN coupling constants in Eq. (2.36). The only contributions which have a different momentum dependence and, therefore, cannot be cast into the form of Eq. (2.36) are the ones $\propto(\delta M_\pi)^2$ and the proton-to-neutron mass difference which involve class-IV operators (Friar *et al.*, 2004; Epelbaum and Meißner, 2005) [see Cheung *et al.* (1980) for a much earlier derivation of these terms]. Notice that the power counting rules in Eq. (2.30) suggest the following hierarchy of the 2NF (van Kolck, 1993): $V_{NN}^{\mathrm{I}} > V_{NN}^{\mathrm{II}} > V_{NN}^{\mathrm{III}} > V_{NN}^{\mathrm{IV}}$ which is consistent with the observations. Next, $\pi\gamma$ exchange also contributes at this order. The resulting CIB potential has been worked out in van Kolck *et al.* (1998) and rederived recently in Kaiser (2006c). It can be written in a rather compact way and leads to negligibly small effects in NN scattering. Kaiser also calculated subleading contributions to the $\pi\gamma$-exchange potential proportional to the large isovector magnetic moment $\kappa_v = 4.7$ of the nucleon and found that the resulting potentials, which are also CIB, have a similar strength as the leading-order one (Kaiser, 2006c).[4] IB 2π-exchange also starts to contribute at $\mathrm{N^3LO}$ and is driven by the neutral-to-charged pion mass difference (CIB) (Friar and van Kolck, 1999) and the strong contribution to the nucleon mass shift (CSB) (Coon and Niskanen, 1996; Niskanen, 2002; Friar *et al.*, 2003; Epelbaum and Meißner, 2005) [see Walzl *et al.* (2001) for the application to NN phase shifts]. Finally, there are also the first IB 3NFs. While the dominant CIB 2π-exchange 2NF is generated by the pion mass difference, the $3N$ diagrams with one insertion of δM_π^2 at $\mathrm{N^3LO}$ are additionally suppressed by the factor $1/m$ if one uses an energy-independent formulation, (see the discussion about the 3NFs at NLO earlier in the text). The nonvanishing 3NFs at $\mathrm{N^3LO}$ result from 1π- and 2π-exchange $3N$ diagrams constructed with the leading-order isospin-invariant vertices and a single insertion of δm as well as 2π-exchange diagram with the leading IB $\pi\pi NN$ interactions $\propto f_{1,2}$ (Epelbaum, Meißner, and Palomar, 2005; Friar *et al.*, 2005). One finds that all these contributions are CSB except the one which is proportional to LEC f_1 and is CIB. We further emphasize that while the value of the LEC f_2 is determined by the electromagnetic nucleon mass shift, the value of the LEC f_1 is unknown. However, see Gasser *et al.* (2002) for an estimation of f_1 based on dimensional analysis and Meißner *et al.* (2006) for an attempt to determine f_1 from data.

Remarkably, even the $\mathrm{N^4LO}$ contributions to the two- and three-nucleon forces have been worked out. At this order, no new structures appear in the 1π-exchange potentials. The corrections to the leading IB 2π-exchange potential result from a single insertion of either the subleading isospin-conserving $\pi\pi\mathrm{NN}$ vertices proportional to the LECs c_i [see Eq. (2.17)], the leading electromagnetic vertex proportional to the LEC f_2 [see Eq. (2.31)],[5] or the (poorly known) leading charge dependence of the pion-nucleon coupling constant (Epelbaum and Meißner, 2005). The resulting IB potentials involve the class-II and -III central, tensor, and spin-spin components. The CIB potentials typically have the strength of a few tens of keV at relative distances $r \sim M_\pi^{-1}$. The CSB tensor and spin-spin potentials are weaker (<10 keV), while the CSB central potential is comparable in size to the CIB contributions. Similarly to the isospin-conserving 2π-exchange potential, the subleading contributions turn out to be numerically large in comparison to the leading-order ones. In particular, for the class-III central 2π-exchange potential one obtains $V_{NN}^{2\pi,(5)}/V_{NN}^{2\pi,(4)} \simeq 3$ for $r \sim M_\pi^{-1}$. The main reason for this unpleasant convergence pattern is the same as in the isospin-conserving case and can be traced back to the (large) Δ-isobar contributions to the LECs $c_{3,4}$. We discuss this issue in more detail in Sec. II.D. Last but not least, there are also numerous IB contact interactions with up to two derivatives involving class-II, -III, and -IV terms [see also Friar *et al.* (2004)]. The corrections to the 3NF at $\mathrm{N^4LO}$ are worked out in Epelbaum, Meißner, and Palomar (2005) and Friar *et al.* (2005). At this order, the first IB but charge symmetry conserving 3NFs show up which result from the neutral-to-charged pion mass difference in the $\mathrm{N^2LO}$ 2π- and 1π-exchange

[4]Notice, however, that these corrections are suppressed by the factor $1/m$ relative to the leading-order contributions and, therefore, appear formally at $\mathrm{N^5LO}$.

[5]The two other LECs $f_{1,3}$ do not contribute to the 2π-exchange 2NF at this order.

diagrams in the second line of Fig. 13 and the 2π-exchange diagram involving the $\pi\pi$NN vertex $\propto f_1$. In addition, there are CSB 3NFs of the 2π- and 1π-exchange types driven by the electromagnetic nucleon mass shift. Again, the strongest 3NFs turn out to be the ones which are proportional to the LECs $c_{3,4}$. They are charge-symmetry conserving and arise from a single insertion of δM_π^2 into the pion propagators of the 2π-exchange $3N$ graph. The expected strength of such IB potentials is $\sim 2\delta M_\pi^2/M_\pi^2 \sim 13\%$ as compared to the isospin-invariant ones given in Eq. (2.22) which are known to yield about $\sim$500–1000 keV to the triton binding energy (the precise numbers are renormalization scheme dependent). Also the strength of the corresponding coordinate-space potentials, e.g., $|g_A^2 \delta M_\pi^2 M_\pi^4 c_3/(64\pi^2 F_\pi^4)| \sim 70$ keV (here we picked out one particular term), indicates that the resulting IB effects in few-nucleon observables might be sizable. The CSB 3NFs, on the other hand, do show a more natural convergence pattern and are considerably weaker. Their contribution to, e.g., the ^{3}H-^{3}He binding energy difference is expected to be of the order of $\sim$10 keV.

Recently, certain classes of even higher-order contributions have been worked out by Kaiser. In particular, he calculated the subleading $\pi\pi\gamma$-exchange potentials proportional to the LECs $c_{3,4}$ at the two-loop level which (formally) contribute at order N^{6}L$\emptyset$ (Kaiser, 2006a, 2006b). The contributions driven by the LEC c_3 were espacially found to generate astonishingly strong CSB and CIB potentials which amount to $\sim$1% of the strongly attractive isoscalar central potential at N^{2}LO and reach a few hundreds of keV at $r \sim M_\pi^{-1}$. Notice, however, that effects of these very strong potentials in S, P, and D waves may, to some extent, be compensated by the corresponding IB contact interactions. The effects in higher partial waves are presumably suppressed due to the shorter range of the 2π-exchange potential compared with the 1π-exchange one.

C. Chiral EFT for few nucleons: Applications

We now turn our attention to applications. As discussed in the previous section, the two-nucleon chiral potential involves the long-range contributions due to the multiple pion exchanges and short-range ones parametrized by contact interactions. Both kinds of terms typically grow with increasing nucleon momenta and become meaningless in the large-momentum region as follows from the very nature of EFT being the low-momentum expansion. As a consequence, the Schrödinger equation is ultraviolet divergent and needs to be regularized (and renormalized). The problem of renormalization in the nonperturbative regime in the context of both pionless (Beane *et al.*, 1998; Phillips *et al.*, 1998, 1999; Birse *et al.*, 1999; Gegelia, 1999; Yang and Huang, 2005; Braaten and Hammer, 2006; Harada and Kubo, 2006; Harada *et al.*, 2009) and pion-full (Lepage, 1997, 2000; Cohen and Hansen, 1998; Frederico *et al.*, 1999; Phillips *et al.*, 2000; Gegelia and Japaridze, 2001; Pavón Valderrama and Ruiz Arriola, 2004a, 2004b, 2006a, 2006b; Nogga *et al.*, 2005; Birse, 2006, 2007; Epelbaum and Meißner, 2006; Gegelia and Scherer, 2006; Pavón Valderrama and Ruiz Arriola, 2006a; Djukanovic *et al.*, 2007; Entem *et al.*, 2008; Higa, Pavón Valderrama, and Ruiz Arriola, 2008; Long and van Kolck, 2008; Shukla *et al.*, 2008; Valderrama and Arriola, 2008; Yang *et al.*, 2008) EFTs has attracted a lot of interest in the past years. The standard procedure to renormalize the Lippmann-Schwinger (LS) equation is based on Wilson's method and implies the following two steps: (Lepage, 1997). First, one solves the LS equation regularized with the finite momentum (or coordinate-space) cutoff and using the potential truncated at a given order in the chiral expansion as the kernel. Second, the LECs accompanying the contact terms in the potential are determined by matching the resulting phase shifts to experimental data which, in this framework, can be viewed as renormalization. Notice that iterating the *truncated* expression for the chiral potential in the LS equation necessarily generates ultraviolet divergencies in the Neumann series which require counterterms beyond the given approximation for the potential. As a consequence, taking the limit of the infinite cutoff in such a manifestly nonrenormalizable (in the above mentioned sense) approach might result, e.g., in impossibility to resolve the (nonlinear) matching conditions for the corresponding LECs. A detailed discussion on the choice of ultraviolet cutoff and its role in renormalization of the Schrödinger equation is given in Lepage (1997, 2000). He argued that the coordinate-space (momentum-space) cutoff should not be decreased (increased) beyond the separation scale after which the description of the data stops to improve. Taking the cutoff near this separation scale is the most efficient choice. This strategy has been followed by the currently most advanced N^{3}LO analyses of the NN system of Entem and Machleidt (2003a) and Epelbaum, Glöckle, and Meißner (2005) where the cutoffs $\Lambda = 450$–600 MeV have been employed. These studies were criticized in Nogga *et al.* (2005) who considered low NN partial waves based on the 1π-exchange potential and contact interactions using a much bigger cutoff variation with $\Lambda < 4$ GeV. They found that higher-order counterterms have to be promoted to LO in the $^3P_0$, $^3P_2$-$^3F_2$, and possibly $^3D_2$ channels in order to stabilize the amplitude. On the other hand, the efficiency of such a modified power counting framework was questioned in Epelbaum and Meißner (2006), where it has been demonstrated that increasing the cutoff and promoting counterterms as suggested in Nogga *et al.* (2005) do not improve the overall description of the scattering observables. For more discussions on the conceptual issues related to the power counting in the NN system see Lepage (1997, 2000), Nogga *et al.* (2005), Birse (2006, 2007), Epelbaum and Meißner (2006), Gegelia and Scherer (2006), Long and van Kolck (2008). More work is needed in the future in order to clarify the relation between the well-established chiral expansion of the nuclear potential and the scattering amplitude.

We further emphasize that it is possible to *nonpertur-*

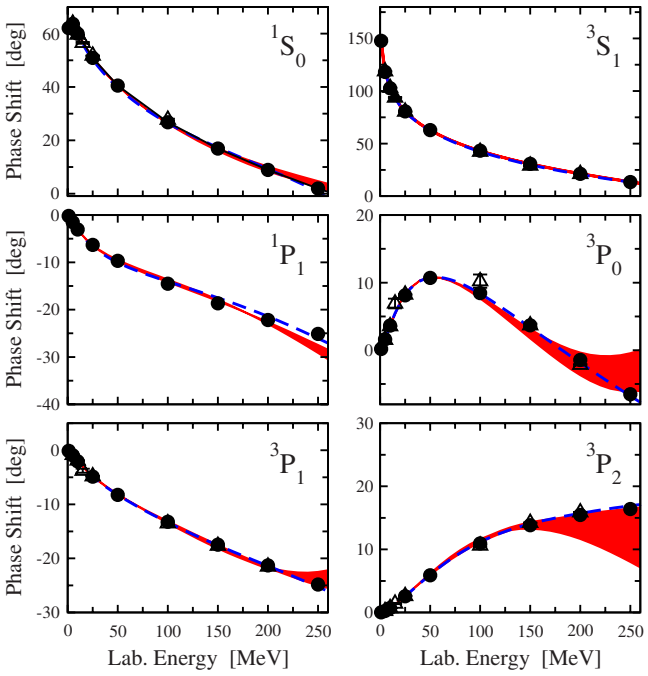

FIG. 15. (Color online) Neutron-proton phase shifts in S and P waves at N^{3}LO in comparison with the Nijmegen (Stoks *et al.*, 1993; Rentmeester *et al.*, 1994) (filled circles) and Virginia Tech (Arndt *et al.*, 2009) (open triangles) PWA. Shaded bands (dashed lines) refer to the calculations by EGM (Epelbaum, Glöckle, and Meißner, 2005) [EM (Entem and Machleidt, 2003a)].

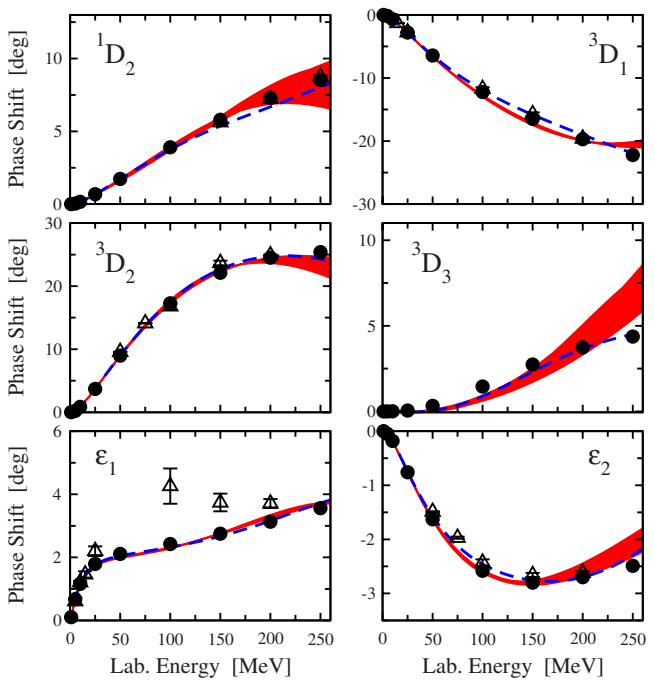

FIG. 16. (Color online) Neutron-proton phase shifts in D waves and the mixing angles $\epsilon_{1,2}$ at N^{3}LO. For notation see Fig. 15.

batively renormalize the partial-wave-projected LS equation with singular $1/r^n$ potentials (Beane *et al.*, 2001; Bawin and Coon, 2003; Braaten and Phillips, 2004; Barford and Birse, 2005; Hammer and Swingle, 2006; Long and van Kolck, 2008). This program was applied to different NN channels based on the 1π- and 2π-exchange potentials at various orders in the chiral expansion by the Granada group (Pavón Valderrama and Ruiz Arriola, 2004a, 2004b, 2005, 2006b; Pavón Valderrama and Ruiz Arriola, 2006a; Entem *et al.*, 2008; Higa, Pavón Valderrama, and Ruiz Arriola, 2008; Valderrama and Arriola, 2008). In these studies, the short-range counterterms are replaced by adjustable parameters entering the short-distance boundary conditions. The number of such parameters in each channel is uniquely determined by the sign (attractive versus repulsive) of the strongest singularity which raises concerns about a systematic improvability (in the EFT sense) of such a framework. Nevertheless, the findings of these studies in attractive channels provide an impressive demonstration of the existence of the long-range correlations in the NN scattering observables.

The most advanced analyses of the two-nucleon system based on the Weinberg power counting take into account the 2NF contributions up to N^{3}LO (Entem and Machleidt, 2003a; Epelbaum, Glöckle, and Meißner, 2005). Most of the LECs c_i, d_i entering the long-range part of the potential are sufficiently well determined in the pion-nucleon system (Fettes *et al.*, 1998).[6] The 24 unknown LECs[7] entering the short-range part of the 2NF at N^{3}LO have been extracted from the low-energy NN data for several choices of the cutoff in the Schrödinger equation. Both N^{3}LO potentials of [Entem and Machleidt (EM) (2003a) and Epelbaum, Glöckle, and Meißner (EGM) (2005)] yield accurate results for the neutron-proton phase shifts up to $E_{\rm lab}\sim 200$ MeV and the deuteron observables. This is exemplified in Figs. 15 and 16 where the EGM and EM results for the neutron-proton S, P, and D waves and the corresponding mixing angles are shown in comparison with PWA results from Stoks *et al.* (1993), Rentmeester *et al.* (1994), and Arndt *et al.* (2009). The bands in the EGM analysis result from the variation in the cutoff in the LS equation (spectral function regularization) in the range $\Lambda = 450-600$ MeV ($\tilde{\Lambda}=500-700$ MeV). It is comforting to see that in most cases the results of both analyses agree with each other within the estimated theoretical uncertainty. Notice, however, that the EM and EGM analyses differ from each other in several important aspects. For example, the so-called spectral function regularization (Epelbaum *et al.*, 2004a, 2004b) of the 2π-exchange contributions has been adopted by EGM while the analysis by EM is based on dimensionally regularized expressions. Further differences can be attributed to the imple-

[6]Notice, however, that the value of the LEC c_4 adopted in Entem and Machleidt (2003a), $c_4=5.4$ GeV^{-1}, is not compatible with pion-nucleon scattering where one finds at order Q^3 (Buettiker and Meißner, 2000): $c_4=3.40\pm0.04$ GeV^{-1}.

[7]This number refers to isospin-invariant contact interactions.

mentation of the momentum-space cutoff in the Schrödinger equation and the treatment of relativistic effects. More precisely, the work by EGM is based on the "relativistic" Schrödinger and Lippmann-Schwinger equation, a natural extension of the usual nonrelativistic equations utilizing the relativistic relation between the CMS energy and momentum [see Friar (1999) for more details]. This equation can be straightforwardly generalized to the case of several nucleons [see Witała *et al.* (2005); Lin, Elster, Polyzou, and Glöckle (2008); and Lin, Elster, Polyzou, Witała, and Glöckle (2008) for recent studies of relativistic effects in $3N$ observables] and can also be cast into equivalent nonrelativisticlike forms (Kamada and Glöckle, 1998; Friar, 1999) (provided the potential is appropriately modified). On the other hand, the analysis of Entem and Machleidt (2003a) uses the static 1π-exchange potential and the $1/m$ and $1/m^2$ corrections to the 2π-exchange potential from Kaiser *et al.* (1997) and Kaiser (2000a), where no particular dynamical equation is specified. Further differences between the EGM and EM analyses result from the fitting procedure: the LECs accompanying the contact interactions were determined by EM and EGM by fitting directly to the scattering data and to the Nijmegen PWA (Stoks *et al.*, 1993; Rentmeester *et al.*, 1994). For this reason, EGM adopted the same treatment of IB effects as followed by the Nijmegen group and did not include, e.g., the leading IB contributions to the 2π-exchange potential. Perhaps, the most important difference between the two studies is related to the estimation of the theoretical uncertainty. In the work by EGM, the theoretical uncertainty was estimated by varying the cutoffs in the Schrödinger equation and the spectral function representation for the 2π-exchange potential restricted by the condition that the resulting LECs are of a natural size which might be viewed as a self-consistency check for calculations carried out within the power counting scheme based on naive dimensional analysis [see Beane *et al.* (2000) and Epelbaum (2006a)]. Notice further that at NLO and N^{2}LO the strengths of various contact interactions are well understood in terms of resonance saturation on the basis of phenomenological one-boson exchange models (Epelbaum, Meißner, Glöckle, and Elster, 2002). No serious attempt to provide a realistic error estimation was done in the analysis of EM. On the other hand, their work clearly demonstrates that for a particularly chosen regularization prescription it is even possible to accurately describe two-nucleon scattering data for $E_{\rm lab}>200$ MeV. For further technical details, results for various scattering observables and the properties of the deuteron, see the original publications (Entem and Machleidt, 2003a; Epelbaum, Glöckle, and Meißner, 2005) and the review article (Epelbaum, 2006a).

To illustrate the convergence of the chiral expansion for NN phase shifts, we show in Fig. 17 the results for the $^1S_0$ partial wave at NLO, N^{2}LO (Epelbaum *et al.*, 2004b), and N^{3}LO (Epelbaum, Glöckle, and Meißner, 2005). We emphasize that the variation in the cutoff at

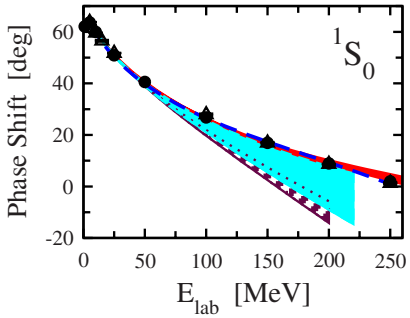

FIG. 17. (Color online) Neutron-proton $^1S_0$ partial wave at NLO (dashed band), N^{2}LO (light-shaded band), and N^{3}LO (dark-shaded band) in comparison with the Nijmegen (Stoks *et al.*, 1993; Rentmeester *et al.*, 1994) (filled circles) and Virginia Tech (Arndt *et al.*, 2009) (open triangles) PWA.

both NLO and N^{2}LO only shows the effects of missing N^{3}LO contact interactions. It, therefore, does not provide a realistic estimation of the theoretical uncertainty at NLO [see Epelbaum (2006a) for an extended discussion].

Applications to the three-nucleon system have so far been carried out up to N^{2}LO. At NLO, no 3NF needs to be taken into account. This allowed for a parameter-free predictions of various $3N$ scattering observables at low energies as well as for the triton and α-particle binding energies (Epelbaum *et al.*, 2001). Using the most recent version of the NLO potential based on the spectral function regularization, one finds at NLO (Epelbaum, 2006a) $B_{^3\rm H}=7.71-8.46$ MeV and $B_{^4\rm He}=24.38-28.77$ MeV to be compared with the experimental values $B_{^3\rm H}=8.482$ MeV and $B_{^4\rm He}=28.30$ MeV. These numbers are similar to the ones obtained in Epelbaum *et al.* (2001) within the framework based on dimensional regularization.

At N^{2}LO one, for the first time, has to take into account the corresponding 3NFs. The two LECs D and E entering the expressions for the 3NF in Eq. (2.22) have been determined by fitting the ^{3}H binding energy and either the nd doublet scattering length (Epelbaum, Nogga, Glöckle, Kamada, Meißner, and Witała, 2002), the ^{4}He binding energy (Nogga *et al.*, 2006), or the properties of light nuclei (Navratil *et al.*, 2007). Notice that the $\pi NNNN$ vertex entering the 1π-exchange-contact 3NF also plays an important role in processes with a completely different kinematics such as, e.g., the pion production in the NN collisions (Hanhart *et al.*, 2000) [see Sec. II.E or weak reactions such as $pp\to de^+\nu_e$ and Nakamura (2008), and references therein]. This offers the possibility to extract the corresponding LEC from these processes [see Nakamura (2008), for a recent attempt]. With the LECs being determined as described above, the resulting nuclear Hamiltonian can be used to describe the dynamics of few-nucleon systems. In particular, $3N$ continuum observables offer a natural and rich testing ground for the chiral forces. In Epelbaum *et al.* (2001), Epelbaum, Nogga, Glöckle, Kamada, and Meißner (2002), Epelbaum, Nogga, Glöckle, Kamada,

Meißner, and Witała (2002), Ermisch *et al.* (2003, 2005), Duweke *et al.* (2005), Kistryn *et al.* (2005), Biegun *et al.* (2006), Ley *et al.* (2006), Witała *et al.* (2006), and Stephan *et al.* (2007) various 3*N* scattering observables have been explored by solving the momentum-space Faddeev equations with chiral two and three-nuclein forces as input. In the formulation of Glöckle *et al.* (1996), one first computes the T matrix by solving the Faddeev-like integral equation,

$$T = tP\phi + (1+tG_0)V_{3N}^1(1+P)\phi + tPG_0T + (1+tG_0)V_{3N}^1(1+P)G_0T, \tag{2.38}$$

where the initial state ϕ is composed of a deuteron and a momentum eigenstate of the projectile nucleon. Here V_{3N}^i is that part of the 3*N* force which singles out the particle i and which is symmetric under the interchange of the two other particles. The complete 3NF is decomposed as $V_{3N}=V_{3N}^1+V_{3N}^2+V_{3N}^3$. Further, $G_0=1/(E-H_0)$ is the free propagator of the nucleons, P is a sum of a cyclical and an anticyclical permutation of the three particles, and t denotes the two-body t matrix. Once T is calculated, the transition operators $U_{\rm el}$ and $U_{\rm br}$ for the elastic and break-up channels can be obtained via

$$U_{\rm el} = PG_0^{-1} + PT + V_{3N}^1(1+P)(1+G_0T),$$

$$U_{\rm br} = (1+P)T. \tag{2.39}$$

For details on solving these equations in momentum space using a partial wave decomposition see Hüber *et al.* (1997). The partial wave decomposition of the 1π exchange and contact 3NF at N^{2}LO and the one-pion-two-pion-exchange topology at N^{3}LO is detailed by Epelbaum, Nogga, Glöckle, Kamada, Meißner, and Witała (2002) and Epelbaum *et al.* (2008), respectively. The expressions for various observables in terms of the transition operators are given by Glöckle *et al.* (1996). The inclusion of the long-range electromagnetic interaction requires a nontrivial generalization of the formalism [see Deltuva *et al.* (2005a, 2005b) for recent progress along this line].

The results for the differential cross section in elastic *nd* scattering are in a good agreement with the data (see Fig. 18 for two representative examples). Notice, however, that the theoretical uncertainty becomes significant already at intermediate energies. Qualitatively, this behavior is consistent with the one observed in the two-nucleon system (Epelbaum, Glöckle, and Meißner, 2005). Notice further that the description of the data improves significantly when going from NLO to N^{2}LO. The situation is similar for vector and tensor analyzing powers [see Epelbaum (2006a) for a recent review article]. More complicated spin observables have also been studied. As a representative example, we show in Fig. 19 a selection of the proton-to-proton and proton-to-deuteron polarization transfer coefficients measured in $d(\vec{p},\vec{p})d$ and $d(\vec{p},\vec{d})p$ reactions at $E_p^{\rm lab}=22.7$ MeV (Glombik *et al.*, 1995; Kretschmer, 1995). The results at N^{2}LO are in a reasonable agreement with the data [see

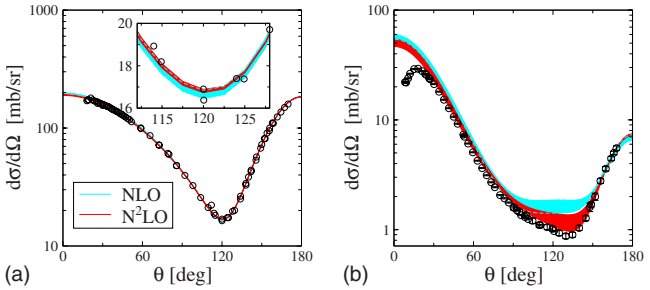

FIG. 18. (Color online) Differential cross section for elastic *nd* scattering at $E_{\rm lab}=10$ MeV (left panel) and 65 MeV (right panel). Light (dark) shaded bands depict the results at NLO (N^{2}LO). The neutron-deuteron data at 10 MeV are from Howell *et al.*, 1987. The remaining data at 10 MeV are the Coulomb and IB-corrected proton-deuteron data from Sperisen *et al.*, 1984, Rauprich *et al.*, 1988, and Sagara *et al.*, 1994. The data at 65 MeV are proton-deuteron data from Witała *et al.*, 1993.

Witała *et al.* (1993) for more examples]. One further observes that the theoretical uncertainty obtained by the cutoff variation is underestimated at NLO [see Epelbaum, Glöckle, and Meißner (2005)]. It is, however, comforting to see that the description of the data improves significantly when going from NLO to N^{2}LO.

The nucleon-deuteron breakup reaction offers even more possibilities than the elastic channel due to the much richer kinematics corresponding to three nucleons in the final state. It has also been studied extensively over the last years, both theoretically and experimentally, leaving one with mixed conclusions. While the differential cross section in some configurations such as, e.g., the recently measured *np* final-state interaction, coplanar star, and an intermediate-star geometries at low energies are in a very good agreement with the data

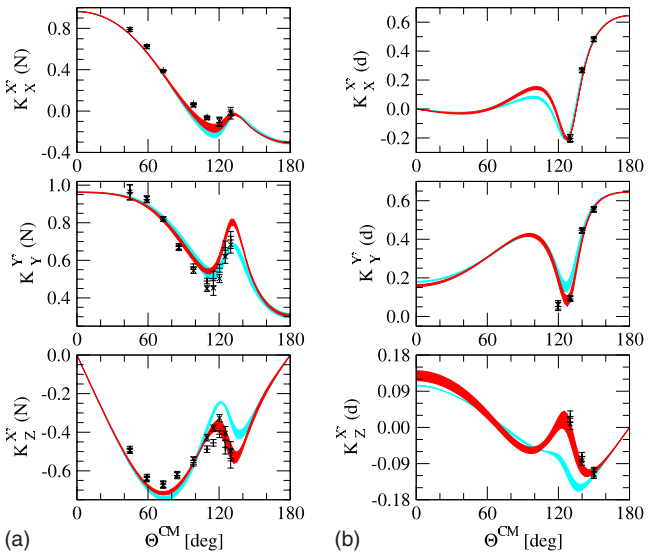

FIG. 19. (Color online) The proton-to-proton (left panel) and proton-to-deuteron (right panel) polarization transfer coefficients in $d(\vec{p},\vec{p})d$ and $d(\vec{p},\vec{d})p$ reactions at $E_p^{\rm lab}=22.7$. Light (dark) shaded bands depict the results at NLO (N^{2}LO). Data are from Glombik *et al.*, 1995; Kretschmer *et al.*, 1995.

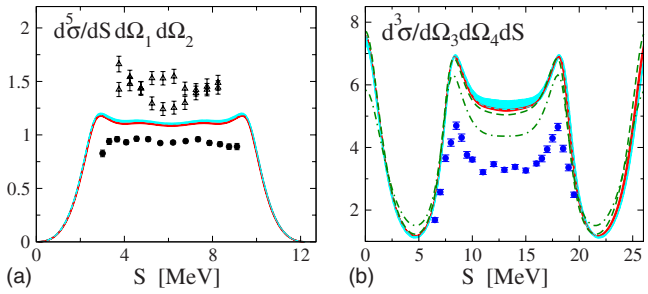

FIG. 20. (Color online) Chiral EFT predictions for neutron-deuteron breakup cross section (in mb MeV^{-1} sr^{-2}) along the kinematical locus *S*. Light shaded (dark shaded) bands refer to the results at NLO ($\mathrm{N^2LO}$). Left panel: The SST at $E_N=13$ MeV. Neutron-deuteron data (open triangles) are from Setze *et al.*, 1996; Strate *et al.*, 1989; proton-deuteron data (filled circles) are from Rauprich *et al.*, 1991. Right panel: The symmetric constant relative-energy (SCRE) configuration with $\alpha=56°$ at $E_N=19$ MeV (Ley *et al.*, 2006). Dashed and dash-dotted lines are results based on the CD Bonn 2000 2NF (Machleidt, 2001) combined with the TM99 3NF (Coon and Han, 2001) and the coupled channel calculation including the explicit Δ and the Coulomb interaction (Deltuva *et al.*, 2005b), respectively.

(Duweke *et al.*, 2005), large deviations are observed in certain other configurations. In particular, the so-called symmetric space-star configuration (SST) appears rather puzzling. In this configuration, the plane in the CMS spanned by the outgoing nucleons is perpendicular to the beam axis, and the angles between the nucleons are 120°. At $E_{\mathrm{lab}}=13$ MeV, the proton-deuteron and neutron-deuteron (*nd*) cross section data deviate significantly from each other. Theoretical calculations based on both phenomenological and chiral nuclear forces have been carried out for the *nd* case and are unable to describe the data (see Fig. 20). Moreover, the Coulomb effect was found to be far too small to explain the difference between the *pd* and *nd* data sets (Deltuva *et al.*, 2005a). Recently, proton-deuteron data for a similar SCRE configuration have been measured in Cologne (Ley *et al.*, 2006). This geometry is characterized by the angle α between the beam axis and the plane in the CMS spanned by the outgoing nucleons. Similar to the SST geometry, one observes large deviations between the theory and the data, in particular for $\alpha=56°$ (see Fig. 20). The included 3NFs have little effect on the cross section while the effect of the Coulomb interaction is significant and removes a part of the discrepancy. Notice that all above cases correspond to rather low energies where one expects good convergence of the chiral expansion. Furthermore, contrary to the A_y puzzle, the cross sections discussed above are mainly sensitive to the two-nucleon *S* waves without any known fine tuning between partial waves. First attempts have been made in the past few years to perform deuteron breakup experiments at intermediate energies, in particular at $E_N=65$ MeV (Kistryn *et al.*, 2005), in which a large part of the phase space is covered at once. Chiral EFT results at $\mathrm{N^2LO}$ for more than 155 data points were shown to be of a comparable quality to the ones based on modern phenomenological nuclear forces.

Recently, first results for the 4*N* continuum based on both phenomenological and chiral nuclear forces and including the Coulomb interactions have become available [see Fisher *et al.* (2006) and Deltuva and Fonseca (2007b) for p-^{3}He scattering, Deltuva and Fonseca (2007a) for the n-^{3}He, p-^{3}H, and d-d scattering, and Lazauskas *et al.* (2005) for the related earlier work]. These studies do not yet include effects of 3NFs but clearly indicate that at least some of the puzzles observed in the 3*N* continuum also persist in the 4*N* continuum [such as, e.g., the A_y puzzle in p-^{3}He scattering (Deltuva and Fonseca, 2007b)]. For a promising new approach to describe scattering states in even heavier systems see Quaglioni and Navratil (2008).

The properties of certain *S*-shell and *P*-shell nuclei with $A\leqslant 13$ have been analyzed recently based on the no-core shell model (NCSM) [see Nogga *et al.* (2006), Navratil *et al.* (2007), and Navratil *et al.* (2008) for an overview]. In Fig. 21 we show some results from Navratil *et al.* (2007) for the spectra of ^{10}B, ^{11}B, ^{12}C, and ^{13}C. We emphasize that the LECs *D* and *E* entering the $\mathrm{N^2LO}$ 3NF were determined in these calculations by the triton binding energy and a global fit to selected properties of ^{6}Li, ^{10}B, and ^{12}C. These studies clearly demonstrate that the chiral 3NF plays an important role in the description of spectra and other properties of light nuclei. The inclusion of the 3NF allows one to considerably improve the agreement with the data. Further results for light nuclei and the dilute neutron matter based on the lattice formulation of chiral EFT are given in Secs. II.G and III.E.

D. The role of the Δ isobar

The chiral expansion for the long-range part of the nuclear force discussed in the previous section exhibits a somewhat unnatural convergence pattern in certain cases such as, e.g., for the central part of the 2π-exchange potential. The origin of the unnaturally strong subleading contribution in this case can be traced back to the large values of the dimension-two low-energy constants (LECs) $c_{3,4}$ which are also responsible for the numerical dominance of the subleading 3π exchange (Kaiser, 2001b) and charge-symmetry breaking 2π-exchange 2NF (Epelbaum and Meißner, 2005) over the corresponding leading contributions. The large values of these LECs are well understood in terms of resonance saturation (Bernard *et al.*, 1997). In particular, the Δ(1232) provides the dominant (significant) contribution to c_3 (c_4). Given its low excitation energy, $\Delta\equiv m_\Delta - m = 293$ MeV, and strong coupling to the πN system, the Δ isobar is known to play an important role in nuclear physics. One can, therefore, expect that the explicit inclusion of Δ in EFT will allow us to resum a certain class of important contributions and improve the convergence as compared to the deltaless theory, provided a proper power counting scheme such as the small scale expan-

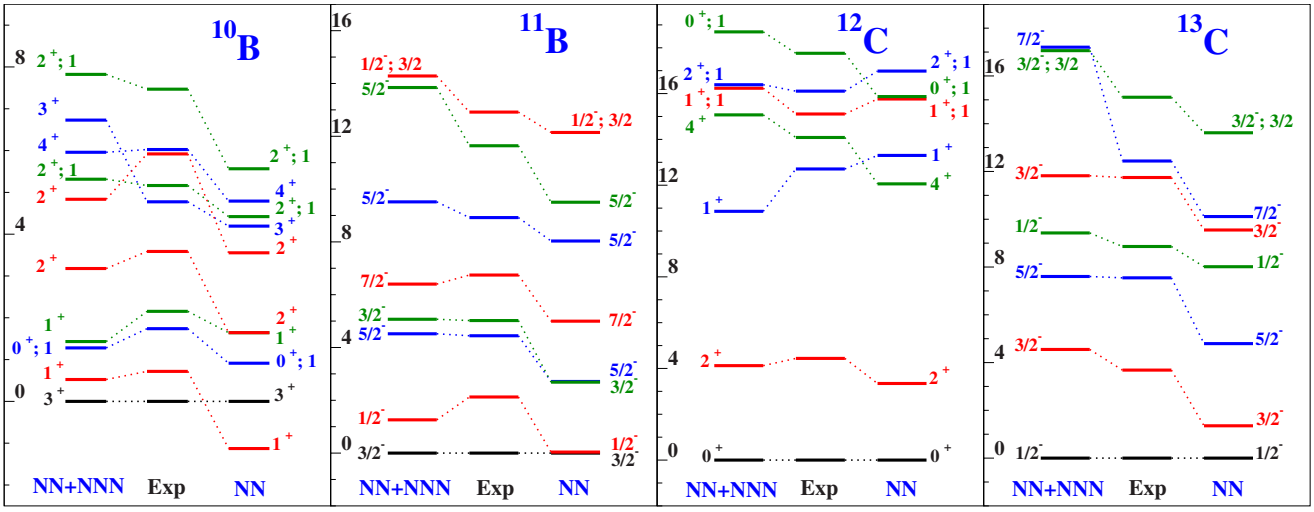

FIG. 21. (Color online) States dominated by P-shell configurations for ^{10}B, ^{11}B, ^{12}C, and ^{13}C. The excitation energy scales are in MeV. The calculation is carried out in the framework of NCSM based on chiral N^{3}LO 2NF from Entem and Machleidt, 2003a and N^{2}LO 3NF. For more details on the calculation see Navratil *et al.*, 2007. Figure is courtesy of Petr Navratil.

sion (SSE) (Hemmert *et al.*, 1998) is employed [see also Jenkins and Manohar (1992)]. The SSE is a phenomenological extension of chiral perturbation theory in which the small expansion parameter includes external momenta, pion masses, and nucleon-delta mass splitting,

$$Q/\Lambda \in \{p/\Lambda, M_\pi/\Lambda, \Delta/\Lambda\}, \tag{2.40}$$

i.e., the delta-nucleon mass splitting is treated as $\Delta \equiv m_\Delta - m \sim M_\pi$ rather than $\Delta \sim \Lambda \gg M_\pi$. The improved convergence has been explicitly demonstrated for pion-nucleon scattering where the description of the phase shifts at third order in the SSE comes out superior (inferior) to the third- (fourth-) order chiral expansion in the deltaless theory (Fettes and Meißner, 2001). In the following, we provide an overview of the additional contributions to the nuclear force which arise in the Δ-full theory as compared to the Δ-less theory and discuss the implications for the convergence of the low-momentum expansion. Notice that in such a setting we do not need to consider the $NN \to N\Delta$, $NN \to \Delta\Delta$, and $N\Delta \to \Delta\Delta$ transitions which would correspond to the coupled-channel approach. The adopted counting rules for the nucleon mass and the delta-nucleon mass difference imply for the momentum scale associated with real delta production $\sqrt{m\Delta} \sim \sqrt{mM_\pi} \sim \Lambda$. For typical external momenta (energies) of the nucleons of the order $|\vec{p}| \sim M_\pi$ ($E_{\rm kin} \sim M_\pi^2/m$) we are interested in, the momenta associated with real delta production can be safely integrated out. We, therefore, only need to consider the contributions to the nuclear force arising due to virtual delta excitations.

The effective Lagrangian can be straightforwardly extended to include the Δ degrees of freedom. To work out Δ contributions up to N^{2}LO, the following additional terms in the heavy-baryon Lagrangian have to be taken into account,

$$\mathcal{L}^{(0)}_{\pi\Delta} = -\bar{T}^i_\mu [iv\cdot D^{ij} - \Delta\delta^{ij}] g^{\mu\nu} T^j_\nu + \cdots,$$

$$\mathcal{L}^{(0)}_{\pi N\Delta} = h_A \bar{T}^i_\mu P^{\mu\nu} \omega^i_\nu N + \text{H.c.},$$

$$\mathcal{L}^{(1)}_{\pi N\Delta} = (b_3 + b_8) \bar{T}^i_\mu i P^{\mu\nu} \omega^i_{\nu\rho} v^\rho N + \text{H.c.} + \cdots, \tag{2.41}$$

where T^i_μ with μ (i) the Lorentz (isospin) index denotes the large component of the delta field. Further, D^{ij}_μ refers to the chiral covariant derivative for the delta fields and $P_{\mu\nu}$ is the standard projector on the 3/2 components, $P_{\mu\nu} = g_{\mu\nu} - v_\mu v_\nu - 4S_\mu S_\nu/(1-d)$, with d the number of space-time dimensions. We also have $w^i_\alpha = \langle \tau^i u_\alpha \rangle/2$ and $w^i_{\alpha\beta} = \langle \tau^i [\partial_\alpha, u_\beta] \rangle/2$. The only relevant LEC in the lowest-order Lagrangian is the $\pi N\Delta$ axial coupling h_A. At subleading order, the combination of $\pi N\Delta$ LECs $b_3 + b_8$ contributes. For more details on the notation, see Hemmert *et al.* (1998) and Fettes and Meißner (2001) [see also Bernard (2008) for a recent review article and Pascalutsa (1998) and Hacker *et al.* (2005) for different formulations]. Finally, it should also be emphasized that the only possible derivativeless $NN N\Delta$ contact interaction,

$$\mathcal{L}^{(0)}_{N\Delta} \propto (\bar{T}^\mu_i N \bar{N} S_\mu \tau^i N + \text{H.c.}), \tag{2.42}$$

vanishes due to the Pauli principle (Epelbaum *et al.*, 2008a).

The values of the LECs in the πN Lagrangian are, clearly, different in the Δ-less and Δ-full theories and can be naturally extracted from πN scattering [see Fettes and Meißner (2001) for such a determination at the leading one-loop level (i.e., order Q^3)]. At subleading order, which is sufficient for our purpose, the determination of c_i from the πN S- and P-wave threshold coefficients yields in the deltaless theory (Krebs *et al.*, 2007),

$$c_1 = -0.57, \quad c_2 = 2.84, \quad c_3 = -3.87, \quad c_4 = 2.89, \tag{2.43}$$

where only central values are given and the units are GeV^{-1}. The above values are somewhat smaller in magnitude than the ones obtained at higher orders [see, e.g., Fettes *et al.* (1998)]. Including the contributions form the Δ, one finds

$$c_1 = -0.57, \quad c_2 = -0.25, \quad c_3 = -0.79, \quad c_4 = 1.33,$$

$$b_3 + b_8 = 1.40. \tag{2.44}$$

Notice that the LECs $c_{2,3,4}$ are strongly reduced in magnitude when the Δ isobar is included. It should also be emphasized that the values of these LECs depend sensitively on the choice of h_A, which in the above case was set to $h_A = 3g_A/(2\sqrt{2})$ from SU(4) (or large N_c). The results for the threshold coefficients and the 2π-exchange potential are, however, rather stable (Krebs *et al.*, 2007). We also emphasize that the description of the P-wave threshold parameters improves significantly upon inclusion of the delta isobar.

We are now in the position to discuss the leading and subleading contributions of the Δ isobar to the nuclear force. Since the appearance of a virtual Δ isobar requires at least one loop, the corresponding contributions first appear at NLO ($\nu=2$). The relevant NN and $3N$ diagrams can be obtained from the ones of Figs. 12 and 13 by replacing the nucleon propagators by the ones of the Δ fields in all intermediate states. We first discuss the 2NF. Similarly to the Δ-less theory, the additional contributions to the 1π-exchange potential and contact interactions at both NLO and N^{2}LO only lead to renormalization of various LECs. The 2π-exchange diagrams were first discussed in Ordonez *et al.* (1996) using time-ordered perturbation theory. These contributions were then calculated in Kaiser *et al.* (1998) using the Feynman graph technique. The corrections at N^{2}LO have been worked out recently (Krebs *et al.*, 2007). We refrain from showing here the resulting expressions which are rather involved and only give the results for the isovector tensor 2π-exchange potential W_T, defined according to $V_{NN} = \boldsymbol{\tau}_1 \cdot \boldsymbol{\tau}_2 \vec{\sigma}_1 \cdot \vec{q}\, \sigma_2 \cdot \vec{q}\, W_T$, which may serve as a representative example,

$$W_T^{(2)} = -\frac{h_A^2}{1296\pi^2 F_\pi^4 \Delta}\{9\pi g_A^2 \omega^2 A^{\tilde{\Lambda}}(q) + h_A^2[2L^{\tilde{\Lambda}}(q) + (4\Delta^2 + \omega^2)D^{\tilde{\Lambda}}(q)]\},$$

$$W_T^{(3)} = -\frac{h_A^2 \Delta}{648\pi^2 F_\pi^4}\{[2(b_3 + b_8)g_A(\omega^2 - 12\Delta^2) - 9c_4(\omega^2 - 4\Delta^2)]D^{\tilde{\Lambda}}(q) + 6[3c_4 - 2(b_3 + b_8)h_A]L^{\tilde{\Lambda}}(q)\}. \tag{2.45}$$

Here the new loop function $D^{\tilde{\Lambda}}(q)$ is defined via

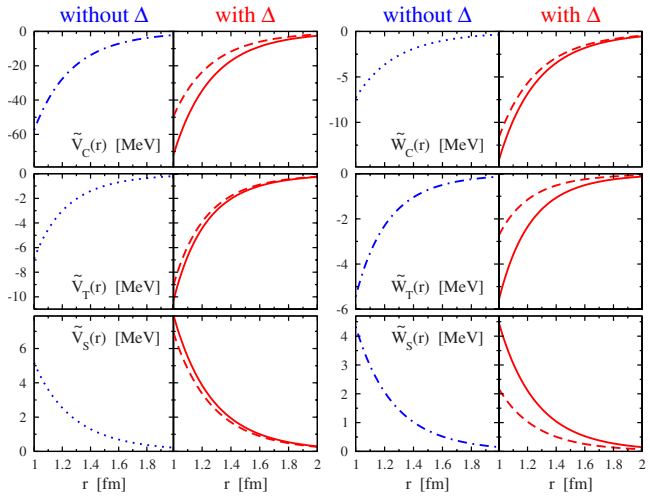

FIG. 22. (Color online) Isoscalar (left panel) and isovector (right panel) components of the 2π-exchange potential in coordinate space for $\tilde{\Lambda} = 700$ MeV. Dashed and solid (dotted and dash-dotted) lines refer to the NLO and N^{2}LO results in the deltafull (deltaless) theory, respectively. There are no contributions to $\tilde{V}_C$ and $\tilde{W}_{T,S}$ ($\tilde{V}_{T,S}$ and $\tilde{W}_C$) at NLO (N^{2}LO) in the deltaless theory.

$$D^{\tilde{\Lambda}}(q) = \frac{1}{\Delta}\int_{2M_\pi}^{\tilde{\Lambda}} \frac{d\mu}{\mu^2 + q^2} \arctan \frac{\sqrt{\mu^2 - 4M_\pi^2}}{2\Delta}. \tag{2.46}$$

The complete results for the Δ contributions can be found in Kaiser *et al.* (1998) and Krebs *et al.* (2007). It is instructive to verify the consistency between the Δ-full and Δ-less theories which requires that the contributions due to intermediate Δ excitations, expanded in powers of $1/\Delta$, can be absorbed into a redefinition of the LECs in the Δ-less theory. This is only possible if the nonpolynomial (in momenta) terms up to N^{2}LO resulting from such an expansion have the same form as expressions in Eqs. (2.14) and (2.18). This indeed turns out to be the case: all expanded nonpolynomial terms up to N^{2}LO are exactly reproduced by the shift in the LECs $c_{3,4}$,

$$c_3 = -2c_4 = -4h_A^2/9\Delta, \tag{2.47}$$

in Eqs. (2.14) and (2.18).

To get more insight into the strength of various 2π-exchange contributions in the Δ-full and Δ-less theories, it is useful to switch to coordinate space. The 2π-exchange potential can then be written as

$$\tilde{V}(r) = \tilde{V}_C + \boldsymbol{\tau}_1 \cdot \boldsymbol{\tau}_2 \tilde{W}_C + [\tilde{V}_S + \boldsymbol{\tau}_1 \cdot \boldsymbol{\tau}_2 \tilde{W}_S]\vec{\sigma}_1 \cdot \vec{\sigma}_2 + [\tilde{V}_T + \boldsymbol{\tau}_1 \cdot \boldsymbol{\tau}_2 \tilde{W}_T]S_{12}, \tag{2.48}$$

where $S_{12} = 3\vec{\sigma}_1 \cdot \hat{r}\vec{\sigma}_2 \cdot \hat{r} - \vec{\sigma}_1 \cdot \vec{\sigma}_2$ is the tensor operator. The scalar functions $\tilde{V}_i(r)$ and $\tilde{W}_i(r)$ are plotted in Fig. 22 using the values for the LECs specified in Eqs. (2.43) and (2.44). As expected, one observes a more natural convergence pattern in the theory with explicit deltas with the N^{2}LO contributions yielding typically only modest corrections to the NLO result. This is, clearly, not the case in the deltaless theory where the entire con-

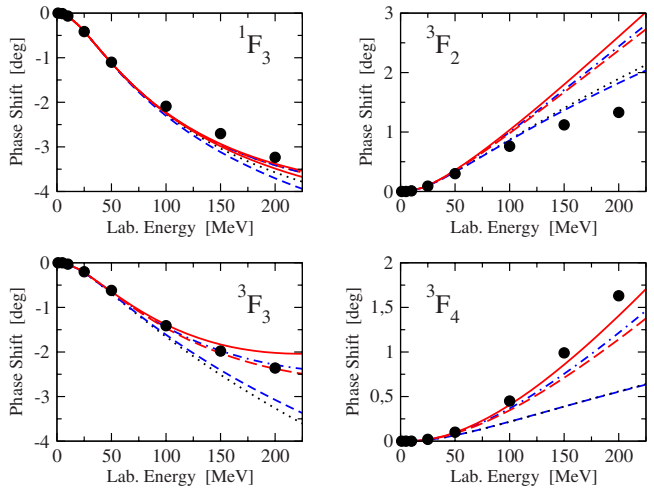

FIG. 23. (Color online) *F*-wave *NN* phase shifts for $\tilde{\Lambda}$ = 700 MeV. The dotted curve is the LO prediction, long-dashed (short-dashed) and solid (dashed-dotted) lines show the NLO and N^{2}LO results with (without) the explicit Δ contributions. The filled circles depict the results from the Nijmegen PWA (Stoks *et al.* 1993).

tributions to $\tilde{V}_C$ and $\tilde{W}_{T,S}$ are generated at N^{2}LO. On the other hand, the N^{2}LO 2π-exchange potential in the deltaless theory provides a very good approximation to the potential resulting at the same order in the deltafull theory. This indicates that the saturation of the LECs $c_{3,4}$ is the most important effect of the Δ isobar at the considered order. The results for *NN F* and other peripheral waves calculated using the Born approximation also clearly demonstrate the improved convergence in the theory with explicit Δ (see Fig. 23).

As explained in Sec. II.B, the first nonvanishing contributions to the 3NF appear in the Δ-less theory at N^{2}LO. The situation is different in the Δ-full theory where the first 3NF contribution is generated at NLO by the second graph in the first line of Fig. 13 with the intermediate nucleon propagator being replaced by the one of the Δ field. In fact, the importance of the πN P_{33} partial wave corresponding to the excitation of the Δ resonance in the 3NF has been realized already 50 years in Fujita and Miyazawa (1957). The resulting expression for the Δ contribution to the 2π-exchange 3NF is exactly reproduced by the first term in Eq. (2.22) if one uses the Δ-saturation values for the LECs c_i from Eq. (2.47). This, in fact, follows from the decoupling theorem and the fact that the static Δ propagator is proportional to Δ^{-1}. Notice that there are no short-range 3NFs with intermediate Δ excitation since the corresponding *NNN*Δ interaction is Pauli forbidden. Stated differently, the LECs *D* and *E* are not saturated by the Δ isobar. Surprisingly, one finds that there are also no Δ contributions to the 3NF at N^{2}LO (Epelbaum *et al.*, 2008a). The 2π-exchange diagrams with one insertion of the subleading $\pi N\Delta$ vertex $\propto b_3+b_8$ generate $1/m$-suppressed terms due to the time derivative entering this vertex. Despite the fact that both the Δ-full and Δ-less theories yield the same expressions for the 2π-exchange 3NF at N^{2}LO, one should keep in mind that the strengths of various terms are different. The extrapolation of the πN amplitude from threshold, where the LECs are determined, to the kinematical region relevant for the 3NF is discussed in Pandharipande *et al.* (2005) who claimed that both theories might yield sizably different results if the expansion is truncated at low orders. Using the values of the LECs from Eqs. (2.43) and (2.44) one, however, finds that the strengths of various terms differ from each other at most by ~7% at N^{2}LO (Epelbaum *et al.*, 2008a). To conclude, the only effect of including the Δ isobar as an explicit degree of freedom in the 3NF up to N^{2}LO is the shift of the major part of the 2π-exchange contribution in Eq. (2.22) from N^{2}LO to NLO and some minor changes in the strengths of various terms in this expression.

We now discuss the role of the Δ for IB nuclear forces. The observed unnatural convergence pattern for the CSB 2π-exchange 2NF and CIB 3NF in the Δ-less theory (see the discussion in Sec. II.B) is very similar to the one for isospin-conserving 2π-exchange 2NF (in all cases the large contributions are proportional to the LECs $c_{3,4}$) and provides a strong motivation to explore the role of the Δ isobar in this case.

The leading IB Δ contributions to the 2π-exchange 2NF result from the corresponding triangle, box, and crossed-box diagrams with one insertion of isospin-breaking pion, nucleon, and delta mass shifts. The latter can be deduced from the corresponding leading strong and electromagnetic Lagrangians (Epelbaum *et al.*, 2008a),

$$\mathcal{L}^{(2)}_{\pi\Delta,\mathrm{IB}} = -\bar{T}^\mu_i c^\Delta_5(\chi_+ - \langle\chi_+\rangle)\delta_{ij}g_{\mu\nu}T^\nu_j,$$

$$\begin{aligned}\mathcal{L}^{(3)}_{\pi\Delta,\mathrm{IB}} = &-\bar{T}^\mu_i F_\pi^2[f^\Delta_1\delta_{ij}\langle Q_+^2 - Q_-^2\rangle + f^\Delta_2\delta_{ij}\langle Q_+\rangle Q_+ \\ &+ f^\Delta_3\delta_{ij}\langle Q_+\rangle^2 + f^\Delta_4\langle\tau^i Q_+\rangle\langle\tau^j Q_+\rangle \\ &+ f^\Delta_5\langle\tau^i Q_-\rangle\langle\tau^j Q_-\rangle]g_{\mu\nu}T^\nu_j + \cdots,\end{aligned} \tag{2.49}$$

where c^Δ_5 and f^Δ_i are the LECs and the ellipsis in the last line refers to strong terms which involve at least one pion field and are irrelevant for the following discussion. The masses of the physical delta fields $(\Delta^{++},\Delta^+,\Delta^0,\Delta^-)$ can be written as

$$m_{\Delta^{++}} = \tilde{m}_\Delta + \frac{\delta m^1_\Delta}{2}, \quad m_{\Delta^+} = \tilde{m}_\Delta + \frac{\delta m^1_\Delta}{6} + \frac{\delta m^2_\Delta}{2},$$

$$m_{\Delta^0} = \tilde{m}_\Delta - \frac{\delta m^1_\Delta}{6} + \frac{\delta m^2_\Delta}{2}, \quad m_{\Delta^-} = \tilde{m}_\Delta - \frac{\delta m^1_\Delta}{2},$$

where $\delta m^1_\Delta/\delta m^2_\Delta$ denote the equidistant/nonequidistant splittings and the mass $\tilde{m}_\Delta$ contains an isospin-invariant shift δm_Δ defined as $\tilde{m}_\Delta = \mathring{m}_\Delta + \delta m_\Delta$, with $\mathring{m}_\Delta$ the delta mass in the chiral limit. The leading strong and electromagnetic contributions to the splittings $\delta m^{1,2}_\Delta$ can be read off from the Lagrangians in Eq. (2.49). While both strong and electromagnetic terms contribute to the equi-

distant splitting δm_Δ^1, the nonequidistant one at this order of pure electromagnetic origin. Epelbaum *et al.* (2008a) determined the values for $\bar{m}_\Delta$ and $\delta m_\Delta^{1,2}$ from the most recent particle data group values for $m_{\Delta^{++}} = 1230.80 \pm 0.30$ MeV and $m_{\Delta^0} = 1233.45 \pm 0.35$ MeV (Amsler *et al.*, 2008) together with the average mass $m_\Delta \equiv (m_{\Delta^{++}} + m_{\Delta^+} + m_{\Delta^0} + m_{\Delta^-})/4 = 1233$ MeV from Arndt *et al.* (2006) which leads to

$$\delta m_\Delta^1 = -5.3 \pm 2.0 \text{ MeV}, \quad \delta m_\Delta^2 = -1.7 \pm 2.7 \text{ MeV}. \tag{2.50}$$

If the quark model relation (Rubinstein *et al.*, 1967) $m_{\Delta^+} - m_{\Delta^0} = m_p - m_n$ is employed instead of using the average delta mass, the results change as follows:

$$\delta m_\Delta^1 = -3.9 \text{ MeV}, \quad \delta m_\Delta^2 = -0.3 \pm 0.3 \text{ MeV}, \tag{2.51}$$

which is consistent with Eq. (2.50). Notice that the values for $\delta m_\Delta^{1,2}$ are of natural size. Indeed, based on naive dimensional analysis one expects $|\delta m_\Delta^1| \sim \epsilon M_\pi^2 / M_\rho \sim 8$ MeV and $|\delta m_\Delta^2| \sim e^2 M_\rho / (4\pi)^2 \sim 0.5$ MeV. For a related discussion on the delta mass splittings in chiral EFT with a particular emphasis on their quark mass dependence see Tiburzi and Walker-Loud (2006).

Having determined the values for the delta mass splittings, it is a straightforward (but tedious) exercise to work out the leading Δ contributions to the IB 2π-exchange potential. Notice that the Δ contributions to the 1π-exchange and contact potentials can be taken into account by a redefinition of various LECs and will, therefore, not be discussed. The explicit expressions for the 2π-exchange contributions can be found in Epelbaum *et al.* (2008b). In Fig. 24 we show the CIB and CSB central, tensor, and spin-spin potentials in coordinate space at $\mathrm{N^3LO}$ in the Δ-full theory in comparison with the $\mathrm{N^3LO}$ and $\mathrm{N^4LO}$ results in the Δ-less theory. While in the Δ-less theory, the leading and subleading class-II 2π-exchange potential arises entirely from the pion mass difference δM_π^2 [(see the discussion in Sec. II.B), in the Δ-full theory one also finds contributions proportional to δm_Δ^2]. Although these contributions are numerically small, they provide a clear manifestation of effects which go beyond the subleading order in the Δ-less theory. Furthermore, it is evident from Fig. 24 that the large portion of the $\mathrm{N^4LO}$ CIB 2π-exchange potential in the Δ-less theory is shifted to $\mathrm{N^3LO}$ in the theory with explicit Δ degrees of freedom leading to a more natural convergence pattern. Similarly, a comparison of the corresponding CSB (i.e., class III) potentials in two theories also indicates toward a more natural convergence in the Δ-full with the main part of the unnaturally large subleading contribution in the Δ-less theory being shifted to the lower order. Notice that the CSB 2π-exchange potential at $\mathrm{N^3LO}$ in the Δ-full theory also receives contributions from the delta splitting δm_Δ^1 which are still absent at $\mathrm{N^4LO}$ in the Δ-less theory. For the central value, $\delta m_\Delta^1 = -5.3$ MeV, these contributions are numerically large and tend to cancel the ones driven by the nucleon mass difference leading to a significantly weaker result-

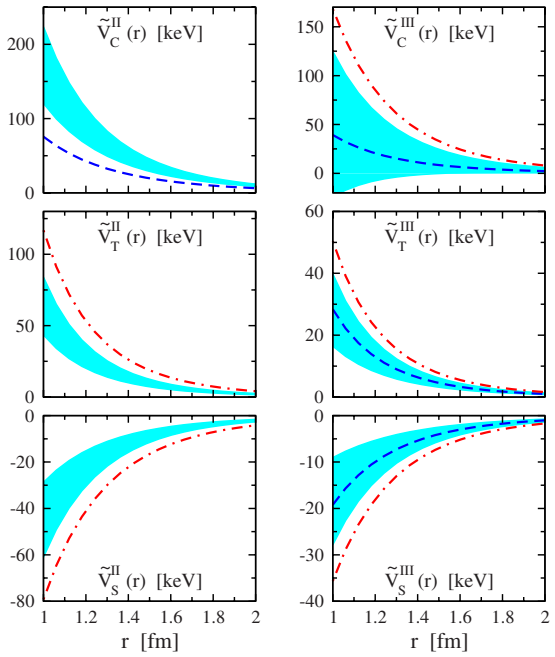

FIG. 24. (Color online) Class-II (left panel) and class-III (right panel) 2π-exchange potentials at $\mathrm{N^3LO}$ in the Δ-full theory (shaded bands) compared to the results in the Δ-less theory at $\mathrm{N^3LO}$ (dashed lines) and $\mathrm{N^4LO}$ (dash-dotted lines). The bands arise from the variation in δm_Δ^1 and δm_Δ^2 according to Eq. (2.50). Notice further that the leading (i.e., $\mathrm{N^3LO}$) contributions to $\tilde{V}_{T,S}^{II}(r)$ and subleading (i.e., $\mathrm{N^4LO}$) contributions to $\tilde{V}_C^{II}(r)$ vanish in the Δ-less theory. In all cases, the spectral function cutoff $\tilde{\Lambda} = 700$ MeV is used.

ing class-III 2π-exchange potentials as compared to the ones at subleading order in the Δ-less theory. This can be viewed as an indication that certain higher-order IB contributions still missing at subleading order in the Δ-less theory are unnaturally large in the theory without explicit delta degrees of freedom. Last but not least, effects from virtual Δ-isobar excitation in the subleading $\pi\gamma$- and 2π-exchange potentials induced by additional one-photon exchange are considered in Kaiser (2006c).

Inclusion of the Δ as an explicit degree of freedom has also important implications for the IB 3NF (Epelbaum *et al.*, 2008a). As discussed in the previous section, the strongest IB 3NF arises from taking into account the charge-to-neutral pion mass difference in the 2π-exchange $3N$ diagrams. In the Δ-less theory, the resulting charge-symmetry conserving 3NF, being formally subleading ($\mathrm{N^3LO}$), is enhanced by the large values of the LECs $c_{4,4}$. In the Δ-full theory, the main part of this strong 2π-exchange contribution appears already at leading order ($\mathrm{N^3LO}$) indicating a more natural convergence pattern. In addition to this obvious effect, one obtains further 2π-exchange contributions at $\mathrm{N^3LO}$ driven by the delta and nucleon mass splittings δm_Δ^2 (charge-symmetry conserving) and δm_Δ^1, δm (charge-symmetry breaking). A close inspection of the resulting expressions, which are all proportional to Δ^{-2}, reveals that they are exactly reproduced in the Δ-less theory by

the saturation of the sub-subleading isospin-conserving (d_i terms in $\mathcal{L}^{(2)}_{\pi N}$) and IB $\pi\pi NN$ vertices. Numerically, the strengths of these CSB 3NFs due to intermediate delta excitation turn out to be rather small, $|\delta m^1_\Delta - 3\delta m_N| g_A^2 h_A^2 M_\pi^6/(432\pi^2 F_\pi^4 \Delta^2) \sim 3$keV, which, however, is comparable to the typical size of the remaining leading CSB 3NF (Epelbaum, Meißner, and Palomar, 2005). $g_A^4 M_\pi^4/(256\pi^2 F_\pi^4) \sim 7$ keV.

E. Few-nucleon reactions involving pions

Few-nucleon reactions involving pions such as, e.g., $\pi d \to \pi d$ (Beane *et al.*, 2003), $\gamma d \to \pi^0 d$ (Beane *et al.*, 1997; Krebs *et al.*, 2004). $\pi\,^3\mathrm{He} \to \pi\,^3\mathrm{He}$ (Baru *et al.*, 2003), $\pi^- d \to \gamma nn$ (Gardestig and Phillips 2006), $\gamma d \to \pi^+ nn$ (Lensky *et al.*, 2007b), and $NN \to NN\pi$ (Baru *et al.*, 2007), where only some of the most recent references are given, provide another fascinating testing ground for the chiral EFT framework. The calculations typically utilize the distorted-wave Born approximation using transition operators derived in chiral EFT and employing either phenomenological or chiral-EFT-based wave functions for the few-nucleon states following Weinberg's original proposal (Weinberg, 1992). An important new ingredient in these applications is the appearance of the momentum scale $p = \sqrt{mM_\pi}$ associated with real pion production which has to be explicitly taken into account and requires an appropriate modification of the power counting (Cohen *et al.*, 1996; Bernard *et al.*, 1999; da Rocha *et al.*, 2000). Such a modified ordering scheme was proposed in Hanhart *et al.* (2000) and applied in Hanhart and Kaiser (2002) to calculate the pion production operator in NN collisions at threshold at NLO. Notice that the rather high energies and momenta of the nucleons in the initial state require the inclusion of the Δ isobar as an explicit degree of freedom. As a characteristic feature of the modified power counting scheme, one observes the appearance of half-integer powers of the small parameter $\chi = M_\pi/m$ in the expansion of the transition operators. One also finds that some pion loop contributions are promoted to significantly lower orders compared to what is expected from Weinberg's original power counting. An application of the modified power counting to P-wave pion production in NN collisions up to N^{2}LO is carried out in Hanhart *et al.* (2000). At this order, only tree diagrams have to be considered. The calculations showed a satisfactory agreement with the data and also demonstrated the feasibility to extract the LEC D which enters the leading 3NF [see Eq. (2.22)] from this reaction. Notice, however, that concerns have been raised in Nakamura (2008) regarding the convergence of the chiral expansion in this reaction. For S-wave pion production, one-loop diagrams already start to contribute at NLO. As pointed out in Lensky *et al.* (2006), it is important to properly separate the truly irreducible contributions in the loop diagrams from the reducible ones in order for the resulting pion production operator to be renormalizable. Numerically, the NLO loop diagrams were found to provide an important contribution to the cross section for $pp \to d\pi^+$. Parametrizing the near-threshold cross section for this reaction as $\sigma = \alpha\eta + \mathcal{O}(\eta^3)$, where η denotes the outgoing pion momentum in units of its mass, the pion S-wave contribution at LO and NLO was found to be $\alpha^{\mathrm{LO}} = 131$ μb and $\alpha^{\mathrm{NLO}} = 220$ μb, respectively (Lensky *et al.*, 2006). The result at NLO agrees nicely with various existing data sets (see Fig. 25). A comprehensive review of meson production reactions in nucleon-nucleon collisions can be found in Hanhart (2004).

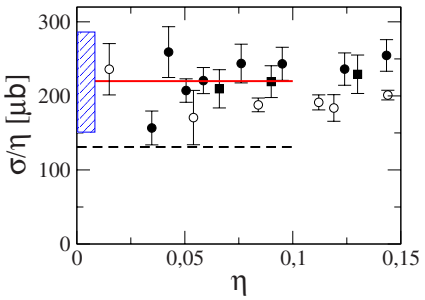

FIG. 25. (Color online) LO (dashed line) and NLO (solid line) results for the total cross section for the reaction $pp \to d\pi^+$ in comparison with the data from Hutcheon *et al.*, 1991 (open circles), Heimberg *et al.*, 1996 (filled circles), and Drochner *et al.*, 1998 (filled squares). The hatched area gives the estimated uncertainty at NLO. Figure is courtesy of C. Hanhart.

Pion production reactions in few-nucleon systems also proved useful to study isospin-violating effects. Recent measurements of the forward-backward asymmetry in the process $pn \to d\pi^0$ (Opper *et al.*, 2003) and the total cross section in the reaction $dd \to \alpha\pi^0$ (Stephenson *et al.*, 2003) yielded a clear evidence of charge-symmetry breaking and serve as excellent testing ground to study isospin violation in the nuclear force and the corresponding transition operators. The first steps toward the theoretical understanding of these reactions have been taken in van Kolck *et al.* (2000) and Gardestig *et al.* (2004); and Nogga *et al.* (2006), respectively. Notice that the appearance of the four-nucleon continuum states makes the theoretical analysis of the process $dd \to \alpha\pi^0$ particularly challenging. We further emphasize that new data on this reaction will be provided by WASA at COSY (Adam *et al.*, 2004). Further details on these studies and related issues can be found in a recent review article (Miller *et al.*, 2006).

The role of the momentum scale $p = \sqrt{mM_\pi}$ and the related issue of the nucleon recoil effects in reactions such as, e.g., πd scattering and pion photoproduction and electroproduction off the deuteron was investigated in the context of chiral EFT in Baru *et al.* (2004) and Lensky *et al.* (2005, 2007a). In particular, it was realized that the importance of the recoil effects in a given process is directly connected to the Pauli principle for the nucleons in the intermediate states. Notice further that the reaction $\gamma d \to nn\pi^+$ (Lensky *et al.*, 2007b) and the similar process $\pi^- d \to \gamma nn$ (Gardestig and Phillips, 2006) were proposed as a tool to extract the value of the neutron-neutron S-wave scattering length. For more de-

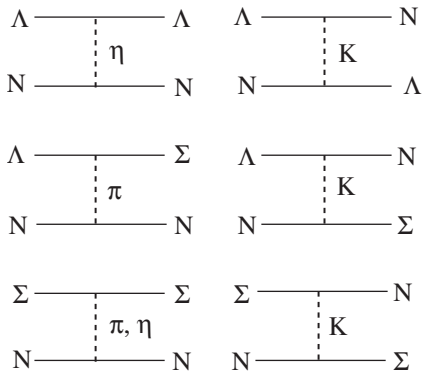

FIG. 26. One-pseudoscalar-meson-exchange diagrams at LO for the hyperon-nucleon interaction.

tails on these and related reactions see Hanhart (2007).

F. Hyperon-nucleon and hyperon-hyperon interactions

The effects of strange quarks in nuclear matter can, e.g., be tested through the determination of the properties of so-called hypernuclei, in which one (or two) nucleon(s) is (are) substituted by a hyperon (hyperons). Such hypernuclei are produced by strangeness-exchange reactions, by associated strangeness production, or by electroproduction reactions at many laboratories worldwide, such as CERN, BNL, KEK, DAΦNE, JLab, MAMI, and GSI [see, e.g., Alberico and Garbarino (2002)]. More generally, nuclear physics with strange quarks has a broad impact on contemporary physics since it lies at the intersection of nuclear and elementary particle physics. Moreover, it has significant implications to the astrophysics of compact objects. Recent progress in the field is reviewed in Bydzovsky *et al.* (2007).

The hyperon-nucleon (YN) interaction is at the heart of the hypernuclear binding and thus a precise determination of its various components is of utmost importance. Here the situation is quite different compared to the two-nucleon case. The data based on YN scattering are quite poor, thus a partial wave analysis is not available and in any theoretical approach one must directly compare to data. The poor status of our information on the YN interaction is most clearly reflected in the present knowledge of the ΛN scattering lengths. For example, Alexander *et al.* (1968) gave for the singlet (s) and triplet (t) scattering lengths $a_s = -1.8^{+2.3}_{-4.2}$ fm, $a_t = -1.8^{+1.1}_{-0.8}$ fm, whereas in the six variants of the Nijmegen soft-core potential model a_s varies in the range $-2.5, \ldots, -0.7$ fm and a_t in the range $-2.2, \ldots, -1.8$ fm (Rijken *et al.* 1999). In the most modern version of the Jülich meson-exchange model one finds $a_s \simeq -2.6$ fm and $a_t \simeq -1.7$ fm (Haidenbauer and Meißner, 2005). However, for the EFT approach it is important to note that all these values are of natural size. For a proposal to extract these scattering lengths with high precision from production data, see Gasparyan *et al.* (2004). Furthermore, since the masses of the Λ and the Σ hyperons are only about 75 MeV apart, the coupling between the ΛN and ΣN channels needs to be taken into account. Moreover, for a sensible comparison with experimental data, it is preferable to solve the scattering equation in the particle basis because then the Coulomb interaction in the charged channels can be incorporated.

The hyperon-nucleon YN interaction has not been investigated using EFT as extensively as the NN interaction. Hyperon and nucleon mass shifts in nuclear matter, using chiral perturbation theory, have been studied in Savage and Wise (1996). They used a chiral interaction containing four-baryon contact terms and pseudoscalar-meson exchanges. The hypertriton (a bound state of a proton, a neutron, and a Λ) and Λd scattering were investigated in the framework of an EFT with contact interactions (Hammer, 2002). Korpa *et al.* (2002) performed a next-to-leading-order (NLO) EFT analysis of YN scattering and hyperon mass shifts in nuclear matter. Three tree-level amplitude contains four-baryon contact terms; pseudoscalar-meson exchanges were not considered explicitly, but SU(3) breaking by meson masses was modeled by incorporating dimension two terms coming from one-pion exchange. The full scattering amplitude was calculated using the Kaplan-Savage-Wise resummation scheme. The hyperon-nucleon scattering data were described successfully for laboratory momenta below

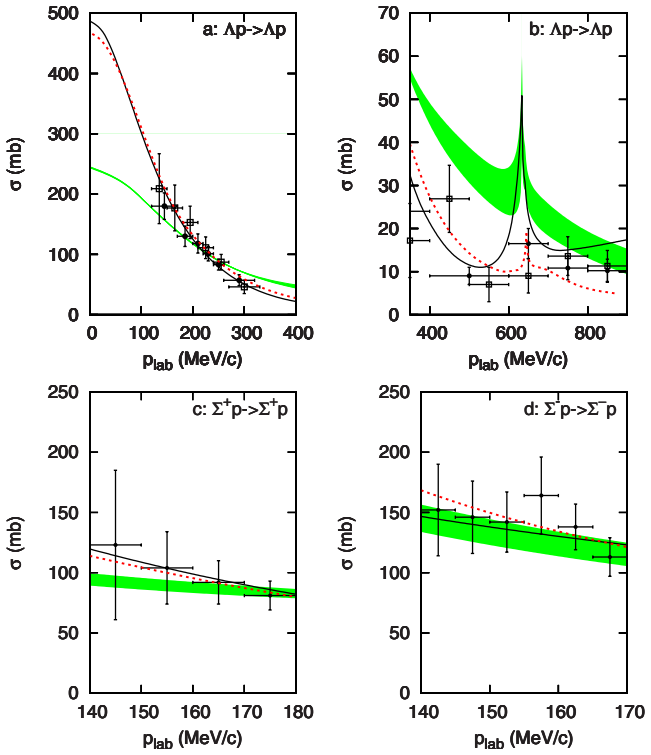

FIG. 27. (Color online) Total cross sections as a function of $p_{\rm lab}$ for $\Lambda p \to \Lambda p$ and $\Sigma^{\pm} p \to \Sigma^{\pm} p$. The shaded band is the LO EFT result for $\Lambda = 550, \ldots 700$,MeV, the dashed curve is the Jülich 04 model (Haidenbauer and Meißner, 2005), and the solid curve is the Nijmegen NSC97f model (Rijken *et al.* 1999). Note that the total cross sections for $\Sigma^{\pm} p \to \Sigma^{\pm} p$ are obtained by integrating the differential data in a limited angular range (see Eisele *et al.*, 1971).

TABLE I. The isospin factors for the various one-pseudoscalar-meson exchanges contributing to the hyperon-nucleon interaction.

Channel	Isospin	π	K	η
	0	−3	0	1
$NN\to NN$	1	1	0	1
$\Lambda N\to\Lambda N$	$\frac{1}{2}$	0	1	1
$\Lambda N\to\Sigma N$	$\frac{1}{2}$	$-\sqrt{3}$	$-\sqrt{3}$	0
	$\frac{1}{2}$	−2	−1	1
$\Sigma N\to\Sigma N$	$\frac{3}{2}$	1	2	1

200 MeV using 12 free parameters. Some aspects of strong ΛN scattering in effective field theory and its relation to various formulations of lattice QCD are discussed in Beane *et al.* (2005).

Within the Weinberg counting scheme, a detailed investigation of the YN interaction at LO was presented in Polinder *et al.* (2006). At LO, the YN potential is given by one-pseudoscalar-Goldstone-boson exchange diagrams (cf. Fig. 26) and contact interactions without derivatives. The spin-space part of the one-pseudoscalar-meson-exchange potential resulting from the LO SU(3) effective chiral meson-baryon Lagrangian is

$$V^{B_1B_2\to B_1'B_2'}=-f_{B_1B_1'P}f_{B_2B_2'P}\frac{\vec{\sigma}_1\cdot\vec{k}\,\vec{\sigma}_2\cdot\vec{k}}{\vec{k}^2+m_P^2},\tag{2.52}$$

where $\vec{k}$ is the momentum transfer, $P=\pi,K,\eta$, and the $f_{B_1B_1'P}$, $f_{B_2B_2'P}$ are the appropriate coupling constants,

$$f_{NN\pi}=f,\quad f_{NN\eta_8}=\frac{1}{\sqrt{3}}(4\alpha-1)f,$$

$$f_{\Lambda NK}=-\frac{1}{\sqrt{3}}(1+2\alpha)f,\quad f_{\Xi\Xi\pi}=-(1-2\alpha)f,$$

$$f_{\Xi\Xi\eta_8}=-\frac{1}{\sqrt{3}}(1+2\alpha)f,\quad f_{\Xi\Lambda K}=\frac{1}{\sqrt{3}}(4\alpha-1)f,$$

$$f_{\Lambda\Sigma\pi}=\frac{2}{\sqrt{3}}(1-\alpha)f,\quad f_{\Sigma\Sigma\eta_8}=\frac{2}{\sqrt{3}}(1-\alpha)f,$$

$$f_{\Sigma NK}=(1-2\alpha)f,\quad f_{\Sigma\Sigma\pi}=2\alpha f,$$

$$f_{\Lambda\Lambda\eta_8}=-\frac{2}{\sqrt{3}}(1-\alpha)f,\quad f_{\Xi\Sigma K}=-f.\tag{2.53}$$

in terms of the coupling constant $f\equiv g_A/2F_\pi$ and the $F/(F+D)$ ratio α (de Swart, 1963). The corresponding isospin factors for the various channels multiplying the spin-space part of the potential in Eq. (2.52) are tabulated in Table I.

It is important to stress that while the interaction potential at LO is SU(3) symmetric, the kinematics of the various channels and the masses of the exchanged mesons are to be taken at their physical values. The LO contact terms for the octet baryon-baryon interactions, which are Hermitian and invariant under Lorentz transformations, are given by the SU(3) invariants,

$$\mathcal{L}^1=C_i^1\langle\bar{B}_a\bar{B}_b(\Gamma_iB)_b(\Gamma_iB)_a\rangle,$$

$$\mathcal{L}^2=C_i^2\langle\bar{B}_a(\Gamma_iB)_a\bar{B}_b(\Gamma_iB)_b\rangle,$$

$$\mathcal{L}^3=C_i^3\langle\bar{B}_a(\Gamma_iB)_a\rangle\langle\bar{B}_b(\Gamma_iB)_b\rangle.\tag{2.54}$$

Here a and b denote the Dirac indices of the particles, B is the usual irreducible octet representation of SU(3) given by

$$B=\begin{pmatrix}\frac{\Sigma^0}{\sqrt{2}}+\frac{\Lambda}{\sqrt{6}} & \Sigma^+ & p\\ \Sigma^- & -\frac{\Sigma^0}{\sqrt{2}}+\frac{\Lambda}{\sqrt{6}} & n\\ -\Xi^- & \Xi^0 & -\frac{2\Lambda}{\sqrt{6}}\end{pmatrix},\tag{2.55}$$

and the brackets denote taking the trace in the three-dimensional flavor space. As an example, we display the resulting partial wave potentials for $\Lambda N\to\Lambda N$,

$$V_{^1S_0}^{\Lambda\Lambda}=4\pi[\tfrac{1}{6}(C_S^1-3C_T^1)+\tfrac{5}{3}(C_S^2-3C_T^2)+2(C_S^3-3C_T^3)]$$

$$V_{^3S_1}^{\Lambda\Lambda}=4\pi[\tfrac{3}{2}(C_S^1+C_T^1)+(C_S^2+C_T^2)+2(C_S^3+C_T^3)].\tag{2.56}$$

Similar expression for the isospin-1/2 and -3/2 $\Sigma N\to\Sigma N$ and the $\Lambda N\to\Sigma N$ potentials are given in Polinder *et al.* (2006). Note that only five of the $\{8\}\times\{8\}=\{27\}+\{10\}+\{10^*\}+\{8\}_s+\{8\}_a+\{1\}$ representations are relevant for NN and YN interactions since the $\{1\}$ occurs only in the $\Lambda\Lambda$, ΞN, and $\Sigma\Sigma$ channels. Equivalently, the six contact terms, C_S^1, C_T^1, C_S^2, C_T^2, C_S^3, C_T^3, enter the NN and YN potentials in only five different combinations. These five contact terms need to be determined by a fit to the experimental data. The resulting chiral potential $V^{\rm LO}=V_{\rm OBE}+V_{\rm cont}$ in the Lippmann-Schwinger equation is regulated with a regulator function $f_\Lambda(p,p')=\exp[-(p^4+p'^4)/\Lambda^4]$, where the cutoff Λ is varied between 550 and 700 MeV. A fit to 35 low-energy data [total cross sections from Engelmann *et al.* (1966), Alexander *et al.* (1968), Sechi-Zorn *et al.* (1968), and Eisele *et al.* (1971) for $\Lambda p\to\Lambda p$, $\Sigma^-p\to\Lambda n$, $\Sigma^\pm p\to\Sigma^\pm p$, and $\Sigma^-p\to\Sigma^0n$ with hyperon laboratory momenta between 110 and 300 MeV and the inelastic capture ratio at rest (de Swart and Dullemond, 1962)] gives a good description of the data (see Fig. 27), with contact interactions of natural size.

Note the strong cusp effect in Λp scattering at the opening of the Σ^+n threshold at $p_{\rm lab}\simeq 600$ MeV [Fig. 27(b)]. The chiral EFT also yields a correctly bound hy-

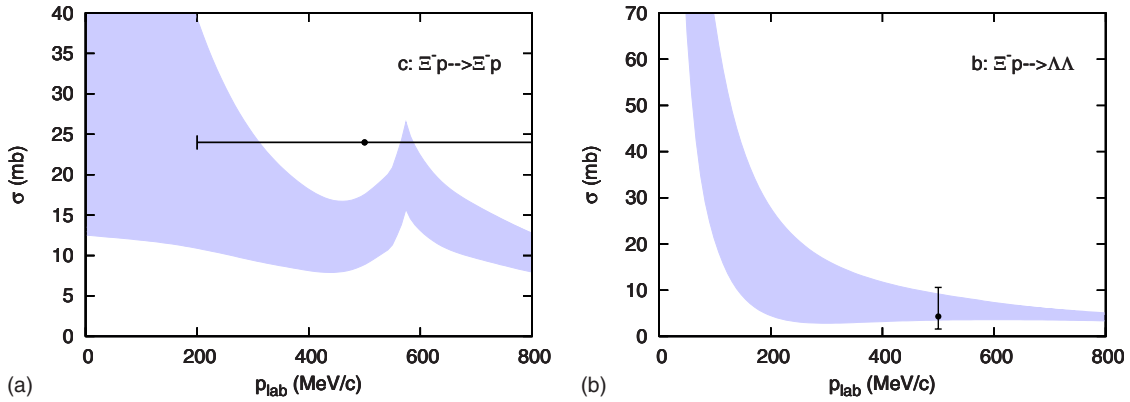

FIG. 28. (Color online) Total cross sections as a function of $p_{\rm lab}$ for $\Xi^- p \to \Xi^- p$ (left panel) and $\Xi^- p \to \Lambda\Lambda$ (right panel). The shaded band is the LO EFT result for $\Lambda = 600$ MeV and varying the LEC $C_{^1S_0}^{\Lambda\Lambda}$ of the additional singlet contact term within natural bounds given a mildly attractive interaction in the $^1S_0$ channel of the $\Lambda\Lambda$ interaction.

pertriton (Haidenbauer *et al.*, 2007) if one fixes the relative strength of the singlet and triplet S waves accordingly. A Λp singlet scattering length of −1.9 fm leads to the correct binding energy. The corresponding triplet scattering length is $a_t^{\Lambda p} = -1.2$ fm and in the $\Sigma^+ p$ system, one finds $a_s = -2.3$ and $a_t = -0.7$ fm. It is quite astonishing that with only six parameters (five LECs and the cutoff Λ) one achieves a quite satisfactory description of the admittedly not very precise YN scattering data. Clearly, a NLO calculation should be performed and fits should be done simultaneously to YN. and NN data. For a more detailed discussion of these results and a comparison to more conventional approaches to the YN interaction, see Polinder *et al.* (2006) and Haidenbauer *et al.* (2007).

The experimental situation on baryon-baryon scattering with $S = -2$, i.e., in the YY and the ΞN, channels, is even poorer. Only recently doubly strange baryon-baryon scattering data at lower energies, below $p_{\rm lab} = 0.8$ GeV, were deduced for the first time (Tamagawa *et al.*, 2001; Ahn *et al.*, 2006). An upper limit of 24 mb at 90% confidence level was provided for elastic $\Xi^- p$ scattering, and for the $\Xi^- p \to \Lambda\Lambda$ cross section at $p_{\rm lab} = 500$ MeV a value of $4.3^{+6.3}_{-2.7}$ mb was reported (Ahn *et al.*, 2006). Within LO chiral EFT, baryon-baryon scattering was analyzed in Polinder *et al.* (2007). The contact terms and the couplings of the pseudoscalar mesons to the baryons are related via SU(3) symmetry to the $S = -1$ hyperon-nucleon channels. There is one additional contact interaction whose strength was varied within natural bounds in the $\Lambda\Lambda \to \Lambda\Lambda$ channel. This fixes its contribution in all other $S = -2$ baryon-baryon channels because of SU(3) symmetry. As a constraint, the information deduced from the recent candidate for ${}^{\;\;6}_{\Lambda\Lambda}$He with a low binding energy (Takahashi *et al.* 2001), the so-called Nagara event, which suggests that the $\Lambda\Lambda$ interaction should be only moderately attractive, was imposed. For a fixed cutoff, the prediction of the $\Xi^- p \to \Xi^- p$ and the $\Xi^- p \to \Lambda\Lambda$ total cross section in comparison to the available data is shown in Fig. 28. The resulting $\Lambda\Lambda$ scattering length in the $^1S_0$ channel is $a_s = -1.83, \ldots, -1.38$ fm. For comparison, in the Nijmegen ESC04 model one finds in this channel $a_s = -1.32$ fm (Rijken and Yamamoto, 2006) and in the constituent quark model of Fujiwara *et al.* (2007), one has $a_s = -0.81$ fm. Note also that this contact interaction does not contribute to certain channels, so that at LO one can make parameter-free predictions for $\Sigma^+\Sigma^+ \to \Sigma^+\Sigma^+$, $\Xi^0 p \to \Xi^0 p$, and $\Xi^0 p \to \Sigma^+\Lambda$. It is expected that in the future better-quality data on the fundamental ΞN and YY interactions as well as much more information about the physics of hypernuclei will become available at the new facilities J-PARC (Japan) and FAIR (Germany). The chiral EFT developed by Polinder *et al.* (2007) can then be used to analyze these upcoming data in a model-independent way.

G. Nuclear lattice simulations

Once the chiral nuclear forces are determined and the low-energy constants appearing in the nuclear forces are fitted (in the two- and three-nucleon sectors) one can make predictions in the four- and more-nucleon sectors based on chiral EFT. However, the explicit numerical treatment of, e.g., the Yakubowsky equations for more than four nucleons is a very difficult task. One possible scheme to solve the many-body problem is to put the chiral effective potential on the lattice and apply powerful Monte Carlo techniques which are already developed to high degree in lattice QCD. One unique feature of the lattice effective field theory approach is the ability to study in one formalism both few- and many-body systems as well as zero- and nonzero-temperature phenomena. A large portion of the nuclear phase diagram can be studied using exactly the same lattice action with exactly the same operator coefficients. A second feature is the computational advantage of many efficient Euclidean lattice methods developed for lattice QCD and condensed matter applications. This includes the use of Markov chain Monte Carlo techniques, Hubbard-Stratonovich transformations, and nonlocal updating schemes such as a hybrid Monte Carlo technique. A third feature is the close theoretical link between

nuclear lattice simulations and chiral effective field theory. One can write down the lattice Feynman rules and calculate lattice Feynman diagrams using precisely the same action used in the nonperturbative simulation. Since the lattice formalism is based on chiral effective field theory, we have a systematic power counting expansion, an *a priori* estimate of errors for low-energy scattering, and a clear theoretical connection to the underlying symmetries of QCD. The first studies combining lattice methods with effective field theory for low-energy nuclear physics looked at infinite nuclear and neutron matter at nonzero density and temperature (see Sec. III.E). Most of the formalism for chiral EFT on the lattice was developed by Lee *et al.* (2004). Nuclear lattice simulations were used to study the triton at leading order in pionless effective field theory with three-nucleon interactions (Borasoy *et al.*, 2006).

We now discuss the principles underlying such nuclear lattice simulations [for a detailed discussion, see Lee *et al.* (2004) and Borasoy *et al.* (2007a)]. In this framework, nucleons are represented as pointlike Grassman fields and pions as pointlike instantaneous pseudoscalar fields. The lattice is defined by a volume $L^3 \times L_t$, with L (L_t) as the spatial (temporal) size. The corresponding lattice spacings are called a and a_t, respectively. Typically, calculations are carried out using a lattice length $L \simeq 20$ fm and the lattice spacing $a \simeq 2$ fm which corresponds to the cutoff $\Lambda = \pi/a \simeq 300$ MeV. At present, computational resources prevent one from using smaller lattice sizes (larger UV cutoffs). Still, the use of various forms of improved actions allows one to access the systematic errors inherent in such simulations.

The basic quantity in nuclear lattice simulations is the correlation function. For A nucleons in Euclidean space it is defined by

$$Z_A(t) = \langle \Psi_A | \exp(-\tau H) | \Psi_A \rangle, \tag{2.57}$$

where $|\Psi_A\rangle$ refers to a Slater determinants for A free nucleons, H is the Hamiltonian of the system, and τ is the Euclidean time. The ground state energy of the A-nucleon system can be derived from the asymptotic behavior of the correlation function for large τ,

$$E_A^0 = -\lim_{\tau \to \infty} \frac{d}{d\tau} \ln Z_A(\tau). \tag{2.58}$$

The expectation value of any normal-ordered operator $\mathcal{O}$ can be derived in a similar way by

$$\langle \Psi_A^0 | \mathcal{O} | \Psi_A^0 \rangle = \lim_{\tau \leftarrow -\infty} \frac{Z_A^{\mathcal{O}}(\tau)}{Z_A(\tau)},$$

$$Z_A^{\mathcal{O}}(t) = \langle \Psi_A | \exp(-\tau H/2) \mathcal{O} \exp(-\tau H/2) | \Psi_A \rangle, \tag{2.59}$$

where $|\Psi_A^0\rangle$ denotes the ground state of the A-nucleon system. It is convenient to describe NN contact interactions by standard bilinear nucleon density operators using the Hubbard-Stratonovich transformation. Using $\exp(\rho^2/2) \sim \int ds \exp(-s^2/2 - s\rho)$ one can express terms quadratic in the nucleon density operator ρ as terms linear in ρ in the presence of auxiliary background fields (collectively denoted by s). In this representation, the full correlation function is related to the path integral over pions and auxiliary fields,

$$Z_A(t) = \mathcal{N} \int Ds \prod_{I=1,2,3} D\pi_I Ds_I \exp(-S_{\pi\pi} - S_{ss}) \times \langle \Psi_A | M^{(L_t-1)}(\pi_I, s, s_I) \cdots M^{(0)}(\pi_I, s, s_I) | \Psi_A \rangle. \tag{2.60}$$

Here $S_{\pi\pi}$ and S_{ss} are free actions for pions and auxiliary fields s, s_I (where s/s_I couples to the isospin-independent/-dependent nucleon bilinear), I denotes isospin indices and $\mathcal{N}$ is an (irrelevant) normalization constant. $M^{(n)}$ is a transfer matrix defined as an n'th step in the temporal direction. We note that the amplitude $\langle \Psi_A | M^{(L_t-1)}(\pi_I, s_i) \cdots M^{(0)}(\pi_I, s_i) | \Psi_A \rangle$ is just a Slater determinant of single nucleon matrix elements $\mathcal{M}_{i,j}$, with $i, j = 1, \ldots, A$.

To be specific, we give here the leading order action starting with the free theory. The presentation here is somewhat sketchy. For an extensive discussion see Borasoy *et al.* (2007a). The free actions for the auxiliary fields and the pions are

$$S_{ss}(s, s_I) = \frac{1}{2} \sum_{\vec{n}} s(\vec{n})^2 + \frac{1}{2} \sum_{I=1}^{3} \sum_{\vec{n}} s_I(\vec{n})^2,$$

$$S_{\pi\pi}(\pi_I) = \frac{\alpha_t}{2} \sum_{I=1}^{3} \sum_{\vec{n}} \pi_I(\vec{n})(-\Delta + M_\pi^2) \pi_I(\vec{n}), \tag{2.61}$$

where M_π is the physical pion mass and $\alpha_t = a_t/a$. For nucleons one may use an $O(a^4)$ improved free lattice Hamiltonian defined by

$$H_{\text{free}} = \frac{1}{m} \sum_{k=0}^{3} \sum_{\vec{n}_s, \hat{l}_s, i,j} f_k \{ a_{i,j}^\dagger(\vec{n}_s) [a_{i,j}(\vec{n}_s + k\hat{l}_s) + a_{i,j}(\vec{n}_s - k\hat{l}_s)] \}, \tag{2.62}$$

where the operators $a_{i,j}^\dagger(\vec{n}_s)$ and $a_{i,j}(\vec{n}_s)$ are the nucleon creation and annihilation operators, $\vec{n}_s$ are spatial coordinates, $\hat{l}_s$ are spatial unit vectors, the indices i and j represent spin and isospin indices, respectively, and the coefficients f_k are $f_{0,1,2,3} = 49/2, -3/4, 3/40, -1/180$. To define the interactions one introduces nucleon-density operators with different spin or isospin polarizations,

$$\rho^{a^\dagger, a}(\vec{n}_s) = \sum_{i,j} a_{i,j}^\dagger(\vec{n}_s) a_{i,j}(\vec{n}_s),$$

$$\rho_I^{a^\dagger, a}(\vec{n}_s) = \sum_{i,j,j'} a_{i,j'}^\dagger(\vec{n}_s) [\tau_I]_{j',j} a_{i,j}(\vec{n}_s),$$

$$\rho_{I,S}^{a^\dagger, a}(\vec{n}_s) = \sum_{i,i',j,j'} a_{i',j'}^\dagger(\vec{n}_s) [\sigma_S]_{i',i} [\tau_I]_{j',j} a_{i,j}(\vec{n}_s). \tag{2.63}$$

The transfer matrix for n_tth step has, besides the free part, two important contributions,

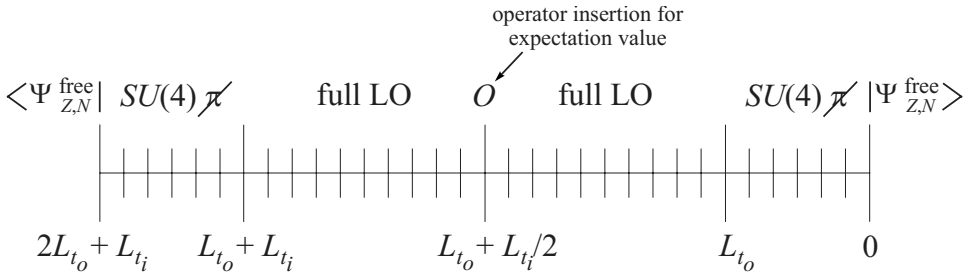

FIG. 29. Overview of the various pieces of the transfer matrix calculation.

$$M^{(n_t)} =: \exp\Bigg\{ - H_{\text{free}}\alpha_t - \frac{g_A\alpha_t}{2F_\pi}\sum_{S,I}\sum_{\vec{n}_s}\nabla_S\pi_I(\vec{n}_s,n_t)\rho^{a^\dagger,a}_{S,I}(\vec{n}_s) + \sqrt{-C\alpha_t}\sum_{\vec{n}_s}\Bigg[s(\vec{n}_s,n_t)\rho^{a^\dagger,a}(\vec{n}_s) + i\sqrt{C_I\alpha_t}\sum_I s_I(\vec{n}_s,n_t)\rho^{a^\dagger,a}_I(\vec{n}_s)\Bigg]\Bigg\}:. \tag{2.64}$$

Here $::$ denotes normal ordering. The first long-range contribution $\sim g_A$ includes the instantaneous pion-nucleon interaction and describes the one-pion exchange in the leading-order effective potential. The second short-range contribution corresponds to the NN contact interactions. The low-energy constants $C=C_S-2C_T$ and $C_I=-C_T$ (cf. Sec. II.B) have different signs, $C<0, C_I>0$. With these signs the pionless theory can be shown to have no sign oscillations if the number of protons and neutrons are equal and they stay pairwise in isospin-singlet states. In this case the multiplication with τ_2 of the single-nucleon matrix elements $\mathcal{M}$ from left and right is well defined and gives $\tau_2\mathcal{M}\tau_2=\mathcal{M}^*$. For this reason, the determinant of $\mathcal{M}$ is real, $\det\mathcal{M}^*=\det\mathcal{M}$. Since τ_2 is antisymmetric, the eigenvalues of $\mathcal{M}$ are doubly degenerate. This leads to a positive Slater determinant (Chen and Kaplan, 2004; Lee, 2004),

$$\det\mathcal{M}\geqslant 0. \tag{2.65}$$

The introduction of pions causes small sign oscillations which, however, are not severe and appear to be suppressed.

To perform simulations in a most efficient way one exploits the approximate SU(4)-Wigner (Wigner, 1937) symmetry in the NN system. The symmetry transformation is given by independent rotations of the spin and isospin degrees of freedom,

$$\delta N = \alpha_{\mu\nu}\sigma^\mu\tau^\nu N \quad \text{with } \sigma^\mu=(1,\vec{\sigma}), \quad \tau^\mu=(1,\vec{\tau}). \tag{2.66}$$

One can show that in the limit where the NN S-wave scattering lengths approach infinity the two-nucleon system becomes invariant under the SU(4) transformation (Mehen *et al.*, 1999). The SU(4)-breaking corrections come from the finite scattering lengths and higher order terms in the chiral expansion; these are of order $\mathcal{O}([1/a(^3S_1)-1/a(^1S_0)],q/\Lambda_\chi)$. Since the NN scattering lengths are very large, the SU(4)-breaking corrections appear to be small. This fact can be used to improve the performance of the lattice simulations. The SU(4) symmetric transfer matrix is given by

$$M^{(n_t)} = :\exp\Bigg[- H_{\text{free}}\alpha_t + \sqrt{-C\alpha_t}\sum_{\vec{n}_s} s(\vec{n}_s,n_t)\rho^{a^\dagger,a}(\vec{n}_s)\Bigg]:. \tag{2.67}$$

In this case there are no sign oscillations for an even number of nucleons (Chen *et al.*, 2004) and one has only one auxiliary field such that the simulations become much cheaper. Although there is no positivity theorem for odd numbers of nucleons, sign oscillations seem to be suppressed also in systems with odd number of nucleons because it is only one particle away from an even system with no sign oscillations. Since the final result is close to the one produced by a SU(4)-symmetric simulation, it pays to divide a simulations into three parts. To simulate the expectation value of some observable one uses SU(4)-symmetric transfer matrices in the first and the last L_{t_0} steps in order to filter the low-energy signal. After this filtering, one starts the simulation with the complete (realistic) transfer matrices. A schematic overview of the transfer matrix calculation is shown in Fig. 29. Having set up the transfer matrix, one utilizes the hybrid Monte Carlo (HMC) method (Duane *et al.*, 1987) to update the field configurations. More specifically, one introduces the conjugate fields p_{π_I}, p_s, p_{s_I} and uses molecular dynamics trajectories to generate new configurations for the fields p_{π_I}, p_s, p_{s_I}, π_I, s, s_I which keep the HMC Hamiltonian

$$H_{\text{HMC}} = \frac{1}{2}\sum_{\vec{n}}\Bigg(\sum_I[p^2_{\pi_I}(\vec{n})+p^2_{s_I}(\vec{n})]+p^2_s(\vec{n})\Bigg) + V(\pi_I,s,s_I) \tag{2.68}$$

constant, where the HMC potential is defined by

$$V(\pi_I,s,s_I) = S_{\pi\pi}+S_{ss}-\log|\det\mathcal{M}|. \tag{2.69}$$

Upon completion of each molecular dynamics trajectory, a Metropolis accept or reject step for the new configuration according to the probability distribution $\exp(-H_{\text{HMC}})$ is applied. This process of molecular dynamics trajectory and Metropolis step is repeated many times.

Already at LO promising results for binding energies, radii, and density correlations for the deuteron, triton, and ^{4}He are obtained (Borasoy *et al.*, 2007a). On a 5^3 lattice, the triton binding energy agrees with experiment

within 5% and the triton root-mean-square radius is accurate to 30%. The binding energy for ^{4}He is within 25% of the experimental value, while the root-mean-square radius agrees within 10%. Note, however, that one has to overcome a zero-range clustering instability that appears for 4 (or more particles) which is mostly a combinatorial effect when more than two particles occupy the same lattice site [for studies of this in other systems, see Lee (2006), and references therein]. To overcome this problem, one can, e.g., smear out the contact interactions with a Gaussian. Such terms improve the lattice action and are formally of higher order [for more details, see, e.g., Borasoy *et al.* (2007a)]. At LO, one can also study the feasibility of simulations for light nuclei with more than four nucleons. It was observed that for $A \leqslant 10$ the CPU time scales approximately linearly with the nucleon number A.

At NLO there appear nine LECs which can be fitted to the Nijmegen *NN* scattering data and deuteron properties. Elastic scattering phase shifts on the lattice are related by Lüscher's formula to the energy levels of two-body states in a finite large volume cubic box with periodic boundary conditions (see Sec. I.E). While this method is useful at low momenta, it is not so useful for determining phase shifts on the lattice at higher energies and higher orbital angular momenta. Furthermore, spin-orbit coupling and partial wave mixing are difficult to measure accurately using Lüscher's method due to multiple-scattering artifacts produced by the periodic cubic boundary conditions. Borasoy *et al.* (2007b) proposed a more robust approach to measure phase shifts for two nonrelativistic point particles on the lattice using a spherical wall boundary. The basic idea is to impose a hard spherical wall boundary on the relative separation between the two interacting particles at some chosen radius. The reason for this spherical wall is to remove copies of the two-particle interactions due to the periodic boundaries on the lattice. This additional boundary condition allows for a direct extraction of the phase shifts and mixing angles from the finite-volume spectrum. For more details, see Borasoy *et al.* (2007b). Using the spherical wall method the values of nine LECs were determined by matching three *S*-wave and four *P*-wave scattering data points, as well as deuteron binding energy and quadrupole moment. In Fig. 30 the *NN* *S*-wave phase shifts and the $^3S_1$-$^3D_1$ mixing angle ϵ_1 for two different actions, called LO_1 and LO_2, are displayed. The action LO_1 is the one given in Eq. (2.64). In the action LO_2 the contact interactions are smeared by a Gaussian. The two actions are identical at leading order and differ only by higher-order terms, thus given an estimate of the higher-order corrections. As can be seen from Fig. 30, the results of the lattice simulations are in a good agreement with the partial wave results for momenta smaller than ~100 MeV. Deviations between the two results for different actions appear merely at larger momenta and

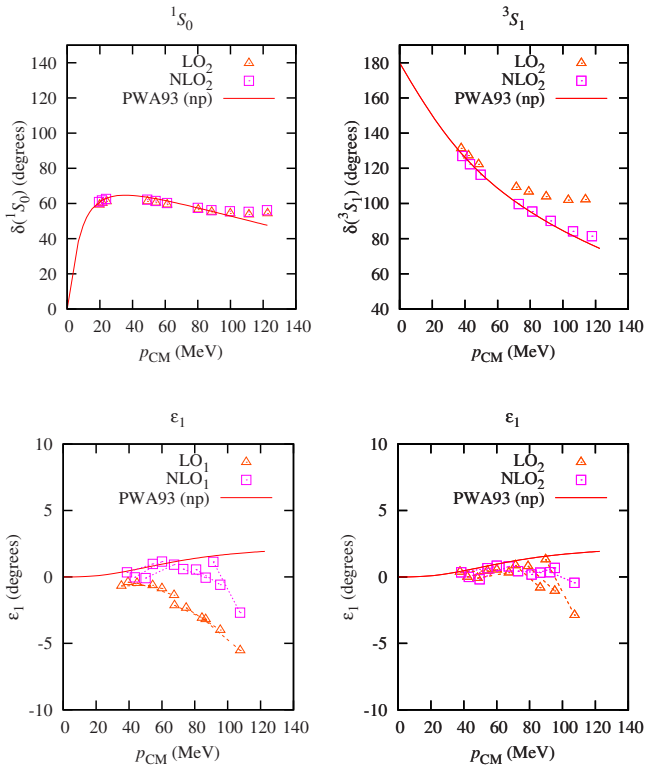

FIG. 30. (Color online) *NN* *S*-wave phase shifts and mixing angles vs center-of-mass momentum with actions LO_1 and LO_2.

are consistent with the expected higher-order effects. In the mean time, a novel action with spin-isospin projected smearing has been developed that gives a good description of the partial waves up to momenta of the order of the pion mass.

At N^{2}LO three-body forces start to show up which depend on two constants. These LECs can be determined from a fit to neutron-deuteron scattering data in the spin-1/2 doublet channel and the triton binding energy. These simulations show a very natural convergence pattern with increasing chiral order. For a box length of ~15 fm the volume dependence already becomes very small and the binding energy approaches its physical value. This is consistent with our expectation that the volume dependence in nuclear lattice EFT simulations should become weak for $L \sim 20$ fm. In Fig. 31 the *S*-wave phase shifts in the spin-3/2 quartet channel versus the square of relative momentum are shown. This channel was not taken into account in the fit procedure. Again one observes a nice convergence with increasing chiral order. The predictions are located between the experimental data for proton-deuteron and neutron-deuteron scattering data. Since isospin breaking was not taken into account in the simulations, the results are very satisfactory. At the same order, the (Coulomb-corrected) binding energy for ^{4}He is overpredicted by 5%, which is consistent with the expected theoretical accuracy of these simulations.

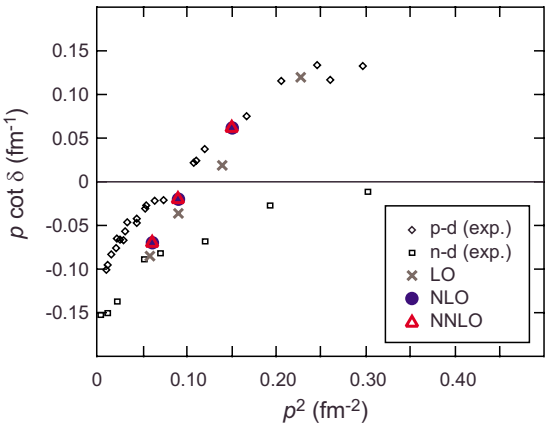

FIG. 31. (Color online) Neutron-deuteron scattering S-wave phase shifts in the spin-3/2 quartet channel vs the square of relative momentum. The data for proton-deuteron and neutron-deuteron scatterings are taken from van Oers and Seagrave, 1967.

The results of these studies demonstrate that lattice EFT is a promising tool for a quantitative description of light nuclei. In the future, it is planned to perform N^{2}LO Monte Carlo simulations of light nuclei and probe neutron matter with larger number of neutrons in a box (see also Sec. III.E). In addition, more detailed studies of finite size effects and further improvements of the lattice action are called for.

H. Quark mass dependence of nuclear forces and IR limit cycle in QCD

The quark mass dependence of the chiral NN interaction was calculated at NLO in the chiral counting in (Beane and Savage (2003) and Epelbaum *et al.* (2003). At this order, the quark mass dependence is synonymous to the pion mass dependence because of the Gell-Mann-Oakes-Renner relation: $M_\pi^2 = -(m_u + m_d)\langle 0|\bar{u}u|0\rangle / F_\pi^2$, where $\langle 0|\bar{u}u|0\rangle \simeq (-290\ \mathrm{MeV})^3$ is the quark condensate. In the following, we therefore refer only to the pion mass dependence which is more convenient for nuclear applications and treat the pion mass as a parameter that can be varied by adjusting the values of the quark masses. In the work of Beane *et al.* (2002), Beane and Savage (2003), and Epelbaum *et al.* (2003) the pion mass dependence of the nucleon-nucleon scattering lengths in the ${}^3S_1$-${}^3D_1$ and ${}^1S_0$ channels as well as the deuteron binding energy, is calculated. To NLO in the chiral power counting, the NN potential can be written as

$$V_{\mathrm{NLO}} = V^{\mathrm{OPE}} + V^{\mathrm{TPE}} + V^{\mathrm{cont}}, \tag{2.70}$$

where V^{OPE}, V^{TPE}, and V^{cont} refer to the one-pion exchange, two-pion exchange, and contact potentials, respectively. Explicit expressions can be found in Epelbaum *et al.* (2003) and Sec. II.B.

In principle, the pion mass dependence of the chiral NN potential is determined uniquely. However, the extrapolation away from the physical pion mass generates errors. The dominating sources are the constants $\bar{C}_{S,T}$ and $\bar{D}_{S,T}$ in V^{cont} which give the corrections to the LO contact terms $\propto M_\pi^2$ and cannot be determined independently from fits to data at the physical pion mass. A smaller effect is due to the error in the LEC $\bar{d}_{16}$, which governs the pion mass dependence of g_A, from the chiral pion-nucleon Lagrangian which is enhanced as one moves away from the physical pion mass. Both effects generate increasing uncertainties as one extrapolates away from the physical point.

In the calculation of Epelbaum *et al.* (2003), the central value $\bar{d}_{16} = -1.23\ \mathrm{GeV}^{-2}$ was used which is the average of three values given by Fettes (2000). In addition, a variation in the LEC $\bar{d}_{16}$ in the range of $\bar{d}_{16} = -0.91, \ldots, -1.76\ \mathrm{GeV}^{-2}$ as given in Fettes (2000) was employed. The size of the two constants $\bar{D}_S$ and $\bar{D}_T$ was constrained from naturalness arguments. It was argued that the corresponding dimensionless constants $F_\pi^2 \Lambda_\chi^2 \bar{D}_{S,T}$ can be expected to satisfy the bounds,

$$-3 \leqslant F_\pi^2 \Lambda_\chi^2 \bar{D}_{S,T} \leqslant 3, \tag{2.71}$$

where $\Lambda_\chi \simeq 1$ GeV is the chiral symmetry breaking scale. A more conservative error estimation was given in Epelbaum, Meißner, and Glöckle (2002). We note that Beane *et al.* (2002) and Beane and Savage (2003) allowed for a larger variation in these LECs. However, the bounds (2.71) are in agreement with resonance saturation estimates and similar relations are obeyed by the LECs whose values are known (Epelbaum, Nogga, Glöckle, Kamada, Meißner, and Witała, 2002). For the constants $C_{S,T}$, this leads to $C_S = -120.8\ \mathrm{GeV}^{-2}$ and $C_T = 1.8\ \mathrm{GeV}^{-2}$ corresponding to the dimensionless coefficients $F_\pi^2 C_S = -1.03$ and $F_\pi^2 C_T = 0.02$, respectively. The unnaturally small value of $F_\pi^2 C_T$ is a consequence of the approximate Wigner SU(4) symmetry.

The ranges from Eq. (2.71) were used to estimate the extrapolation errors of two-nucleon observables such as the deuteron binding energy and the spin-singlet and spin-triplet scattering lengths in Epelbaum *et al.* (2003). The resulting pion mass dependence of the deuteron binding energy is shown in Fig. 32. In the chiral limit the binding energy is of natural size, $B_D \sim F_\pi^2/m \simeq 10$ MeV. Note, however, that in the calculation of Beane *et al.* (2002) and Beane and Savage (2003) the assumed larger uncertainties in the LECs prevent one from making a definite statement about the binding of the deuteron in the chiral limit. For pion masses above the physical value the differences between the two calculations are considerably smaller. The recent study of Mondejar and Soto seems to indicate that two-loop diagrams generate a peculiar quark mass dependence of the contact interactions which are parametrically large (Mondejar and Soto, 2007). The influence of these effects on the quark

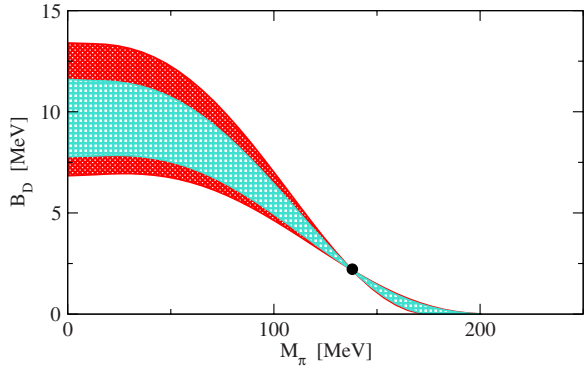

FIG. 32. (Color online) Deuteron binding energy as a function of the pion mass M_π. The shaded areas correspond to the allowed values. The light shaded band gives the uncertainty due to the unknown value of the LECs $\bar{D}_{S,T}$ using the central value $\bar{d}_{16}-1.23$ GeV^{-2}. The dark shaded band gives the uncertainty if, in addition to the variation in $\bar{D}_{S,T}$, the LEC $\bar{d}_{16}$ is varied in the range from $\bar{d}_{16}-0.91$ GeV^{-2} to $\bar{d}_{16}-1.76$ GeV^{-2} given in Fettes, 2000. The heavy dot shows the binding energy for the physical value of the pion mass.

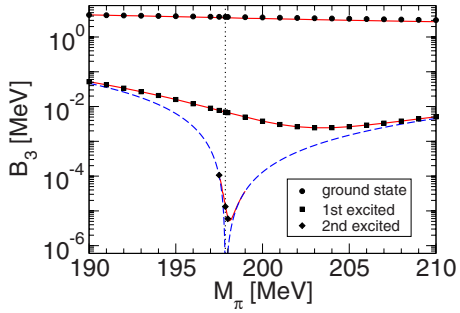

FIG. 34. (Color online) Binding energies B_3 of the triton ground and first two excited states as a function of M_π. The circles, squares, and diamonds give the chiral EFT result, while the solid lines are calculations in the pionless theory. The vertical dotted line indicates the critical pion mass M_π^{crit} and the dashed lines are the bound state thresholds.

mass dependence of, e.g., the deuteron binding energy remains to be worked out in detail. In Fig. 33, we show the inverse scattering lengths in the spin-triplet and spin-singlet channels from Epelbaum *et al.* (2003) together with some recent lattice results (Beane *et al.*, 2006). However, the errors and pion masses are still too large to draw any conclusions about the physical point.

Figure 33 also shows that a scenario where both inverse scattering lengths vanish simultaneously at a critical pion mass of about 200 MeV is possible. For pion masses below the critical value, the spin-triplet scattering length would be positive and the deuteron would be bound. As the inverse spin-triplet scattering length decreases, the deuteron would becomes more and more shallow and finally would become unbound at the critical mass. Above the critical pion mass the deuteron would exist as a shallow virtual state. In the spin-singlet channel, the situation is reversed: the "spin-singlet deuteron" would be a virtual state below the critical pion mass and would become bound above. It is unlikely that this scenario of both inverse scattering lengths vanishing simultaneously is realized in QCD at the physical values of the quark masses. However, based on this behavior it was conjectured that one should be able to reach the critical point by varying the up- and down-quark masses m_u and m_d independently because the spin-triplet and spin-singlet channels have different isospin (Braaten and Hammer, 2003). In this case, the triton would display the Efimov effect which corresponds to the occurrence of an infrared limit cycle in QCD. It is evident that a complete investigation of this issue requires the inclusion of isospin breaking corrections and therefore higher orders in the chiral EFT. However, a number of studies have investigated the universal properties of the limit cycle by considering specific values of $\bar{D}_S$ and $\bar{D}_T$.

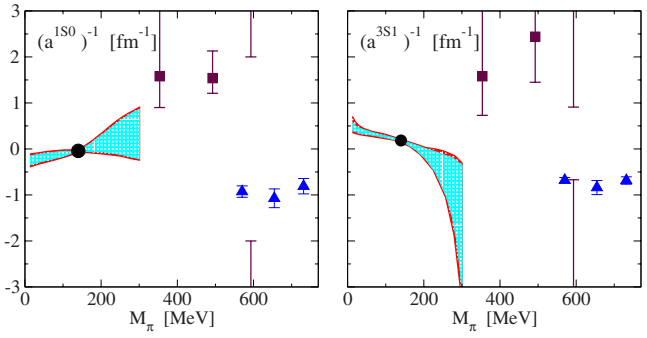

FIG. 33. (Color online) Inverse of the S-wave scattering lengths in the spin-triplet and spin-singlet nucleon-nucleon channels as a function of the pion mass M_π. Filled triangles and rectangles show the lattice calculations from Fukugita *et al.*, 1994, 1995 and Beane *et al.*, 2006, respectively. For remaining notation see Fig. 32.

In an exploratory study of the three-nucleon system (Braaten and Hammer, 2003), the mean values of the error bands from Epelbaum *et al.* (2003) were used as input for the three-body calculations in the pionless EFT. Even though both scattering lengths were large for the mean values, they did not become infinite at the same value of the pion mass and there was no exact limit cycle for this choice of parameters. However, different sets of values for $\bar{D}_S$ and $\bar{D}_T$ that lie within the bound given by Eq. (2.71) and cause the spin-singlet and spin-triplet scattering lengths to become infinite at the same value of the pion mass can be found.

Epelbaum *et al.* (2006) studied the properties of the triton around the critical pion mass for one particular solution with a critical pion mass $M_\pi^{\text{crit}}=197.8577$ MeV. From the solution of the Faddeev equations, the binding energies of the triton and the first two excited states in the vicinity of the limit cycle were calculated for this scenario in chiral EFT. The binding energies are given in Fig. 34 by the circles (ground state), squares (first excited state), and diamonds (second excited state). The dashed lines indicate the neutron-deuteron ($M_\pi \leqslant M_\pi^{\text{crit}}$) and neutron-spin-singlet-deuteron ($M_\pi \geqslant M_\pi^{\text{crit}}$) thresholds

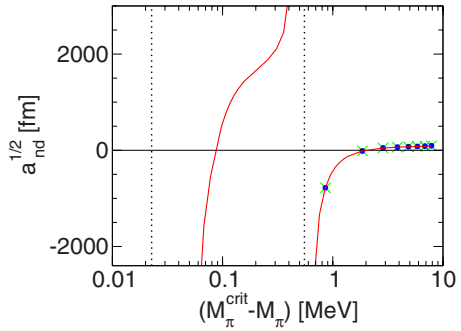

FIG. 35. (Color online) Doublet neutron-deuteron scattering length $a_{nd}^{1/2}$ in the critical region computed in the pionless EFT. The solid line gives the LO result, while the crosses and circles show the NLO and N^{2}LO results. The dotted lines indicate the pion masses at which $a_{nd}^{1/2}$ diverges.

where the three-body states become unstable. Directly at the critical mass, these thresholds coincide with the three-body threshold and the triton has infinitely many excited states. The solid lines are leading-order calculations in the pionless theory using the pion mass dependence of the nucleon-nucleon scattering lengths and one triton state from chiral EFT as input. The chiral EFT results for the other triton states in the critical region are reproduced very well. The binding energy of the triton ground state varies only weakly over the whole range of pion masses and is about one-half of the physical value at the critical point. The excited states are influenced by the thresholds and vary much more strongly.

These studies were extended to N^{2}LO in the pionless EFT and neutron-deuteron scattering observables in Hammer *et al.* (2007). It was demonstrated that the higher-order corrections in the vicinity of the critical pion mass are small. This is illustrated in Fig. 35, where we show the doublet scattering length $a_{nd}^{1/2}$ in the critical region. The solid line gives the LO result, while the crosses and circles show the NLO and N^{2}LO results. The dotted lines indicate the pion masses at which $a_{nd}^{1/2}$ diverges because the second and third excited states of the triton appear at the neutron-deuteron threshold. These singularities in $a_{nd}^{1/2}(M_\pi)$ are a clear signature that the limit cycle is approached in the critical region. Considering the specific case of the doublet scattering length at $M_\pi = 190$ MeV, we have

$$a_{nd}^{1/2}(M_\pi = 190\ \text{MeV}) = 93.18 + 0.80 + 0.14\ \text{fm}. \quad (2.72)$$

At this pion mass we are fairly far away from any singular points in the function $a_{nd}^{1/2}(M_\pi)$. Consequently, the pionless results follow a natural convergence pattern with the expansion parameter γr_0, which is ≈ 0.08 at this value of M_π. For three-body scattering observables in the critical region no calculation in chiral EFT is available. The above example shows that both approaches complement each other. If the pion mass dependence of one three-body observable is known, the pionless theory can be used to predict all other observables with high precision and less computational effort. Figure 35 demonstrates clearly that the pionless theory converges rapidly in the critical region.

A final answer on the question of whether an infrared limit cycle can be realized in QCD can only be given by solving QCD directly. In particular, it would be interesting to know whether this can be achieved by appropriately tuning the quark masses in a lattice QCD simulation (Wilson, 2005). As a first step, the finite volume dependence of Efimov energies in the pionless theory was studied in Kreuzer and Hammer (2009). Finally, we note that the dependence of nuclear binding on hadronic mass variation has also been studied based on the Argonne potential (Flambaum and Wiringa, 2007).

III. TOWARD A MANY-BODY EFT FOR NUCLEI

The EFT approach to the nuclear many-body problem is much less established than the one for the forces and few-nucleon systems. This is, on the one hand, related to the appearance of new scales such as the Fermi momentum or induced by collective excitations and, on the other hand, to the computational problems related to solve the many-body problem. Thus, a variety of pathways is being explored and here we can only give an overview about the existing attempts and their status. For a pedagogical review on the application of EFTs to finite density systems, see Furnstahl *et al.* (2008).

A. In-medium chiral perturbation theory

Early attempts to formulate in-medium chiral perturbation theory were mostly triggered by the pioneering paper of Kaplan and Nelson on kaon condensation (Nelson and Kaplan, 1987). Most of these calculations were based on chiral Lagrangians at most bilinear in the nucleon fields and performed in the mean-field approximation, $\bar{N}DN \to \rho_p \,\mathrm{Tr}\, D_{11} + \rho_n \,\mathrm{Tr}\, D_{22}$ with ρ_p (ρ_n) the proton (neutron) density, D represents a generic differential operator including the coupling to pions and external sources, the trace runs over spinor indices, and the subscripts run in flavor space. Proceeding in this way, one keeps track about the vacuum CHPT Lagrangians, but the chiral counting in the medium is lost, as, e.g., nucleon correlations are not considered. The most elegant formulation of this approach based on the path-integral formulation is due to Wirzba and collaborators [see, e.g., Thorsson and Wirzba (1995) and Kirchbach and Wirzba (1996, 1997)].

To go beyond the mean-field approximation, the in-medium generating functional for pions coupled to nucleons and external sources was developed in Meißner *et al.* (2002) and Oller (2002). Leaving out multinucleon interactions a systematic in-medium CHPT can be developed by expanding around the nuclear matter ground state at asymptotic times and integrating out the nucleon fields in the path integral representation, giving rise to the in-medium generating functional [for the detailed derivation, we refer to Oller (2002)],

$$e^{i\tilde{Z}[v,a,s,p]} = \int [dU] \exp\left\{ i \int dx \mathcal{L}_{\pi\pi} - i \int \frac{d\vec{p}}{(2\pi)^3 2E(p)} \int dx dy e^{ip(x-y)} \mathrm{Tr}(A\,[I_4 - D_0^{-1}A]^{-1}|_{(x,y)}(\not{p}+m)n(p)) \right.$$
$$+ \frac{1}{2} \int \frac{d\vec{p}}{(2\pi)^3 2E(p)} \int \frac{d\vec{q}}{(2\pi)^3 2E(q)} \int dx dx' dy dy' e^{ip(x-y)}$$
$$\left. \times e^{-iq(x'-y')}\, \mathrm{Tr}(A\,[I_4 - D_0^{-1}A]^{-1}|_{(x,x')}(\not{q}+m)n(q) A\,[I_4 - D_0^{-1}A]^{-1}|_{(y',y)}(\not{p}+m)n(p)) + \cdots \right\}$$
$$\equiv \int [dU] \exp\left\{ i \int dx \tilde{\mathcal{L}}_{\pi\pi}[U;v,a,s,p] \right\}, \tag{3.1}$$

where the operator A is defined as the difference between the full and the free Dirac operators,

$$\mathcal{L}_{\bar{\psi}\psi} = \bar{\psi}(x) D(x) \psi(x) = \bar{\psi}(x)[D_0(x) - A(x)]\psi(x), \tag{3.2}$$

with $D_0 = i\gamma_\mu \partial^\mu - m$, while the diagonal flavor matrix $n(p) = \mathrm{diag}[\theta(k_F^{(p)} - |\vec{p}|), \theta(k_F^{(n)} - |\vec{p}|)]$ parametrizes the upper cutoff of the three-momentum integrations in terms of the proton and neutron Fermi momenta, respectively. Furthermore I_4 is the unit operator in four dimensions, $E(p)$ is the on-shell energy of a nucleon with mass m, and v, a, s, p are vector, axial-vector, scalar, and pseudoscalar sources. The resulting in-medium effective Lagrangian $\tilde{\mathcal{L}}$ is given in terms of pions and external sources only and thus the problem is reduced to that of vacuum CHPT, with the important difference that the $\tilde{\mathcal{L}}$ is *noncovariant* as well as *nonlocal* [for a general analysis of the structure of nonrelativistic but local EFTs, see Leutwyler (1994)]. In particular, we note the appearance of the nonlocal vacuum vertex $\Gamma = -iA(I_4 - D_0^{-1}A)^{-1}$ that generates a geometric series in terms of the local interaction operator A and the free Dirac propagator, with A itself being subject to the standard chiral expansion, $A = A^{(1)} + A^{(2)} + \cdots$ [see Bernard *et al.* (1992)]. The generalized *in-medium* vertices (cf Fig. 36) consist of several nonlocal vacuum vertices Γ connected through the exchange of on-shell Fermi-sea states. These are the building blocks for the systematic expansion in small momenta, counting the Fermi momentum $k_F \sim 2M_\pi$ at nuclear saturation as $\mathcal{O}(p)$. The in-medium chiral counting including the contributions from nucleon propagators can now be given. The choice of the counting scheme depends on the energy flowing through the nucleon lines, inducing a separate consideration of the so-called *standard* and *nonstandard* cases. We consider first the former. Here the energy flow is of order $M_\pi \sim \mathcal{O}(p)$ and thus the nucleon propagator counts as $D_0^{-1} \sim \mathcal{O}(p^{-1})$. The chiral dimension for a many-particle diagram with L_π pion loops and V_T vacuum and/or in-medium vertices of dimension δ_i is

$$\nu = 2L_\pi + 2 + \sum_{j=1}^{V_T} (\delta_j - 2). \tag{3.3}$$

Consequently, the lowest-order in-medium contributions arise at $\mathcal{O}(p^4)$ since the lowest order in-medium vertices have dimension four due to the four-momentum Dirac delta function attached to any Γ vertex. The first corrections at NLO arise at $\mathcal{O}(p^5)$, which should be contrasted to the vacuum case where LO [NLO] is $\mathcal{O}(p^2)$ [$\mathcal{O}(p^4)$]. In the absence of multinucleon interactions, the breakdown scale is $\Lambda = \sqrt{6}\pi F_\pi \simeq 700$ MeV for S waves and $\Lambda = \sqrt{6}\pi F_\pi / g_A \simeq 560$ MeV for P waves. However, there is one subtlety with this power counting. Quite similar to what happens in case of the TPE NN interaction, the energy flowing into a nucleon line can vanish, so that the nucleon propagator scales as $\mathcal{O}(p^{-2})$. To deal with this nonstandard case, one has to separately count the number of nucleon lines with energy $E \leqslant k_F^2/2m$ and the normal lines with $E \sim M_\pi$. The explicit expression for the modified counting index ν can be found in Meißner *et al.* (2002). In this case, the breakdown scale is $6\pi^2 F_\pi^2/2m \simeq 270$ MeV for S waves and further reduced by a factor of $1/g_A^2$ for P-wave interactions. Note that the so-defined in-medium CHPT not only encompasses but also transcends the so-called low-energy theorems of Drukarev and Levin (1990), Furnstahl *et al.* (1992), and Birse (1994).

We now discuss some results obtained in this scheme. The density dependence of the light quark condensates is given at NLO by

$$\langle \Omega | \bar{u}u | \Omega \rangle = \langle \bar{u}u \rangle_{\mathrm{vac}} \left[1 - \frac{2\sigma}{F_\pi^2 M_\pi^2} \hat{\rho} + \frac{4c_5}{F_\pi^2} \bar{\rho} \right],$$

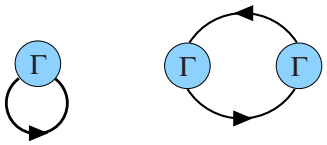

FIG. 36. (Color online) Generalized in-medium vertices of lowest order. The thick solid lines correspond to insertions of a Fermi sea and each circle to the insertion of the operator Γ as defined in the text.

$$\langle\Omega|\bar{d}d|\Omega\rangle = \langle\bar{d}d\rangle_{\rm vac}\left[1 - \frac{2\sigma}{F_\pi^2 M_\pi^2}\hat{\rho} - \frac{4c_5}{F_\pi^2}\bar{\rho}\right], \tag{3.4}$$

with $|\Omega\rangle$ the nuclear matter background, $\hat{\rho}=(\rho_p+\rho_n)/2$, $\bar{\rho}=(\rho_p-\rho_n)/2$ are the isospin symmetric and asymmetric combinations of the proton and the neutron densities, while σ is the pion-nucleon sigma term, $\sigma=-4c_1M_\pi^2$ at $\mathcal{O}(p^2)$. The small isospin-breaking contribution is given in terms of the LEC $c_5=-(0.09\pm0.01)$ GeV. Furthermore, the subscript vac refers to the vacuum value of the corresponding quantity. Higher-order corrections in the density will be discussed in the next section.

The propagation of pions in the medium can be analyzed by calculating the spectral relations between the energy ω and the three-momentum $\vec{q}$ for on-shell neutral and charged pions. For symmetric nuclear matter (with density $\hat{\rho}$) and in the chiral limit one obtains the dispersion law

$$\omega^2 = \vec{q}^2\left(1 - \frac{4\hat{\rho}}{F_\pi^2}c_2\right). \tag{3.5}$$

Since the in-medium pion velocity $\tilde{v}=d\omega/d|\vec{q}|=1-2\hat{\rho}c_2/F_\pi^2$ must be smaller than the velocity of light (Leutwyler, 1994; Pisarski and Tytgat, 1996), this imposes the constraint $c_2\geqslant 0$, which is satisfied by the actual value of this LEC. It was also established in Meißner *et al.* (2002) that for standard values of the LEC c_3, chiral symmetry can account for the observed mass shift of the negatively charged pion in deeply bound pionic states in ^{207}Pb (Gilg *et al.*, 2000; Itahashi *et al.*, 2000). At NLO, one obtains $\Delta M_\pi=18\pm5$ MeV which is compatible with the experimental result, $\Delta M_\pi=23-27$ MeV. Of interest is also splitting of the temporal like and spacelike components of the pion decay constant, which read at NLO in symmetric nuclear matter,

$$F_t = F_\pi\left\{1 - \frac{\hat{\rho}}{\rho_0}(0.26\pm0.04)\right\},$$

$$F_s = F_\pi\left\{1 - \frac{\hat{\rho}}{\rho_0}(1.23\pm0.07)\right\}, \tag{3.6}$$

with ρ_0 the nuclear matter density. The ratio $F_s/F_t=\tilde{v}^2<1$ is consistent with the discussion about the in-medium pion velocity. One can also show that the corrections at $\mathcal{O}(p^5)$ do not spoil the validity of the Gell-Mann–Oakes–Renner relation [see also Thorsson and Wirzba (1995)], in particular both F_t and the quark condensate decrease with increasing density. For a more detailed discussion of two-, three-, and four point functions in the medium, see Meißner *et al.* (2002).

The missing ingredients in these calculations are the effects of multinucleon interactions. It has recently been shown how these can be included in the path integral formulation (Oller 2008; Oller *et al.* 2009). For that, one introduces heavy fields H that couple to nucleon bilinears in appropriate spin-isospin combinations, $\tilde{\mathcal{L}}[U;v,a,s,p]\to\tilde{\mathcal{L}}[U;H;v,a,s,p]$, and letting the mass of the H fields tends to infinity (cf. Fig. 3). In that way, one can formally integrate out the multifermion interactions from the generating functional.

Further progress has been made in Girlanda *et al.* (2004). They developed a generalization of in-medium CHPT for finite systems. This provides a framework to study pion-nuclear bound states, for which the finite volume and the surface of the nucleus are important ingredients. The corresponding chiral counting is applied to the underlying pion-nucleon interactions and also to the relevant nuclear matrix elements. The central object of this approach is the Green's function in the presence of a nucleus, $G_A(X\to Y)$, which describes the general process $A+X\to A+Y$, where X,Y represent some number of external pions and photons and A is a nucleus made of A nucleons. The presence of the nucleus is parametrized in terms of proton and neutron distribution functions that are taken from phenomenology. In the limit of uniform density, this approach reduce to the in-medium CHPT described above. As an example, the pion-nucleus optical potential is calculated at NLO,

$$U(E;\vec{q}\,',\vec{q}) = \int d^3\vec{x}\,e^{-i(\vec{q}'-\vec{q})\cdot\vec{x}}[\tilde{U}(E;\vec{q}\,',\vec{q},\vec{x}) + \mathcal{O}(p^6)],$$

$$\tilde{U}(E;\vec{q}\,',\vec{q},\vec{x}) = -\int d^3\vec{r}\,\frac{e^2E}{4\pi|\vec{x}-\vec{r}|}2\rho_p(\vec{r}) + \cdots, \tag{3.7}$$

where E is the pion energy, $\vec{q},\vec{q}$ are the outgoing and the incoming three-momenta, in order, and ρ_p is the proton charge density. The ellipsis in Eq. (3.7) stands for the contributions from the hard virtual photons and from the strong interaction [for details see Girlanda *et al.* (2004)]. As stressed by Girlanda *et al.* (2005) this approach allows one to identify unambiguously the nuclear finite size effects and to disentangle the S-, P-, and D-wave contributions to the optical potential without invoking the local density approximation. For a more detailed discussion concerning also the comparison with more traditional approaches to pion-nucleus physics, see Girlanda *et al.* (2004).

B. Perturbative chiral nuclear dynamics

A somewhat different path, which has turned out to be successful phenomenologically, has been taken by the Munich group (Kaiser *et al.*, 2002a, 2002b; Fritsch *et al.* 2005) [for a related work, see Lutz *et al.* (2000)]. Its key element is the separation of long- and short-distance dynamics. The ordering scheme counts pion masses and momentum, the Fermi momentum, and the nucleon-delta mass splitting as small quantities,[8] motivated by the fact that at nuclear matter density $k_F\simeq 2M_\pi$. Therefore, pions must be included and propagation effects of the delta will be resolved. The long-distance physics is calculated perturbatively including one- and two-pion

[8]We unify here the two formulations with and without explicit deltas presented by this group.

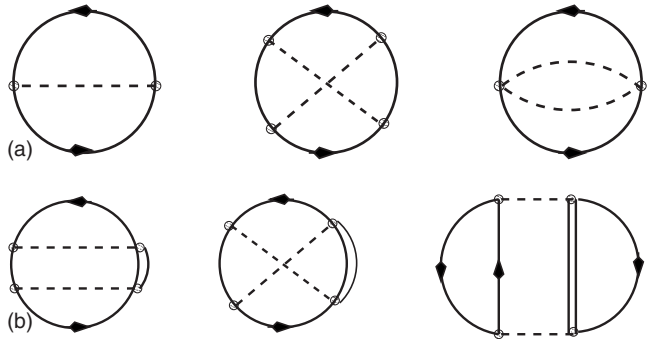

FIG. 37. Diagrams contributing to E/N in nuclear matter. Upper panel: One- and two-pion exchange diagrams contributing to the energy per particle at two and three loops. Solid and dashed lines denote nucleons and pions, respectively. Lower panel: Three-body diagrams related to 2π exchange with single delta excitations (double lines). These represent interactions between three nucleons in the Fermi sea.

exchange Hartree and Fock graphs (see Fig. 37 for some typical diagrams contributing to the energy per particle in nuclear matter). The short-distance dynamics is also treated perturbatively by either fine tuning of an UV cutoff or adjusting the parameters that appear at a given observable at a given order. This differs from the treatment of the contact interactions in free NN scattering. Within this scheme, one can reproduce the empirical saturation point of nuclear matter by adjusting (fine tuning) one parameter related to the short-distance dynamics. This corresponds to a novel mechanism for nuclear matter saturation due to the repulsive contribution to the energy per particle generated by Pauli blocking in second-order (iterated) one-pion exchange. This can be better understood by considering the realistic parametrization of the energy per particle in isospin symmetric nuclear matter,

$$\bar{E}(k_F) = 3k_F^2/10m - \alpha k_F^3/m^2 + \beta k_F^4/m^3, \tag{3.8}$$

where α,β are dimensionless parameters. If $\alpha,\beta>0$, a saturation minimum will be obtained. In the deltaless theory, one obtains exactly such a form in the chiral limit and the parameters can be given in closed form. In fact, the expression for β is parameter-free. Fine tuning the short-distance contribution to α, one obtains the proper binding energy of nuclear matter. Qualitatively, this picture is not changed when the effects related to the finite pion mass and the delta excitation are included. Furthermore, one obtains as a by-product a realistic value of the nuclear matter compressibility.

This approach has been applied and extended in various ways. Spin-orbit interactions in nuclei and hypernuclei were considered in Kaiser (2002b, 2003) and Kaiser and Weise (2005, 2008). This led to a nice explanation of the very strong spin-orbit interactions in ordinary nuclei contrasted to the remarkably weak spin-orbit splitting in Λ hypernuclei. Corrections to the in-medium chiral condensate beyond the linear density approximation were calculated in Kaiser *et al.* (2008) and Kaiser and Weise (2009). Further, a systematic analysis of the nuclear energy density functional based on a unification of chiral pion nuclear dynamics with strong scalar and vector mean fields was performed and applied to the properties of nuclear matter and finite nuclei [see Finelli *et al.* (2003, 2004, 2007) and Kaiser *et al.* (2003)]. For more details on these interesting calculations, the interested reader is referred to the original articles.

C. EFT for halo nuclei

A special class of nuclear systems exhibiting universal behavior are *halo nuclei*. A halo nucleus consists of a tightly bound core surrounded by one or more loosely bound valence nucleons. The valence nucleons are characterized by a very low separation energy compared to those in the core. As a consequence, the radius of the halo nucleus is large compared to the radius of the core. A trivial example is the deuteron, which can be considered a two-body halo nucleus. The root-mean-square radius of the deuteron $\langle r^2\rangle^{1/2}\approx 2$ fm is about three times larger than the size of the constituent nucleons. Halo nuclei with two valence nucleons are particularly interesting examples of three-body systems. If none of the two-body subsystems are bound, they are called *Borromean* halo nuclei. This name is derived from the heraldic symbol of the Borromeo family of Italy, which consists of three rings interlocked in such way that if any one of the rings is removed the other two separate. The most carefully studied Borromean halo nuclei are ^{6}He and ^{11}Li, which have two weakly bound valence neutrons (Zhukov *et al.*, 1993; Jensen *et al.*, 2004). In the case of ^{6}He, the core is a ^{4}He nucleus, which is also known as the α particle. The two-neutron separation energy for ^{6}He is about 1 MeV, small compared to the binding energy of the α particle which is about 28 MeV. The neutron-α ($n\alpha$) system has no bound states and the ^{6}He nucleus is therefore Borromean. There is, however, a strong P-wave resonance in the $J=3/2$ channel of $n\alpha$ scattering which is sometimes referred to as ^{5}He. This resonance is responsible for the binding of ^{6}He. Thus ^{6}He can be interpreted as a bound state of an α particle and two neutrons, both of which are in $P_{3/2}$ configurations.

Because of the separation of scales in halo nuclei, they can be described by extensions of the pionless EFT. One can assume the core to be structureless and treat the nucleus as a few-body system of the core and the valence nucleons. Corrections from the structure of the core appear in higher orders and can be included in perturbation theory. Cluster models of halo nuclei then appear as leading-order approximations in the EFT. A new facet is the appearance of resonances as in the neutron-alpha system which leads to a more complicated singularity structure and renormalization compared to the few-nucleon system discussed above (Bertulani *et al.*, 2002).

The first application of effective field theory methods to halo nuclei was carried out in Bertulani *et al.* (2002)

and Bedaque, Hammer, and van Kolck (2003), where the $n\alpha$ system (^{5}He) was considered. It was found that for resonant P-wave interactions both the scattering length and effective range have to be resummed at leading order. At threshold, however, only one combination of coupling constants is fine tuned and the EFT becomes perturbative. More recent studies have focused on the consistent inclusion of the Coulomb interaction in two-body halo nuclei such as the $p\alpha$ and $\alpha\alpha$ systems (Higa, 2008; Higa, Hammer, and van Kolck, 2008). In particular, the $\alpha\alpha$ system shows a surprising amount of fine tuning between the strong and electromagnetic interaction. It can be understood in an expansion around the limit where, when electromagnetic interactions are turned off, the ^{8}Be ground state is exactly at threshold and exhibits conformal invariance. In this scenario, the Hoyle state in ^{12}C would appear as a remnant of an excited Efimov state (Efimov, 1981). In order to better understand the modification of the Efimov spectrum and limit cycles by long-range interactions such as the Coulomb interaction, a one-dimensional inverse square potential supplemented with a Coulomb interaction was investigated in Hammer and Higa (2008). The results indicate that the counterterm required to renormalize the inverse square potential alone is sufficient to renormalize the full problem. However, the breaking of the discrete scale invariance through the Coulomb interaction leads to a modified bound state spectrum. The shallow bound states are strongly influenced by the Coulomb interaction while the deep bound states are dominated by the inverse square potential.

Three-body halo nuclei composed of a core and two valence neutrons are of particular interest due to the possibility of these systems to display the Efimov effect (Efimov, 1970). Since the scattering length cannot easily be varied in halo nuclei, one has to look for excited states. Such studies have previously been carried out in cluster models and the renormalized zero-range model (Fedorov *et al.*, 1994; Amorim *et al.*, 1997; Mazumdar *et al.*, 2000). A comprehensive study of S-wave halo nuclei in EFT including structure calculations with error estimates was recently carried out by Canham and Hammer (2008). Currently, the only possible candidate for an excited Efimov state is ^{20}C, which consists of a core nucleus with spin and parity quantum numbers $J^P=0^+$ and two valence neutrons. The nucleus ^{19}C is expected to have a $\frac{1}{2}^+$ state near threshold, implying a shallow neutron-core bound state and therefore a large neutron-core scattering length. The value of the ^{19}C energy, however, is not known well enough to make a definite statement about the appearance of an excited state in ^{20}C. The matter form factors of halo nuclei can also be calculated in the halo EFT. As an example, we show the various one- and two-body matter density form factors with leading-order error bands for the ground state of ^{20}C at low momentum transfers in Fig. 38: $\mathcal{F}_{nn}(k^2)$, $\mathcal{F}_{nc}(k^2)$, $\mathcal{F}_n(k^2)$, and $\mathcal{F}_c(k^2)$. A definition of the form factors can be found in Canham and Hammer (2008). The theory breaks down for momentum transfers of the order of the pion-mass squared ($k^2 \approx 0.5$ fm^{-2}) where the one-pion exchange interaction cannot be approximated by short-range contact interactions anymore. From the slope of the matter form factors one can extract the corresponding radii,

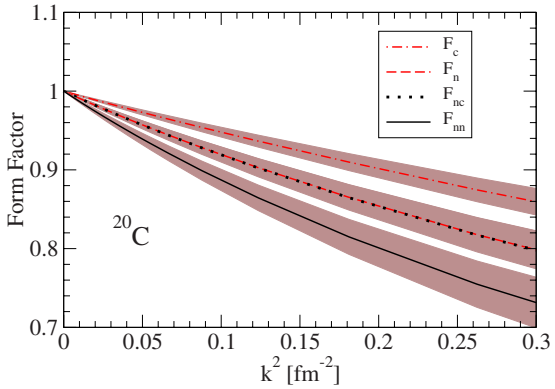

FIG. 38. (Color online) The various one- and two-body matter density form factors with leading-order error bands for the ground state of ^{20}C in the low-energy region: $\mathcal{F}_{nn}(k^2)$, solid line; $\mathcal{F}_{nc}(k^2)$, dotted line; $\mathcal{F}_n(k^2)$, lighter dashed line; and $\mathcal{F}_c(k^2)$, lighter dot-dashed line.

$$\mathcal{F}(k^2) = 1 - \tfrac{1}{6}k^2\langle r^2\rangle + \cdots . \tag{3.9}$$

Information on these radii has been extracted from experiment for some halo nuclei. For the neutron-neutron radius of the Borromean halo nucleus ^{14}Be, for example, the leading-order halo EFT result is $\sqrt{\langle r_{nn}^2\rangle}=4.1\pm0.5$ fm. The value $\sqrt{\langle r_{nn}^2\rangle_{\rm exp}}=5.4\pm1.0$ fm was obtained from three-body correlations in the dissociation of ^{14}Be using a technique based on intensity interferometry and Dalitz plots (Marques *et al.*, 2001). Within the errors there is good agreement between both values. However, one should also keep in mind that there is some model dependence in the experimental result. Results for further halo nuclei are given by Canham and Hammer (2008). A few recent studies have also investigated scattering observables. In particular, in Mazumdar *et al.* (2006) and Yamashita *et al.* (2008) extended the trajectory of the possible ^{20}C excited state into the scattering region in order to find a resonance in n-^{19}C scattering.

The simplest strange halo nucleus is the hypertriton, a three-body bound state of a proton, a neutron, and the Λ. The total binding energy is only about 2.4 MeV. The hypertriton is not Borromean because the proton-neutron subsystem has a bound state, the deuteron. The separation energy for the Λ, $E_\Lambda=0.13\pm0.05$ MeV, is small compared to the binding energy $B_D=2.224$ MeV of the deuteron. The hypertriton can therefore also be considered a two-body halo nucleus. It has been studied in both two- and three-body approaches (Congleton, 1992; Cobis *et al.*, 1997; Fedorov and Jensen, 2002). A study of the hypertriton in the halo EFT was carried out by Hammer (2002). An important feature of the halo EFT is the possibility to quantify theoretical errors through error bands. Calculations can be improved sys-

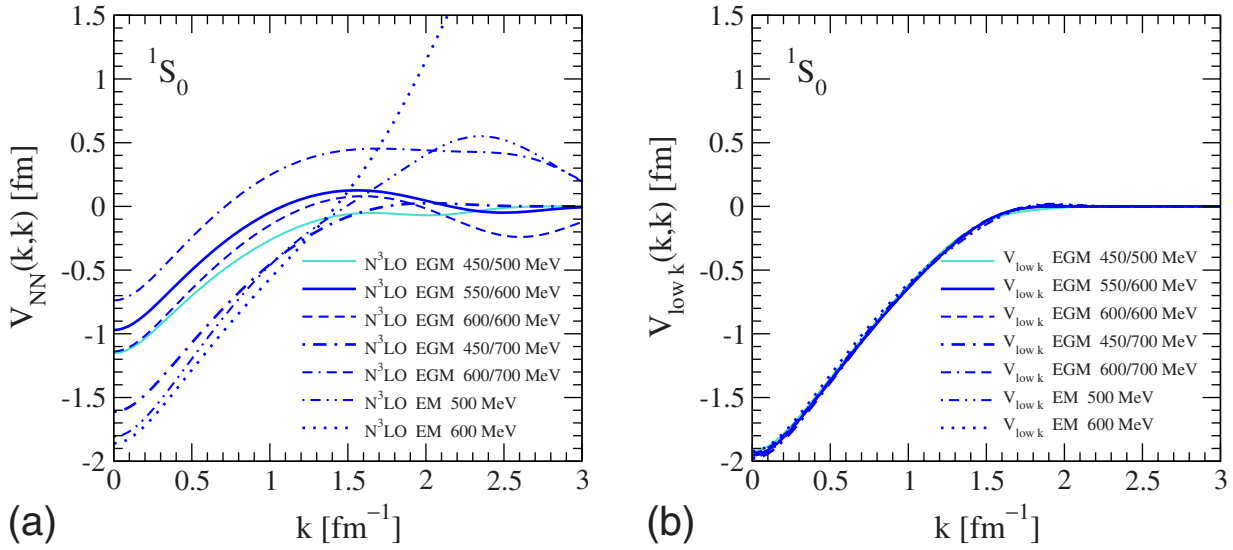

FIG. 39. (Color online) The diagonal matrix elements of the nucleon-nucleon potential in the $^1S_0$ partial wave. Left panel: Chiral nucleon-nucleon potentials at N^{3}LO by EGM (Epelbaum, Glöckle, and Meißner, 2005) and EM (Entem and Machleidt, 2003a) for various cutoffs. Right panel: Same potentials evolved down to a cutoff $\Lambda=2.2$ fm^{-1}. Figure courtesy of A. Schwenk.

tematically through the inclusion of higher-order terms.

Another interesting application of this effective theory will be the study of Coulomb excitation data from existing and future facilities with exotic beams (such as FAIR and FRIB). In these experiments a nuclear beam scatters off the Coulomb field of a heavy nucleus. Such processes can populate excited states of the projectile which subsequently decay, leading to its "Coulomb dissociation" (Bertulani and Baur, 1988). Effective theories offer a systematic framework for a full quantum-mechanical treatment of these reactions. In summary, with new improved experimental data for these weakly bound nuclei, much more knowledge can be obtained about the structure of these interesting systems as well as discovering whether they show universal behavior and excited Efimov states.

D. $V_{low\ k}$ potentials: Construction and applications

Nuclear interactions, like all interactions, depend on the resolution scale. For a momentum cutoff Λ, only details of the interactions at distances larger than $1/\Lambda$ can be resolved. The interaction potential V consists of two-, three-, and higher-body terms and can be written as

$$V(\Lambda) = V_2(\Lambda) + V_3(\Lambda) + V_4(\Lambda) + \cdots . \tag{3.10}$$

While V depends on Λ, observables are independent of Λ. This property can be used to construct so-called low-momentum potentials with a cutoff $\Lambda' < \Lambda$ that describe low-energy physics in terms of low-energy degrees of freedom only. Various methods for constructing such low-momentum potentials are known [see, e.g., Bogner *et al.* (2003) for a review]. The first construction of a low-momentum potential was carried out by Epelbaum *et al.* (1998a, 1999) based on the Okubo method (Fukuda *et al.*, 1954; Okubo, 1954). Bogner and collaborators have pushed this idea further and constructed low-momentum potentials for various realistic nucleon-nucleon interactions using renormalization group (RG) techniques. They showed that these potentials all converge to the same universal $V_{low\ k}$ if the cutoff is lowered to low enough values ($\Lambda \lesssim 2$ fm^{-1}). This is illustrated in Fig. 39 for the $^1S_0$ partial wave. The left panel shows the chiral nucleon-nucleon potentials at N^{3}LO by EGM (Epelbaum, Glöckle, and Meißner, 2005) and EM (Entem and Machleidt, 2003a) for various cutoffs. The right panel shows the same potentials evolved down to a cutoff $\Lambda=2.2$ fm^{-1}. At this cutoff all potentials have collapsed to the same universal curve.

As the resolution scale is lowered the physics previously present in high-momentum modes now appears in many-body forces that are generated through the RG transformation. The low-momentum potential constructed this way is phase equivalent by construction. In most early calculations, the many-body forces generated by the RG have been neglected for simplicity. In this case phase equivalence only holds in the two-body subspace. Recent advances based on similarity RG techniques, however, suggest that these limitations can be overcome soon (Bogner *et al.*, 2007; Jurgenson and Furnstahl, 2009). Low-momentum potentials have also been constructed for hyperon-nucleon interactions (Schaefer *et al.*, 2006; Dapo *et al.*, 2008). Here the various realistic potentials are less constrained by data and the $V_{low\ k}$ interactions show only convergence in some channels.

Nogga *et al.* (2004) studied the three- and four-nucleon systems using the $V_{low\ k}$ potential supplemented by the leading-order chiral $3N$ forces. This procedure was motivated by the expectation that the many-body forces have to reduce to the leading-order chiral forces at low enough momentum. The free parameters in the chiral $3N$ force were then fitted to experiment for each value

of the cutoff. If the chiral 3*N* force is left out, the cutoff variation generates the Tjon line. Since the RG evolution leaves the two-body observables unchanged by construction, the variation can only go along the Tjon line. This is in agreement with the findings in the pionless EFT (Platter *et al.*, 2005). For a study of potential problems arising when using *NN* low-momentum potentials without the corresponding 3*N* potentials in few-nucleon systems, see Fujii *et al.* (2004).

Because of the low cutoff, the low-momentum potential has advantages in nuclear structure calculations where smaller model spaces are desirable because of the computational effort involved. For a summary of recent applications, see Schwenk and Holt (2008). As the RG evolution shifts contributions between the potential and the integrals over intermediate states in loop integrals which are restricted by Λ, the RG transformation can eliminate sources of nonperturbative behavior such as strong short-range repulsion or tensor forces (Bogner *et al.*, 2005, 2006). This suggests that perturbative nuclear matter calculations are possible. At these low resolution scales, nuclear matter saturation would be largely driven by three-body forces. Moreover, perturbative nuclear matter calculations would also provide a solid basis for the construction of a universal density functional for nuclei with controlled errors (Bertsch *et al.*, 2007; Furnstahl, 2007). A first step toward such a universal energy density functional based on low-momentum interactions was taken in Bogner *et al.* (2008) using the density matrix expansion of Negele and Vautherin.

E. Lattice simulations of many-nucleon systems

Nuclear matter studies utilizing lattice simulations were pioneered by Brockmann and Frank (1992), who calculated the quantum corrections to the Walecka model (Serot and Walecka, 1986) and by Muller *et al.* (2000), who investigated nuclear matter properties utilizing a Hamiltonian that accommodates on-site and next-to-neighbor parts of the central spin- and isospin-exchange nucleon-nucleon interactions. The first connection between chiral EFT and the properties of nucleon and neutron matter using Monte Carlo methods was done in the work of Borasoy, Lee, and Schäfer (Lee *et al.*, 2004). They laid out the framework for nuclear lattice simulations with chiral EFT and presented leading-order results for hot neutron matter at temperatures $T=20-40$ K and densities below twice the nuclear matter density. Neutron matter in a periodic box based on the lattice representation of the chiral NLO potential (see Sec. II.G) was performed in Borasoy *et al.* (2008), probing the density range from 2% to 8% of normal nuclear matter density. Dilute neutron matter is a particularly good testing ground for chiral EFT applied to many-nucleon systems because of the Pauli suppression of three-body forces. Furthermore, neutron matter at $k_F \sim 80$ MeV, with $k_F=(3\pi^2 N)^{1/3}/L$ (for N neutrons in a box of volume L^3), is close to the so-called unitary limit. In this limit, the scattering length is infinite and the range of the interaction is zero, so that the scattering amplitude takes its largest possible value (as given by unitarity). In this limit, the only dimensionful parameter describing the ground state of the many-fermion system is the particle density. Thus, the ground state energy E_0 of the system obeys the simple relation

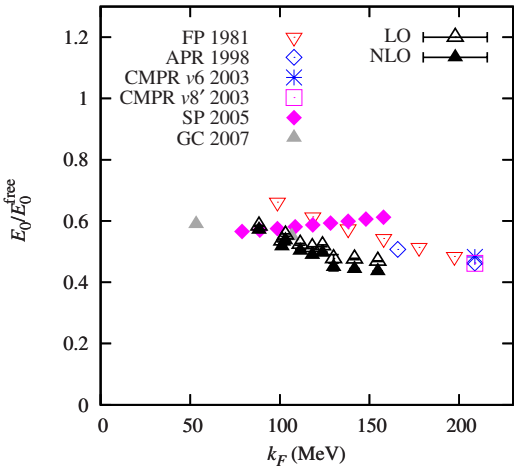

FIG. 40. (Color online) Results for $E_0/E_0^{\rm free}$ vs the Fermi momentum k_F at LO (open triangles) and NLO (filled triangles). For comparison, we also display the results of FP 1981 (Friedman and Pandharipande, 1981), APR 1998 (Akmal *et al.*, 1998), CMPR $v6$ and $v8'$ 2003 (Carlson *et al.*, 2003), SP 2005 (Schwenk and Pethick, 2005), and GC 2007 (Gezerlis and Carlson, 2008).

$$E_0 = \xi E_0^{\rm free}, \tag{3.11}$$

where ξ is a dimensionless measurable constant and $E_0^{\rm free}$ is the ground state energy of a free Fermi gas. Due to its universal nature, the unitary limit can be studied in ultracold atomic systems such as ^{6}Li or ^{40}K a utilizing Feshbach-resonance techniques. Recently measured values for ξ scatter considerably and have sizable error bars [for a review, see Giorgini *et al.* (2008)]. There also have been numerous calculations of ξ employing very different many-body techniques [see Furnstahl *et al.* (2008) for a recent review].

Recent EFT simulations at LO and NLO with an improved action for 8, 12, and 16 neutron boxes of length $L=10$, 12, and 14 fm are shown in Fig. 40 (Epelbaum *et al.*, 2009). The chiral EFT results are consistent with most earlier calculations based on different methods. A good fit to the lattice data is obtained by [the structure of the correction terms is discussed in Borasoy *et al.* (2008)]

$$\frac{E_0}{E_0^{\rm free}} \simeq \xi - \frac{\xi_1}{k_F a} + 0.16 k_F r_0 - (0.51\ \text{fm}^3) k_F^3, \tag{3.12}$$

with $\xi \simeq 0.31$ and $\xi_1 \simeq 0.81$. This is consistent with the Monte Carlo studies of many-fermion systems in Lee (2008) but smaller than the value for ξ obtained in fixed-node Green's function Monte Carlo calculations [see, e.g., Carlson *et al.* (2003)]. This suggests that the upper bound on the ground state energy in that type of approach might be lowered further by a more optimal fer-

mionic nodal surface. Clearly, such numerical simulations of many-nucleon systems have become a valuable tool to further constrain the nuclear equation of state at moderate densities and lead to further insight into the physics of strongly coupled many-body systems. In particular, they provide another link between nuclear and atomic physics as discussed in Sec. II.A.

IV. SUMMARY AND PERSPECTIVES

In this review, we have described the theory that has emerged by applying effective field theory methods to the nuclear force problem. This method allows for a systematic derivation of nuclear forces with a direct connection to QCD via its symmetries. The review focused on the derivation of the forces and their application in the few-nucleon problem where most work has been carried out so far. However, there are many frontiers where future work is required. These include a better understanding of nonperturbative renormalization and improved renormalization schemes, the consistent inclusion of electroweak currents, and the development of a consistent EFT for the nuclear many-body problem. The application of new techniques and advanced calculational methods for the many-body problem will be decisive to achieve the latter. Promising approaches include the renormalization group, nuclear lattice calculations, coupled cluster approaches, the no-core shell model, and density functional theory. For very low-energy processes, these approaches can be complemented by the pionless or halo EFT which is an ideal tool to unravel universal properties and establish connections to other fields of physics.

ACKNOWLEDGMENTS

We thank all our collaborators for sharing their insights into the topics discussed here. The work of E.E. was supported in parts by funds provided from the Helmholtz Association to the young investigator group "Few-Nucleon Systems in Chiral Effective Field Theory" (Grant No. VH-NG-222). This work was further supported by the BMBF under Contract No. 06BN411, by the DFG (Grant No. SFB/TR 16 "Subnuclear Structure of Matter"), by the Helmholtz Association through funds provided to the virtual institute "Spin and strong QCD" (VH-VI-231), and by the European Community-Research Infrastructure Integrating Activity "Study of Strongly Interacting Matter" (acronym HadronPhysics2, Grant Agreement n. 227431) under the Seventh Framework Programme of the EU.

REFERENCES

Adam, H. H., *et al.* (WASA-at-COSY), 2004, e-print arXiv:nucl-ex/0411038.
Afnan, I. R., and D. R. Phillips, 2004, Phys. Rev. C **69**, 034010.
Afnan, I. R., and F. J. D. Serduke, 1973, Phys. Lett. **44B**, 143.
Ahn, J. K., *et al.*, 2006, Phys. Lett. B **633**, 214.
Akmal, A., V. R. Pandharipande, and D. G. Ravenhall, 1998, Phys. Rev. C **58**, 1804.
Alberico, W. M., and G. Garbarino, 2002, Phys. Rep. **369**, 1.
Alexander, G., *et al.*, 1968, Phys. Rev. **173**, 1452.
Amghar, A., and B. Desplanques, 1995, Nucl. Phys. A **585**, 657.
Amorim, A. E. A., T. Frederico, and L. Tomio, 1997, Phys. Rev. C **56**, R2378.
Amsler, C., *et al.* (Particle Data Group), 2008, Phys. Lett. B **667**, 1.
Ando, S.-I., 2007, Eur. Phys. J. A **33**, 185.
Ando, S.-I., and M. C. Birse, 2008, Phys. Rev. C **78**, 024004.
Aoki, S., *et al.* (CP-PACS), 2005, Phys. Rev. D **71**, 094504.
Arndt, R. A., W. J. Briscoe, I. I. Strakovsky, and R. L. Workman, 2006, Phys. Rev. C **74**, 045205.
Arndt, R. A., W. J. Briscoe, R. L. Workman, I. I. Strakovsky, and M. Paris, 2009, SAID online program, http://gwdac.phys.gwu.edu
Arzt, C., 1995, Phys. Lett. B **342**, 189.
Austen, G. J. M., and J. J. de Swart, 1983, Phys. Rev. Lett. **50**, 2039.
Banks, T., and A. Casher, 1980, Nucl. Phys. B **169**, 103.
Barford, T., and M. C. Birse, 2005, J. Phys. A **38**, 697.
Baru, V., J. Haidenbauer, C. Hanhart, and J. A. Niskanen, 2003, Eur. Phys. J. A **16**, 437.
Baru, V., C. Hanhart, A. E. Kudryavtsev, and U.-G. Meißner, 2004, Phys. Lett. B **589**, 118.
Baru, V., *et al.*, 2007, e-print arXiv:0711.2748.
Bawin, M., and S. A. Coon, 2003, Phys. Rev. A **67**, 042712.
Beane, S. R., P. F. Bedaque, W. C. Haxton, D. R. Phillips, and M. J. Savage, 2000, e-print arXiv:nucl-th/0008064.
Beane, S. R., P. F. Bedaque, K. Orginos, and M. J. Savage, 2006, Phys. Rev. Lett. **97**, 012001.
Beane, S. R., P. F. Bedaque, A. Parreño, and M. J. Savage, 2004, Phys. Lett. B **585**, 106.
Beane, S. R., P. F. Bedaque, A. Parreño, and M. J. Savage, 2005, Nucl. Phys. A **747**, 55.
Beane, S. R., P. F. Bedaque, M. J. Savage, and U. van Kolck, 2002, Nucl. Phys. A **700**, 377.
Beane, S. R., V. Bernard, E. Epelbaum, U.-G. Meißner, and D. R. Phillips, 2003, Nucl. Phys. A **720**, 399.
Beane, S. R., V. Bernard, T. S. H. Lee, U.-G. Meißner, and U. van Kolck, 1997, Nucl. Phys. A **618**, 381.
Beane, S. R., T. D. Cohen, and D. R. Phillips, 1998, Nucl. Phys. A **632**, 445.
Beane, S. R., K. Orginos, and M. J. Savage, 2007, Nucl. Phys. B **768**, 38.
Beane, S. R., K. Orginos, and M. J. Savage, 2008, Int. J. Mod. Phys. E **17**, 1157.
Beane, S. R., and M. J. Savage, 2003, Nucl. Phys. A **717**, 91.
Beane, S. R., *et al.*, 2001, Phys. Rev. A **64**, 042103.
Beane, S. R., *et al.* (NPLQCD), 2007, Nucl. Phys. A **794**, 62.
Becher, T., and H. Leutwyler, 1999, Eur. Phys. J. C **9**, 643.
Bedaque, P. F., H.-W. Hammer, and U. van Kolck, 1998, Phys. Rev. C **58**, R641.
Bedaque, P. F., H.-W. Hammer, and U. van Kolck, 1999a, Phys. Rev. Lett. **82**, 463.
Bedaque, P. F., H.-W. Hammer, and U. van Kolck, 1999b, Nucl. Phys. A **646**, 444.
Bedaque, P. F., H.-W. Hammer, and U. van Kolck, 2000, Nucl. Phys. A **676**, 357.
Bedaque, P. F., H.-W. Hammer, and U. van Kolck, 2003, Phys. Lett. B **569**, 159.
Bedaque, P. F., G. Rupak, H. W. Grießhammer, and H.-W. Hammer, 2003, Nucl. Phys. A **714**, 589.

Bedaque, P. F., and U. van Kolck, 1998, Phys. Lett. B **428**, 221.
Bedaque, P. F., and U. van Kolck, 2002, Annu. Rev. Nucl. Part. Sci. **52**, 339.
Belitsky, A. V., and T. D. Cohen, 2002, Phys. Rev. C **65**, 064008.
Bernard, V., 2008, Prog. Part. Nucl. Phys. **60**, 82.
Bernard, V., E. Epelbaum, H. Krebs, and U.-G. Meißner, 2008, Phys. Rev. C **77**, 064004.
Bernard, V., N. Kaiser, J. Kambor, and U.-G. Meißner, 1992, Nucl. Phys. B **388**, 315.
Bernard, V., N. Kaiser, and U.-G. Meißner, 1995, Nucl. Phys. B **457**, 147.
Bernard, V., N. Kaiser, and U.-G. Meißner, 1997, Nucl. Phys. A **615**, 483.
Bernard, V., N. Kaiser, and U.-G. Meißner, 1999, Eur. Phys. J. A **4**, 259.
Bernard, V., and U.-G. Meißner, 2007, Annu. Rev. Nucl. Part. Sci. **57**, 33.
Bertsch, G. F., D. J. Dean, and W. Nazarewicz, 2007, SciDAC Rev. **6**, 42.
Bertulani, C. A., and G. Baur, 1988, Phys. Rep. **163**, 299.
Bertulani, C. A., H.-W. Hammer, and U. Van Kolck, 2002, Nucl. Phys. A **712**, 37.
Biegun, A., *et al.*, 2006, Acta Phys. Pol. B **37**, 213.
Birse, M. C., 1994, J. Phys. G **20**, 1537.
Birse, M. C., 2006, Phys. Rev. C **74**, 014003.
Birse, M. C., 2007, Phys. Rev. C **76**, 034002.
Birse, M. C., 2008, Phys. Rev. C **77**, 047001.
Birse, M. C., and J. A. McGovern, 2004, Phys. Rev. C **70**, 054002.
Birse, M. C., J. A. McGovern, and K. G. Richardson, 1999, Phys. Lett. B **464**, 169.
Bogner, S. K., R. J. Furnstahl, and R. J. Perry, 2007, Phys. Rev. C **75**, 061001.
Bogner, S. K., R. J. Furnstahl, and L. Platter, 2008, e-print arXiv:0811.4198.
Bogner, S. K., R. J. Furnstahl, S. Ramanan, and A. Schwenk, 2006, Nucl. Phys. A **773**, 203.
Bogner, S. K., T. T. S. Kuo, and A. Schwenk, 2003, Phys. Rep. **386**, 1.
Bogner, S. K., A. Schwenk, R. J. Furnstahl, and A. Nogga, 2005, Nucl. Phys. A **763**, 59.
Borasoy, B., E. Epelbaum, H. Krebs, D. Lee, and U.-G. Meißner, 2007a, Eur. Phys. J. A **31**, 105.
Borasoy, B., E. Epelbaum, H. Krebs, D. Lee, and U.-G. Meißner, 2007b, Eur. Phys. J. A **34**, 185.
Borasoy, B., E. Epelbaum, H. Krebs, D. Lee, and U.-G. Meißner, 2008, Eur. Phys. J. A **35**, 357.
Borasoy, B., H. Krebs, D. Lee, and U.-G. Meißner, 2006, Nucl. Phys. A **768**, 179.
Braaten, E., and H.-W. Hammer, 2003, Phys. Rev. Lett. **91**, 102002.
Braaten, E., and H.-W. Hammer, 2006, Phys. Rep. **428**, 259.
Braaten, E., and H.-W. Hammer, 2007, Ann. Phys. **322**, 120.
Braaten, E., and D. Phillips, 2004, Phys. Rev. A **70**, 052111.
Brockmann, R., and J. Frank, 1992, Phys. Rev. Lett. **68**, 1830.
Brown, G. E., 1970, Comments Nucl. Part. Phys. **4**, 140.
Buettiker, P., and U.-G. Meißner, 2000, Nucl. Phys. A **668**, 97.
Burgess, C. P., 2007, Annu. Rev. Nucl. Part. Sci. **57**, 329.
Bydzovsky, P., A. Gal, and J. Mares, 2007, *Topics in Strangeness Nuclear Physics*, Lecture Notes in Physics Vol. 724 (Springer, Heidelberg).
Canham, D. L., and H.-W. Hammer, 2008, Eur. Phys. J. A **37**, 367.
Carlson, J., J. Morales, J. V. R. Pandharipande, and D. G. Ravenhall, 2003, Phys. Rev. C **68**, 025802.
Chen, J.-W., and D. B. Kaplan, 2004, Phys. Rev. Lett. **92**, 257002.
Chen, J.-W., D. Lee, and T. Schafer, 2004, Phys. Rev. Lett. **93**, 242302.
Cheung, C. Y., E. M. Henley, and G. A. Miller, 1980, Nucl. Phys. A **348**, 365.
Christlmeier, S., and H. W. Grießhammer, 2008, Phys. Rev. C **77**, 064001.
Cobis, A., A. S. Jensen, and D. V. Fedorov, 1997, J. Phys. G **23**, 401.
Coelho, H. T., T. K. Das, and M. R. Robilotta, 1983, Phys. Rev. C **28**, 1812.
Coester, F., S. Cohen, B. Day, and C. M. Vincent, 1970, Phys. Rev. C **1**, 769.
Cohen, T. D., 2002, Phys. Rev. C **66**, 064003.
Cohen, T. D., J. L. Friar, G. A. Miller, and U. van Kolck, 1996, Phys. Rev. C **53**, 2661.
Cohen, T. D., and B. A. Gelman, 2002, Phys. Lett. B **540**, 227.
Cohen, T. D., and J. M. Hansen, 1998, Phys. Lett. B **440**, 233.
Cohen, T. D., and J. M. Hansen, 1999a, Phys. Rev. C **59**, 13.
Cohen, T. D., and J. M. Hansen, 1999b, Phys. Rev. C **59**, 3047.
Coleman, S. R., J. Wess, and B. Zumino, 1969, Phys. Rev. **177**, 2239.
Congleton, J. G., 1992, J. Phys. G **18**, 339.
Coon, S. A., and J. L. Friar, 1986, Phys. Rev. C **34**, 1060.
Coon, S. A., and H. K. Han, 2001, Few-Body Syst. **30**, 131.
Coon, S. A., and J. A. Niskanen, 1996, Phys. Rev. C **53**, 1154.
Coon, S. A., M. D. Scadron, and B. R. Barrett, 1975, Nucl. Phys. A **242**, 467.
Cottingham, W. N., M. Lacombe, B. Loiseau, J. M. Richard, and R. Vinh Mau, 1973, Phys. Rev. D **8**, 800.
da Rocha, C., G. Miller, and U. van Kolck, 2000, Phys. Rev. C **61**, 034613.
Danilov, G., 1961, Sov. Phys. JETP **13**, 349.
Dapo, H., B.-J. Schaefer, and J. Wambach, 2008, Eur. Phys. J. A **36**, 101.
Delfino, A., T. Frederico, V. S. Timóteo, and L. Tomio, 2006, Phys. Lett. B **634**, 185.
Deltuva, A., and A. C. Fonseca, 2007a, Phys. Rev. C **76**, 021001.
Deltuva, A., and A. C. Fonseca, 2007b, Phys. Rev. Lett. **98**, 162502.
Deltuva, A., A. C. Fonseca, and P. U. Sauer, 2005a, Phys. Rev. Lett. **95**, 092301.
Deltuva, A., A. C. Fonseca, and P. U. Sauer, 2005b, Phys. Rev. C **72**, 054004.
de Swart, J. J., 1963, Rev. Mod. Phys. **35**, 916.
de Swart, J. J., and C. Dullemond, 1962, Ann. Phys. **19**, 485.
de Swart, J. J., M. C. M. Rentmeester, and R. G. E. Timmermans, 1997, πN Newslett. **13**, 96.
Djukanovic, D., J. Gegelia, S. Scherer, and M. R. Schindler, 2007, Few-Body Syst. **41**, 141.
Drochner, M., *et al.* (GEM), 1998, Nucl. Phys. A **643**, 55.
Drukarev, E. G., and E. M. Levin, 1990, Nucl. Phys. A **511**, 679.
Duane, S., A. D. Kennedy, B. J. Pendleton, and D. Roweth, 1987, Phys. Lett. B **195**, 216.
Durand, L., 1957, Phys. Rev. **108**, 1597.
Duweke, C., *et al.*, 2005, Phys. Rev. C **71**, 054003.
Eden, J. A., and M. F. Gari, 1996, Phys. Rev. C **53**, 1510.
Efimov, V., 1970, Phys. Lett. B **33**, 563.

Efimov, V., 1981, Nucl. Phys. A **362**, 45 .
Efimov, V., 1991, Phys. Rev. C **44**, 2303.
Eisele, F., H. Filthuth, W. Foehlisch, V. Hepp, and G. Zech, 1971, Phys. Lett. B **37**, 204.
Engelmann, R., H. Filthuth, V. Hepp, and E. Kluge, 1966, Phys. Lett. **21**, 587.
Entem, D. R., and R. Machleidt, 2002, Phys. Rev. C **66**, 014002.
Entem, D. R., and R. Machleidt, 2003a, Phys. Rev. C **68**, 041001.
Entem, D. R., and R. Machleidt, 2003b, e-print arXiv:nucl-th/0303017.
Entem, D. R., E. Ruiz Arriola, M. Pavón Valderrama, and R. Machleidt, 2008, Phys. Rev. C **77**, 044006.
Epelbaum, E., 2000, Ph.D. thesis, Ruhr-University Bochum.
Epelbaum, E., 2006a, Prog. Part. Nucl. Phys. **57**, 654.
Epelbaum, E., 2006b, Phys. Lett. B **639**, 456.
Epelbaum, E., 2007, Eur. Phys. J. A **34**, 197.
Epelbaum, E., W. Glöckle, A. Krüger, and U.-G. Meißner, 1999, Nucl. Phys. A **645**, 413.
Epelbaum, E., W. Glöckle, and U.-G. Meißner, 1998a, Phys. Lett. B **439**, 1.
Epelbaum, E., W. Glöckle, and U.-G. Meißner, 1998b, Nucl. Phys. A **637**, 107.
Epelbaum, E., W. Glöckle, and U.-G. Meißner, 2000, Nucl. Phys. A **671**, 295.
Epelbaum, E., W. Glöckle, and U.-G. Meißner, 2004a, Eur. Phys. J. A **19**, 125.
Epelbaum, E., W. Glöckle, and U.-G. Meißner, 2004b, Eur. Phys. J. A **19**, 401.
Epelbaum, E., W. Glöckle, and U.-G. Meißner, 2005, Nucl. Phys. A **747**, 362.
Epelbaum, E., H.-W. Hammer, U.-G. Meißner, and A. Nogga, 2006, Eur. Phys. J. C **48**, 169.
Epelbaum, E., H. Kamada, A. Nogga, H. Witała, W. Glöckle, and U.-G. Meißner, 2001, Phys. Rev. Lett. **86**, 4787.
Epelbaum, E., H. Krebs, D. Lee, and U.-G. Meißner, 2009, unpublished.
Epelbaum, E., H. Krebs, and U.-G. Meißner, 2008a, Nucl. Phys. A **806**, 65.
Epelbaum, E., H. Krebs, and U.-G. Meißner, 2008b, Phys. Rev. C **77**, 034006.
Epelbaum, E., and U.-G. Meißner, 2005, Phys. Rev. C **72**, 044001.
Epelbaum, E., and U. G. Meißner, 2006, e-print arXiv:nucl-th/0609037.
Epelbaum, E., U.-G. Meißner, and W. Glöckle, 2002, e-print arXiv:nucl-th/0208040.
Epelbaum, E., U.-G. Meißner, and W. Glöckle, 2003, Nucl. Phys. A **714**, 535.
Epelbaum, E., U.-G. Meißner, W. Glöckle, and C. Elster, 2002, Phys. Rev. C **65**, 044001.
Epelbaum, E., U.-G. Meißner, and J. E. Palomar, 2005, Phys. Rev. C **71**, 024001.
Epelbaum, E., A. Nogga, W. Glöckle, H. Kamada, and U.-G. Meißner, 2002, Eur. Phys. J. A **15**, 543.
Epelbaum, E., A. Nogga, W. Glöckle, H. Kamada, U.-G. Meißner, and H. Witała, 2002, Phys. Rev. C **66**, 064001.
Ermisch, K., *et al.*, 2003, Phys. Rev. C **68**, 051001.
Ermisch, K., *et al.*, 2005, Phys. Rev. C **71**, 064004.
Fearing, H. W., 1998, Phys. Rev. Lett. **81**, 758.
Fearing, H. W., and S. Scherer, 2000, Phys. Rev. C **62**, 034003.
Fedorov, D. V., and A. S. Jensen, 2002, Nucl. Phys. A **697**, 783.
Fedorov, D. V., A. S. Jensen, and K. Riisager, 1994, Phys. Rev. Lett. **73**, 2817.
Fettes, N., 2000, Ph.D. thesis, University of Bonn.
Fettes, N., and U.-G. Meißner, 2001, Nucl. Phys. A **679**, 629.
Fettes, N., U.-G. Meißner, M. Mojžiš, and S. Steininger, 2000, Ann. Phys. **283**, 273.
Fettes, N., U.-G. Meißner, and S. Steininger, 1998, Nucl. Phys. A **640**, 199.
Finelli, P., N. Kaiser, D. Vretenar, and W. Weise, 2003, Eur. Phys. J. A **17**, 573.
Finelli, P., N. Kaiser, D. Vretenar, and W. Weise, 2004, Nucl. Phys. A **735**, 449.
Finelli, P., N. Kaiser, D. Vretenar, and W. Weise, 2007, Phys. Lett. B **658**, 90.
Fisher, B. M., *et al.*, 2006, Phys. Rev. C **74**, 034001.
Flambaum, V. V., and R. B. Wiringa, 2007, Phys. Rev. C **76**, 054002.
Fleming, S., T. Mehen, and I. W. Stewart, 2000, Nucl. Phys. A **677**, 313.
Frederico, T., V. S. Timóteo, and L. Tomio, 1999, Nucl. Phys. A **653**, 209.
Friar, J. L., 1977, Ann. Phys. **104**, 380.
Friar, J. L., 1997, Few-Body Syst. **22**, 161.
Friar, J. L., 1999, Phys. Rev. C **60**, 034002.
Friar, J. L., and S. A. Coon, 1994, Phys. Rev. C **49**, 1272.
Friar, J. L., D. Hüber, and U. van Kolck, 1999, Phys. Rev. C **59**, 53.
Friar, J. L., D. G. Madland, and B. W. Lynn, 1996, Phys. Rev. C **53**, 3085.
Friar, J. L., G. L. Payne, and U. van Kolck, 2005, Phys. Rev. C **71**, 024003.
Friar, J. L., and U. van Kolck, 1999, Phys. Rev. C **60**, 034006.
Friar, J. L., U. van Kolck, G. L. Payne, and S. A. Coon, 2003, Phys. Rev. C **68**, 024003.
Friar, J. L., U. van Kolck, M. C. M. Rentmeester, and R. G. E. Timmermans, 2004, Phys. Rev. C **70**, 044001.
Friedman, B., and V. R. Pandharipande, 1981, Nucl. Phys. A **361**, 502.
Fritsch, S., N. Kaiser, and W. Weise, 2005, Nucl. Phys. A **750**, 259.
Fujii, S., *et al.*, 2004, Phys. Rev. C **70**, 024003.
Fujita, J., and H. Miyazawa, 1957, Prog. Theor. Phys. **17**, 360.
Fujita, J.-I., M. Kawai, and M. Tanifuji, 1962, Nucl. Phys. **29**, 252.
Fujiwara, Y., Y. Suzuki, and C. Nakamoto, 2007, Prog. Part. Nucl. Phys. **58**, 439.
Fukuda, N., K. Sawada, and M. Taketani, 1954, Prog. Theor. Phys. **12**, 156.
Fukugita, M., Y. Kuramashi, H. Mino, M. Okawa, and A. Ukawa, 1994, Phys. Rev. Lett. **73**, 2176.
Fukugita, M., Y. Kuramashi, M. Okawa, H. Mino, and A. Ukawa, 1995, Phys. Rev. D **52**, 3003.
Furnstahl, R. J., 2007, e-print arXiv:nucl-th/0702040.
Furnstahl, R. J., D. K. Griegel, and T. D. Cohen, 1992, Phys. Rev. C **46**, 1507.
Furnstahl, R. J., and H.-W. Hammer, 2002, Phys. Lett. B **531**, 203.
Furnstahl, R. J., H.-W. Hammer, and N. Tirfessa, 2001, Nucl. Phys. A **689**, 846.
Furnstahl, R. J., G. Rupak, and T. Schafer, 2008, Annu. Rev. Nucl. Part. Sci. **58**, 1.
Gabbiani, F., P. F. Bedaque, and H. W. Grießhammer, 2000, Nucl. Phys. A **675**, 601.
Gardestig, A., and D. R. Phillips, 2006, Phys. Rev. C **73**,

014002.
Gardestig, A., *et al.*, 2004, Phys. Rev. C **69**, 044606.
Gasparyan, A., J. Haidenbauer, C. Hanhart, and J. Speth, 2004, Phys. Rev. C **69**, 034006.
Gasser, J., M. A. Ivanov, E. Lipartia, M. Mojzis, and A. Rusetsky, 2002, Eur. Phys. J. C **26**, 13.
Gasser, J., and H. Leutwyler, 1982, Phys. Rep. **87**, 77.
Gasser, J., and H. Leutwyler, 1984, Ann. Phys. **158**, 142.
Gasser, J., and H. Leutwyler, 1985, Nucl. Phys. B **250**, 465.
Gasser, J., M. E. Sainio, and A. Svarc, 1988, Nucl. Phys. B **307**, 779.
Gegelia, J., 1998, e-print arXiv:nucl-th/9802038.
Gegelia, J., 1999, J. Phys. G **25**, 1681.
Gegelia, J., and G. Japaridze, 2001, Phys. Lett. B **517**, 476.
Gegelia, J., and S. Scherer, 2006, Int. J. Mod. Phys. A **21**, 1079.
Georgi, H., 1991, Nucl. Phys. B **361**, 339.
Georgi, H., 1993, Annu. Rev. Nucl. Part. Sci. **43**, 209.
Gezerlis, A., and J. Carlson, 2008, Phys. Rev. C **77**, 032801.
Gilg, H., *et al.*, 2000, Phys. Rev. C **62**, 025201.
Giorgini, S., L. P. Pitaevskii, and S. Stringari, 2008, Rev. Mod. Phys. **80**, 1215.
Girlanda, L., A. Rusetsky, and W. Weise, 2004, Ann. Phys. **312**, 92.
Girlanda, L., A. Rusetsky, and W. Weise, 2005, Nucl. Phys. A **755**, 653.
Giusti, L., and S. Necco, 2007, J. High Energy Phys. **04**, 090.
Glöckle, W., H. Witała, D. Hüber, H. Kamada, and J. Golak, 1996, Phys. Rep. **274**, 107.
Glombik, A., *et al.*, 1995, AIP Conf. Proc. **334**, 486.
Goldstone, J., 1961, Nuovo Cimento **19**, 154.
Goldstone, J., A. Salam, and S. Weinberg, 1962, Phys. Rev. **127**, 965.
Gonzalez Trotter, D. E., *et al.*, 1999, Phys. Rev. Lett. **83**, 3788.
Grießhammer, H. W., 2004, Nucl. Phys. A **744**, 192.
Grießhammer, H. W., 2005, Nucl. Phys. A **760**, 110.
Haag, R., 1958, Phys. Rev. **112**, 669.
Hacker, C., N. Wies, J. Gegelia, and S. Scherer, 2005, Phys. Rev. C **72**, 055203.
Haidenbauer, J., and U.-G. Meißner, 2005, Phys. Rev. C **72**, 044005.
Haidenbauer, J., U.-G. Meißner, A. Nogga, and H. Polinder, 2007, Lect. Notes Phys. **724**, 113.
Hamber, H. W., E. Marinari, G. Parisi, and C. Rebbi, 1983, Nucl. Phys. B **225**, 475.
Hammer, H.-W., 2002, Nucl. Phys. A **705**, 173.
Hammer, H.-W., and R. J. Furnstahl, 2000, Nucl. Phys. A **678**, 277.
Hammer, H.-W., and R. Higa, 2008, Eur. Phys. J. A **37**, 193.
Hammer, H.-W., and T. Mehen, 2001, Nucl. Phys. A **690**, 535.
Hammer, H.-W., D. R. Phillips, and L. Platter, 2007, Eur. Phys. J. A **32**, 335.
Hammer, H.-W., and L. Platter, 2007, Eur. Phys. J. A **32**, 113.
Hammer, H.-W., and B. G. Swingle, 2006, Ann. Phys. **321**, 306.
Hanhart, C., 2004, Phys. Rep. **397**, 155.
Hanhart, C., 2007, e-print arXiv:nucl-th/0703028.
Hanhart, C., and N. Kaiser, 2002, Phys. Rev. C **66**, 054005.
Hanhart, C., U. van Kolck, and G. A. Miller, 2000, Phys. Rev. Lett. **85**, 2905.
Harada, K., and H. Kubo, 2006, Nucl. Phys. B **758**, 304.
Harada, K., H. Kubo, and A. Ninomiya, 2009, Int. J. Mod. Phys. A **24**, 3191.
Heimberg, P., *et al.*, 1996, Phys. Rev. Lett. **77**, 1012.
Hemmert, T. R., B. R. Holstein, and J. Kambor, 1998, J. Phys. G **24**, 1831.
Henley, E. M., and G. A. Miller, 1979, *Rho M. Wilkinson D: Mesons in Nuclei* (North-Holland, Amsterdam), Vol. I, pp. 405–434.
Higa, R., 2008, e-print arXiv:0809.5157.
Higa, R., H.-W. Hammer, and U. van Kolck, 2008, Nucl. Phys. A **809**, 171.
Higa, R., M. Pavón Valderrama, and E. Ruiz Arriola, 2008, Phys. Rev. C **77**, 034003.
Higa, R., and M. R. Robilotta, 2003, Phys. Rev. C **68**, 024004.
Higa, R., M. R. Robilotta, and C. A. da Rocha, 2004, Phys. Rev. C **69**, 034009.
Higa, R., M. R. Robilotta, and C. A. da Rocha, 2005, e-print arXiv:nucl-th/0501076.
Howell, C. R., 2008, e-print arXiv:0805.1177.
Howell, C. R., *et al.*, 1987, Few-Body Syst. **2**, 19.
Howell, C. R., *et al.*, 1998, Phys. Lett. B **444**, 252.
Hüber, D., H. Witała, A. Nogga, W. Glöckle, and H. Kamada, 1997, Few-Body Syst. **22**, 107.
Huhn, V., *et al.*, 2000, Phys. Rev. Lett. **85**, 1190.
Hutcheon, D. A., *et al.*, 1991, Nucl. Phys. A **535**, 618.
Ishii, N., S. Aoki, and T. Hatsuda, 2007a, PoS **LAT2007**, 146.
Ishii, N., S. Aoki, and T. Hatsuda, 2007b, Phys. Rev. Lett. **99**, 022001.
Ishikawa, S., and M. R. Robilotta, 2007, Phys. Rev. C **76**, 014006.
Itahashi, K., *et al.*, 2000, Phys. Rev. C **62**, 025202.
Jackson, A. D., D. O. Riska, and B. Verwest, 1975, Nucl. Phys. A **249**, 397.
Jaminon, M., and C. Mahaux, 1990, Phys. Rev. C **41**, 697.
Jenkins, E., and A. V. Manohar, 1991, Phys. Lett. B **255**, 558.
Jenkins, E., and A. V. Manohar, 1992, Phys. Lett. B **281**, 336.
Jensen, A. S., K. Riisager, D. V. Fedorov, and E. Garrido, 2004, Rev. Mod. Phys. **76**, 215.
Jurgenson, E. D., and R. J. Furnstahl, 2009, Nucl. Phys. A **818**, 152.
Kaiser, N., 2000a, Phys. Rev. C **62**, 024001.
Kaiser, N., 2000b, Phys. Rev. C **61**, 014003.
Kaiser, N., 2001a, Phys. Rev. C **64**, 057001.
Kaiser, N., 2001b, Phys. Rev. C **63**, 044010.
Kaiser, N., 2002a, Phys. Rev. C **65**, 017001.
Kaiser, N., 2002b, Nucl. Phys. A **709**, 251.
Kaiser, N., 2003, Phys. Rev. C **68**, 054001.
Kaiser, N., 2006a, Phys. Rev. C **74**, 067001.
Kaiser, N., 2006b, Phys. Rev. C **73**, 064003.
Kaiser, N., 2006c, Phys. Rev. C **73**, 044001.
Kaiser, N., R. Brockmann, and W. Weise, 1997, Nucl. Phys. A **625**, 758.
Kaiser, N., S. Fritsch, and W. Weise, 2002a, Nucl. Phys. A **697**, 255.
Kaiser, N., S. Fritsch, and W. Weise, 2002b, Nucl. Phys. A **700**, 343.
Kaiser, N., S. Fritsch, and W. Weise, 2003, Nucl. Phys. A **724**, 47.
Kaiser, N., S. Gerstendorfer, and W. Weise, 1998, Nucl. Phys. A **637**, 395.
Kaiser, N., P. de Homont, and W. Weise, 2008, Phys. Rev. C **77**, 025204.
Kaiser, N., M. Muhlbauer, and W. Weise, 2007, Eur. Phys. J. A **31**, 53.
Kaiser, N., and W. Weise, 2005, Phys. Rev. C **71**, 015203.
Kaiser, N., and W. Weise, 2008, Nucl. Phys. A **804**, 60.
Kaiser, N., and W. Weise, 2009, Phys. Lett. B **671**, 25.

Kamada, H., and W. Glöckle, 1998, Phys. Rev. Lett. **80**, 2547.
Kamada, H., *et al.*, 2008, AIP Conf. Proc. **1011**, 59.
Kaplan, D. B., 1997, Nucl. Phys. B **494**, 471.
Kaplan, D. B., M. J. Savage, and M. B. Wise, 1998a, Phys. Lett. B **424**, 390.
Kaplan, D. B., M. J. Savage, and M. B. Wise, 1998b, Nucl. Phys. B **534**, 329.
Kaplan, D. B., M. J. Savage, and M. B. Wise, 1999, Phys. Rev. C **59**, 617.
Kharchenko, V. F., 1973, Sov. J. Nucl. Phys. **16**, 173.
Kievsky, A., M. Viviani, and L. E. Marcucci, 2004, Phys. Rev. C **69**, 014002.
Kilian, W., and T. Ohl, 1994, Phys. Rev. D **50**, 4649.
Kirchbach, M., and A. Wirzba, 1996, Nucl. Phys. A **604**, 395.
Kirchbach, M., and A. Wirzba, 1997, Nucl. Phys. A **616**, 648.
Kistryn, S., *et al.*, 2005, Phys. Rev. C **72**, 044006.
Knecht, M., and R. Urech, 1998, Nucl. Phys. B **519**, 329.
Korpa, C. L., A. E. L. Dieperink, and R. G. E. Timmermans, 2002, Phys. Rev. C **65**, 015208.
Krebs, H., V. Bernard, and U.-G. Meißner, 2004, Eur. Phys. J. A **22**, 503.
Krebs, H., E. Epelbaum, and U.-G. Meißner, 2007, Eur. Phys. J. A **32**, 127.
Kretschmer, W., 1995, AIP Conf. Proc. **339**, 355.
Kreuzer, S., and H.-W. Hammer, 2009, Phys. Lett. B **673**, 260.
Krippa, B., M. C. Birse, J. A. McGovern, and N. R. Walet, 2003, Phys. Rev. C **67**, 031301.
Lazauskas, R., *et al.*, 2005, Phys. Rev. C **71**, 034004.
Lee, D., 2004, Phys. Rev. C **70**, 064002.
Lee, D., 2006, Phys. Rev. A **73**, 063204.
Lee, D., 2008, Phys. Rev. C **78**, 024001.
Lee, D., B. Borasoy, and T. Schafer, 2004, Phys. Rev. C **70**, 014007.
Lensky, V., *et al.*, 2005, Eur. Phys. J. A **26**, 107.
Lensky, V., *et al.*, 2006, Eur. Phys. J. A **27**, 37.
Lensky, V., *et al.*, 2007a, Phys. Lett. B **648**, 46.
Lensky, V., *et al.*, 2007b, Eur. Phys. J. A **33**, 339.
Lepage, G. P., 1989, in *From Actions to Answers* (TASI-89), edited by T. DeGrand and D. Toussaint (World Scientific, Singapore, 1989); e-print arXiv:hep-ph/0506330.
Lepage, G. P., 1997, e-print arXiv:nucl-th/9706029.
Lepage, G. P., 2000, Talk given at the program "Effective Field Theories and Effective Interactions," INT, Seattle, June 25–August 2.
Leutwyler, H., 1994, Phys. Rev. D **49**, 3033.
Leutwyler, H., 1996, Phys. Lett. B **378**, 313.
Leutwyler, H., and A. V. Smilga, 1992, Phys. Rev. D **46**, 5607.
Ley, J., *et al.*, 2006, Phys. Rev. C **73**, 064001.
Lin, T., C. Elster, W. N. Polyzou, and W. Glöckle, 2008, Phys. Lett. B **660**, 345.
Lin, T., C. Elster, W. N. Polyzou, H. Witała, and W. Glöckle, 2008, Phys. Rev. C **78**, 024002.
Long, B., and U. van Kolck, 2008, Ann. Phys. **323**, 1304.
Lüscher, M., 1986, Commun. Math. Phys. **105**, 153.
Lüscher, M., 1991, Nucl. Phys. B **354**, 531.
Lutz, M., 2000, Nucl. Phys. A **677**, 241.
Lutz, M., B. Friman, and Ch. Appel, 2000, Phys. Lett. B **474**, 7.
Machleidt, R., 2001, Phys. Rev. C **63**, 024001.
Machleidt, R., and I. Slaus, 2001, J. Phys. G **27**, R69.
Manohar, A. V., 1996, e-print arXiv:hep-ph/9606222.
Marques, F. M., *et al.*, 2001, Phys. Rev. C **64**, 061301.
Mazumdar, I., V. Arora, and V. S. Bhasin, 2000, Phys. Rev. C **61**, 051303.
Mazumdar, I., A. R. P. Rau, and V. S. Bhasin, 2006, Phys. Rev. Lett. **97**, 062503.
McKellar, B. H. J., and R. Rajaraman, 1968, Phys. Rev. Lett. **21**, 450.
McManus, H., and D. O. Riska, 1980, Phys. Lett. **92B**, 29.
Mehen, T., I. W. Stewart, and M. B. Wise, 1999, Phys. Rev. Lett. **83**, 931.
Meißner, U.-G., G. Müller, and S. Steininger, 1997, Phys. Lett. B **406**, 154.
Meißner, U.-G., J. A. Oller, and A. Wirzba, 2002, Ann. Phys. **297**, 27.
Meißner, U.-G., U. Raha, and A. Rusetsky, 2006, Phys. Lett. B **639**, 478.
Meißner, U.-G., and S. Steininger, 1998, Phys. Lett. B **419**, 403.
Miller, G. A., B. M. K. Nefkens, and I. Slaus, 1990, Phys. Rep. **194**, 1.
Miller, G. A., A. K. Opper, and E. J. Stephenson, 2006, Annu. Rev. Nucl. Part. Sci. **56**, 253.
Miller, G. A., and W. T. H. Van Oers, 1994, e-print arXiv:nucl-th/9409013.
Mohr, R. F., R. J. Furnstahl, H.-W. Hammer, R. J. Perry, and K. G. Wilson,2006, Ann. Phys. **321**, 225.
Mondejar, J., and J. Soto, 2007, Eur. Phys. J. A **32**, 77.
Müller, G., and U.-G. Meißner, 1999, Nucl. Phys. B **556**, 265.
Muller, H. M., S. E. Koonin, R. Seki, and U. van Kolck, 2000, Phys. Rev. C **61**, 044320.
Nakamura, S. X., 2008, Phys. Rev. C **77**, 054001.
Navratil, P., V. G. Gueorguiev, J. P. Vary, W. E. Ormand, and A. Nogga, 2007, Phys. Rev. Lett. **99**, 042501.
Navratil, P., *et al.*, 2008, Few-Body Syst. **43**, 129.
Nelson, A. E., and D. B. Kaplan, 1987, Phys. Lett. B **192**, 193.
Nemura, H., N. Ishii, S. Aoki, and T. Hatsuda, 2008, e-print arXiv:0806.1094.
Neufeld, H., and H. Rupertsberger, 1996, Z. Phys. C **71**, 131.
Niskanen, J. A., 2002, Phys. Rev. C **65**, 037001.
Nogga, A., S. K. Bogner, and A. Schwenk, 2004, Phys. Rev. C **70**, 061002.
Nogga, A., H. Kamada, and W. Glöckle, 2000, Phys. Rev. Lett. **85**, 944.
Nogga, A., P. Navratil, B. R. Barrett, and J. P. Vary, 2006, Phys. Rev. C **73**, 064002.
Nogga, A., R. G. E. Timmermans, and U. van Kolck, 2005, Phys. Rev. C **72**, 054006.
Nogga, A., *et al.*, 2006, Phys. Lett. B **639**, 465.
Okubo, S., 1954, Prog. Theor. Phys. **12**, 603.
Oller, J. A., 2002, Phys. Rev. C **65**, 025204.
Oller, J. A., 2003, Nucl. Phys. A **725**, 85.
Oller, J. A., 2008, private communication.
Oller, J. A., A. Lacour, and U. G. Meißner, 2009, e-print arXiv:0902.1986.
Opper, A. K., *et al.*, 2003, Phys. Rev. Lett. **91**, 212302.
Ordonez, C., and U. van Kolck, 1992, Phys. Lett. B **291**, 459.
Ordonez, C., L. Ray, and U. van Kolck, 1994, Phys. Rev. Lett. **72**, 1982.
Ordonez, C., L. Ray, and U. van Kolck, 1996, Phys. Rev. C **53**, 2086.
Pandharipande, V. R., D. R. Phillips, and U. van Kolck, 2005, Phys. Rev. C **71**, 064002.
Pascalutsa, V., 1998, Phys. Rev. D **58**, 096002.
Pavón Valderrama, M., and E. Ruiz Arriola, 2004a, Phys. Rev. C **70**, 044006.
Pavón Valderrama, M., and E. Ruiz Arriola, 2004b, Phys. Lett. B **580**, 149.

Pavón Valderrama, M., and E. Ruiz Arriola, 2005, Phys. Rev. C **72**, 054002.
Pavón Valderrama, M., and E. R. Arriola, 2006a, Phys. Rev. C **74**, 054001.
Pavón Valderrama, M., and E. Ruiz Arriola, 2006b, Phys. Rev. C **74**, 064004.
Peccei, R. D., 2008, Lect. Notes Phys. **741**, 3.
Phillips, A., 1968, Nucl. Phys. A **107**, 209.
Phillips, D. R., I. R. Afnan, and A. G. Henry-Edwards, 2000, Phys. Rev. C **61**, 044002.
Phillips, D. R., S. R. Beane, and M. C. Birse, 1999, J. Phys. A **32**, 3397.
Phillips, D. R., S. R. Beane, and T. D. Cohen, 1998, Ann. Phys. **263**, 255.
Phillips, D. R., G. Rupak, and M. J. Savage, 2000, Phys. Lett. B **473**, 209.
Phillips, R. J. N., 1959, Rep. Prog. Phys. **22**, 562.
Pieper, S. C., V. R. Pandharipande, R. B. Wiringa, and J. Carlson, 2001, Phys. Rev. C **64**, 014001.
Pieper, S. C., and R. B. Wiringa, 2001, Annu. Rev. Nucl. Part. Sci. **51**, 53.
Pisarski, R. D., and M. Tytgat, 1996, Phys. Rev. D **54**, R2989.
Platter, L., 2006, Phys. Rev. C **74**, 037001.
Platter, L., and H.-W. Hammer, 2006, Nucl. Phys. A **766**, 132.
Platter, L., H.-W. Hammer, and U.-G. Meißner, 2004, Phys. Rev. A **70**, 052101.
Platter, L., H.-W. Hammer, and U.-G. Meißner, 2005, Phys. Lett. B **607**, 254.
Platter, L., C. Ji, and D. R. Phillips, 2008, e-print arXiv:0808.1230.
Platter, L., and D. R. Phillips, 2006, Few-Body Syst. **40**, 35.
Polinder, H., J. Haidenbauer, and U.-G. Meißner, 2006, Nucl. Phys. A **779**, 244.
Polinder, H., J. Haidenbauer, and U.-G. Meißner, 2007, Phys. Lett. B **653**, 29.
Politzer, H. D., 1980, Nucl. Phys. B **172**, 349.
Polyzou, W. N., and W. Glöckle, 1990, Few-Body Syst. **9**, 97.
Pudliner, B. S., V. R. Pandharipande, J. Carlson, S. C. Pieper, and R. B. Wiringa, 1997, Phys. Rev. C **56**, 1720.
Pupin, J. C., and M. R. Robilotta, 1999, Phys. Rev. C **60**, 014003.
Quaglioni, S., and P. Navratil, 2008, Phys. Rev. Lett. **101**, 092501.
Rauprich, G., *et al.*, 1988, Few-Body Syst. **5**, 67.
Rauprich, G., *et al.*, 1991, Nucl. Phys. A **535**, 313.
Rentmeester, M. C. M., R. G. E. Timmermans, and J. J. de Swart, 2003, Phys. Rev. C **67**, 044001.
Rentmeester, M. C. M., R. G. E. Timmermans, J. L. Friar, and J. J. de Swart, 1999, Phys. Rev. Lett. **82**, 4992.
Rentmeester, M. C. M., *et al.*, 1994, *NN* online program, http://nn-online.org
Rijken, T. A., V. G. J. Stoks, and Y. Yamamoto, 1999, Phys. Rev. C **59**, 21.
Rijken, T. A., and Y. Yamamoto, 2006, e-print arXiv:nucl-th/0608074.
Robilotta, M. R., 1985, Phys. Rev. C **31**, 974.
Robilotta, M. R., 2001, Phys. Rev. C **63**, 044004.
Robilotta, M. R., 2006, Phys. Rev. C **74**, 044002.
Rozpedzik, D., *et al.*, 2006, Acta Phys. Pol. B **37**, 2889.
Rubinstein, H. R., F. Scheck, and R. H. Sokolov, 1967, Phys. Rev. **154**, 1608.
Rupak, G., and X.-W. Kong, 2003, Nucl. Phys. A **717**, 73.
Ryezayeva, N., *et al.*, 2008, Phys. Rev. Lett. **100**, 172501.
Sadeghi, H., and S. Bayegan, 2005, Nucl. Phys. A **753**, 291.
Sadeghi, H., S. Bayegan, and H. W. Grießhammer, 2006, Phys. Lett. B **643**, 263.
Sagara, K., *et al.*, 1994, Phys. Rev. C **50**, 576.
Savage, M. J., and M. B. Wise, 1996, Phys. Rev. D **53**, 349.
Schaefer, B. J., M. Wagner, J. Wambach, T. T. S. Kuo, and G. E. Brown, 2006, Phys. Rev. C **73**, 011001.
Scherer, S., and H. W. Fearing, 1995a, Phys. Rev. C **51**, 359.
Scherer, S., and H. W. Fearing, 1995b, Phys. Rev. D **52**, 6445.
Schwenk, A., and J. D. Holt, 2008, AIP Conf. Proc. **1011**, 159.
Schwenk, A., and C. J. Pethick, 2005, Phys. Rev. Lett. **95**, 160401.
Sechi-Zorn, B., B. Kehoe, J. Twitty, and R. A. Burnstein, 1968, Phys. Rev. **175**, 1735.
Serot, B. D., and J. D. Walecka, 1986, Adv. Nucl. Phys. **16**, 1.
Setze, H. R., *et al.*, 1996, Phys. Lett. B **388**, 229.
Shukla, D., D. R. Phillips, and E. Mortenson, 2008, J. Phys. G **35**, 115009.
Skorniakov, G. V., and K. A. Ter-Martirosian, 1957, Sov. Phys. JETP **4**, 648.
Soto, J., and J. Tarrus, 2008, Phys. Rev. C **78**, 024003.
Sperisen, F., *et al.*, 1984, Nucl. Phys. A **422**, 81.
Srivastava, M. K., and D. W. L. Sprung, 1975, Adv. Nucl. Phys. **8**, 131.
Stephan, E., *et al.*, 2007, Phys. Rev. C **76**, 057001.
Stephenson, E. J., *et al.*, 2003, Phys. Rev. Lett. **91**, 142302.
Stern, J., 1998, e-print arXiv:hep-ph/9801282.
Stetcu, I., B. R. Barrett, and U. van Kolck, 2007, Phys. Lett. B **653**, 358.
Stetcu, I., B. R. Barrett, U. van Kolck, and J. P. Vary, 2007, Phys. Rev. A **76**, 063613.
Stoks, V. G., 1990, Ph.D. thesis, University Nijmegen.
Stoks, V. G. J., R. A. M. Klomp, M. C. M. Rentmeester, and J. J. de Swart, 1993, Phys. Rev. C **48**, 792.
Stoks, V. G. J., R. A. M. Klomp, C. P. F. Terheggen, and J. J. de Swart, 1994, Phys. Rev. C **49**, 2950.
Strate, J., *et al.*, 1989, Nucl. Phys. A **501**, 51.
Takahashi, H., *et al.*, 2001, Phys. Rev. Lett. **87**, 212502.
Tamagawa, T., *et al.*, 2001, Nucl. Phys. A **691**, 234.
Thorsson, V., and A. Wirzba, 1995, Nucl. Phys. A **589**, 633.
Tiburzi, B. C., and A. Walker-Loud, 2006, Nucl. Phys. A **764**, 274.
Uehling, E. A., 1935, Phys. Rev. **48**, 55.
Urech, R., 1995, Nucl. Phys. B **433**, 234.
Vafa, C., and E. Witten, 1984, Nucl. Phys. B **234**, 173.
Valderrama, M. P., and E. R. Arriola, 2008, e-print arXiv:0809.3186.
van Kolck, U., 1994, Phys. Rev. C **49**, 2932.
van Kolck, U., 1999, Nucl. Phys. A **645**, 273.
van Kolck, U., J. L. Friar, and T. Goldman, 1996, Phys. Lett. B **371**, 169.
van Kolck, U., J. A. Niskanen, and G. A. Miller, 2000, Phys. Lett. B **493**, 65.
van Kolck, U., M. C. M. Rentmeester, J. L. Friar, T. Goldman, and J. J. de Swart, 1998, Phys. Rev. Lett. **80**, 4386.
van Kolck, U. L., 1993, Ph.D. thesis, University of Texas, Austin.
van Oers, W. T. H., and J. D. Seagrave, 1967, Phys. Lett. **24B**, 562.
von Neumann-Cosel, P., A. Richter, G. Schrieder, A. Shevchenko, A. Stiller, and H. Arenhövel, 2002, Phys. Rev. Lett. **88**, 202304.
von Stecher, J., J. D'Incao, and C. Greene, 2009, Nat. Phys. **5**,

417.
Walzl, M., U.-G. Meißner, and E. Epelbaum, 2001, Nucl. Phys. A **693**, 663.
Weinberg, S., 1979, Physica A **96**, 327.
Weinberg, S., 1990, Phys. Lett. B **251**, 288.
Weinberg, S., 1991, Nucl. Phys. B **363**, 3.
Weinberg, S., 1992, Phys. Lett. B **295**, 114.
Wigner, E., 1937, Phys. Rev. **51**, 947.
Wilczek, F., 2007, Nature (London) **445**, 156.
Wilson, K. G., 1983, Rev. Mod. Phys. **55**, 583.
Wilson, K. G., 2005, Nucl. Phys. B, Proc. Suppl. **140**, 3.
Wiringa, R. B., V. G. J. Stoks, and R. Schiavilla, 1995, Phys. Rev. C **51**, 38.
Witała, H., J. Golak, W. Glöckle, and H. Kamada, 2005, Phys. Rev. C **71**, 054001.
Witała, H., J. Golak, R. Skibinski, C. R. Howell, and W. Tornow, 2003, Phys. Rev. C **67**, 064002.
Witała, H., *et al.*, 1993, Few-Body Syst. **15**, 67.
Witała, H., *et al.*, 2006, Phys. Rev. C **73**, 044004.
Yamashita, M. T., T. Frederico, and L. Tomio, 2008, Phys. Lett. B **660**, 339.
Yamashita, M. T., L. Tomio, A. Delfino, and T. Frederico, 2006, Europhys. Lett. **75**, 555.
Yang, C. J., C. Elster, and D. R. Phillips, 2008, Phys. Rev. C **77**, 014002.
Yang, J.-F., and J.-H. Huang, 2005, Phys. Rev. C **71**, 034001.
Yukawa, H., 1935, Proc. Phys. Math. Soc. Jpn. **17**, 48.
Zhukov, M. V., *et al.*, 1993, Phys. Rep. **231**, 151.